A Correlation-Based Transition Model using Local Variables for Unstructured Parallelized CFD codes

An der Universität Stuttgart, Fakultät Maschinenbau
zur Erlangung des akademischen Grades eines Doktor-Ingenieurs (Dr.-Ing.) eingereichte und genehmigte Abhandlung

vorgelegt von
Robin Blair Langtry
aus Ottawa, Kanada

Hauptberichter: ***Prof. M. Casey, D. Phil.***
Universität Stuttgart

Mitberichter: ***Prof. Dr. Wolfgang Rodi***
Universität Karlsruhe

Tag der mündlichen Prüfung: 31. Mai 2006

Institut für Thermische Strömungsmaschinen
und Maschinenlaboratorium
Universität Stuttgart
2006

Acknowledgments

I would like to express my profound gratitude to Prof. M. Casey for agreeing to supervise this thesis and to Prof. Dr. W. Rodi for agreeing to act as a co-supervisor. Both their input and guidance over the course of writing this thesis have been truly invaluable.

I would also like to especially thank Dr. F.R. Menter who supervised the technical work described in this thesis over the course of my employment at ANSYS CFX. Dr. Menter has been a terrific mentor, and a great friend.

As well, I would like to thank Prof. B. Suzen, Prof. G. Huang, Dr S. Völker and Dr. W. Solomon for their insight and numerous thoughtful discussions over the course of the transition model development. I would also like to thank all of my colleagues at ANSYS CFX who have made my time in Germany such a wonderful experience.

Also, I would like to express my gratitude to Frau Euler for all of her help with the administrative tasks associated with submitting this thesis.

Finally, I would like to thank my family and especially Stacie Langtry for all of their love and encouragement.

Financial support for this study was provided by ANSYS CFX, GE Global Research and GE Aircraft Engines and is gratefully acknowledged.

Table of Contents

Nomenclature

AoA	Angle of attack (deg.)
C_p	Pressure coefficient, $p_{oinlet}-p/(0.5\rho U_{ref}^2)$
C_f	Skin friction coefficient, $\tau/(0.5\rho U_{ref}^2)$
FSTI	Freestream turbulence intensity (%), $100(2k/3)^{1/2}/U_{ref}$
k	Turbulent kinetic energy
K	Flow acceleration parameter
L	Axial reference length
P	Local static pressure
$p_{t,inlet}$	Inlet total pressure
$p_{t,outlet}$	Outlet total pressure
$p_{dyn,outlet}$	Outlet dynamic pressure
Re_x	Reynolds number, $\rho L U_{ref}/\mu$
Re_θ	Momentum thickness Reynolds number, $\rho\theta U_0/\mu$
$Re_{\theta t}$	Transition onset momentum thickness Reynolds number (based on freestream conditions), $\rho\theta_t U_0/\mu$
$\tilde{R}e_{\theta t}$	Local transition onset momentum thickness Reynolds number (obtained from a transport equation)
R_T	Viscosity ratio
R_y	Wall-distance based turbulent Reynolds number
R_v	Vorticity Reynolds number
S	Absolute value of strain rate, $(2S_{ij}S_{ij})^{1/2}$
S_{ij}	Strain rate tensor, $0.5(\partial u_i/\partial x_j + \partial u_j/\partial x_i)$
Tu	Turbulence intensity, $100(2k/3)^{1/2}/U$
U	Local velocity
U_o	Local freestream velocity
U_{ref}	Inlet reference velocity
u’	Local fluctuating streamwise velocity
x/C	Axial distance over axial chord
y	Distance to nearest wall
Yp	Loss coefficient, $(p_{t,inlet} - p_{t,outlet})/ p_{dyn,outlet}$
y^+	Distance in wall coordinates, $\rho y\mu_\tau/\mu$
δ	Boundary layer thickness
θ	Momentum thickness
λ_θ	Pressure gradient parameter, $(\rho\theta^2/\mu)(dU/ds)$
μ	Molecular viscosity
μ_t	Eddy viscosity
μ_τ	Friction velocity
ρ	Density
τ	Wall shear stress
Ω	Absolute value of vorticity, $(2\Omega_{ij}\Omega_{ij})^{1/2}$
Ω_{ij}	Vorticity tensor, $0.5(\partial u_i/\partial x_j - \partial u_j/\partial x_i)$
ω	Specific turbulence dissipation rate

Subscripts

t	Transition onset
s	Streamline

Abstract

A new correlation-based transition model has been developed that is based strictly on local variables. As a result, the transition model is compatible with modern CFD techniques such as unstructured grids and massive parallel execution. The model is based on two transport equations, one for intermittency and one for a transition onset criterion in terms of momentum thickness Reynolds number. The proposed transport equations do not attempt to model the physics of the transition process (unlike e.g. turbulence models), but form a framework for the implementation of transition correlations into general-purpose CFD methods. The transition model has been extensively validated for predicting transition in both aerodynamic and turbomachinery flows. An incremental approach was used to validate the model, first on simple flat plate experiments, 2D airfoils/blades and then on progressively more complicated 3D test cases such as a low-aspect ratio compressor, a transonic wing, a full helicopter configuration and an actual wind turbine blade. In all cases good agreement with the available experimental data was observed. The author believes that the current formulation is a significant step forward in engineering transition modeling, as it allows the combination of transition correlations with general purpose CFD codes. There is a strong potential that the model will allow the 1st order effects of transition to be included in everyday industrial CFD simulations.

Kurzfassung

Im Rahmen der vorliegenden Arbeit wurde ein neues Transitionsmodell entwickelt, dass auf empirischen Korrelationen basiert. Durch die Beschränkung auf lokale Variablen in den verwendeten Korrelationen lässt sich dieses Modell innerhalb moderner CFD-Methoden einsetzen, die unstrukturierte Rechengitter und massiv parallele Berechnungsmethoden verwenden. Das Modell basiert auf zwei Transportgleichungen für die Intermittenz und die mit der Impulsverlustdicke gebildete Reynolds-Zahl, welche als Kriterium für das Einsetzen der Transition verwendet wird. Die vorgeschlagenen Transportgleichungen versuchen nicht, die Physik der Transition zu modellieren (entsprechend der Turbulenzmodellierung mit statistischen Turbulenzmodellen) sondern bilden einen Rahmen für die Implementierung empirischer Transitionskorrelationen in universelle CFD-Methoden. Das entwickelte Modell wurde eingehend für die Transition aerodynamischer Strömungen und Strömungen innerhalb von Turbomaschinen validiert. Diese Validierung wurde stufenweise durchgeführt. Am Anfang standen einfache Grenzschichtströmungen und zweidimensionale Tragflügelumströmungen . Im weiteren Verlauf wurde die Validierung auf komplexere Strömungen wie zum Beispiel die Strömungen in einem Kompressor und um einen transsonischen Tragflügel ausgedehnt. Abgeschlossen wurde die Validierung anhand einer kompletten Hubschrauberkonfiguration und einer Tragflügelumströmung eines Windkraftwerks. In allen Fällen konnte eine gute Übereinstimmung mit verfügbaren experimentellen Ergebnissen festgestellt werden. Der Autor ist zuversichtlich, dass die durchgeführten Arbeiten ein wichtiger Beitrag für den Einsatz empirischer Transitionskorrelationen sind, da das entwickelte Modell die Kombination der Transitionskorrelationen mit modernen CFD-Berechnungsverfahren erlaubt. Potenziell besteht damit eine leistungsfähige Methode, um die Vorhersage der maßgeblichen Transitionseffekte in industrielle CFD-Simulationen zu integrieren.

Chapter 1
Introduction

In the past few decades a significant amount of progress has been made in the development of reliable turbulence models that can accurately simulate a wide range of fully turbulent engineering flows. The efforts by different groups have resulted in a spectrum of models that can be used in many different applications, while balancing the accuracy requirements and the computational resources available to a CFD user. However, the important effect of laminar-turbulent transition is not included in the majority of today's engineering CFD simulations. The reason for this is that transition modelling does not offer the same wide spectrum of CFD-compatible model formulations that is currently available for turbulent flows, even though a large body of publications are available on the subject. There are several reasons for this unsatisfactory situation.

The first is that transition occurs through different mechanisms in different applications. In aerodynamic flows, transition is typically the result of a flow instability (Tollmien-Schlichting waves or cross-flow instability), where the resulting exponential growth of two-dimensional waves eventually results in a non-linear break-down to turbulence. This is often referred to as natural transition (Schlichting, 1979). In turbomachinery applications, the main transition mechanism is bypass transition (Morkovin, 1969) imposed on the boundary layer by high levels of turbulence in the freestream. The high freestream turbulence levels are for instance generated by upstream blade rows. Another important transition mechanism is separation-induced transition (Mayle, 1996), where a laminar boundary layer separates under the influence of a pressure gradient and transition develops within the separated shear layer (which may or may not reattach). As well, a turbulent boundary layer can re-laminarize under the influence of a strong favourable pressure gradient (Mayle, 1991). While the importance of transition phenomena for aerodynamic and heat transfer simulations is widely accepted, it is difficult to include all of these effects in a single model.

The second complication arises from the fact that conventional Reynolds averaged Navier-Stokes (RANS) procedures do not lend themselves easily to the description of transitional flows, where both linear and non-linear effects are relevant. RANS averaging eliminates the effects of linear disturbance growth and is therefore difficult to apply to the transition process. While methods based on the stability equations such as the e^n method of Smith & Gamberoni (1956) and van Ingen (1956) avoid this limitation, they are not compatible with general-purpose CFD methods as typically applied in complex geometries. The reason is that these methods require a priori knowledge of the geometry and the grid topology. In addition, they involve numerous non-local operations (e.g. tracking the disturbance growth along each streamline) that are difficult to implement

into today's CFD methods (Stock & Haase, 2000). This is not to argue against the stability approaches, as they are an essential part of the desired "spectrum" of transition models required for the vastly different application areas and accuracy requirements. However, much like in turbulence modelling, it is important to develop engineering models that can be applied in day-to-day operations by design engineers on complicated 3D geometries.

It should be noted that at least for 2D flows, the efforts of various groups has resulted in a number of engineering design tools intended to model transition for very specific applications. The most notable efforts are those of Drela and Giles (1987) who developed the XFOIL code which can be used for modeling transition on 2D airfoils and the MISES code of Youngren and Drela (1991), which is used for modeling transition on 2D turbomachinery blade rows. Both of these codes use a viscous – inviscid coupling approach which allows the classical boundary layer formulation tools to be used. Transition prediction is accomplished using either an e^n method or an empirical correlation. A 3D wing or blade design is performed by stacking the 2D profiles (with the basic assumption that span wise flow is negligible) to create the geometry at which point a 3D CFD analysis is preformed.

Closer inspection shows that hardly any of the current transition models are CFD-compatible. Most formulations suffer from non-local operations that cannot be carried out (with reasonable effort) in general-purpose CFD codes. This is because modern CFD codes use mixed elements and massive parallel execution and do not provide the infrastructure for computing integral boundary layer parameters or allow the integration of quantities along the direction of external streamlines. Even if structured boundary layer grids are used (typically hexahedra), the codes are based on data structures for unstructured meshes. The information on a body-normal grid direction is therefore not easily available. In addition, most industrial CFD simulations are carried out on parallel computers using a domain decomposition methodology. This means in the most general case that boundary layers can be split and computed on different processors, prohibiting any search or integration algorithms. Consequently, the main requirements for a fully CFD-compatible transition model are:

1. Allow the *calibrated* prediction of the onset and the length of transition
2. Allow the inclusion of different transition mechanisms
3. Be formulated locally (no search or line-integration operations)
4. Avoid multiple solutions (same solution for initially laminar or turbulent boundary layer)
5. Do not affect the underlying turbulence model in fully turbulent regimes
6. Allow a robust integration down to the wall with similar convergence as the underlying turbulence model
7. Be formulated independent of the coordinate system
8. Applicable to three-dimensional boundary layers

Considering the main classes of engineering transition models (stability analysis, correlation based models, low-Re models) one finds that none of these methods can meet all of the above requirements.

The only transition models that have historically been compatible with modern CFD methods are the low-Re models (Jones & Launder, 1973, Rodi & Scheuerer 1984). However, they typically suffer from a close interaction with the transition capability and the viscous sublayer modeling and this can prevent an independent calibration of both phenomena (Savill 1993, 1996). At best, the low-Re models can only be expected to simulate bypass transition which is dominated by diffusion effects from the freestream. This is because the standard low-Re models rely exclusively on the ability of the wall damping terms to capture the effects of transition. Realistically, it would be very surprising if these models that were calibrated for viscous sublayer damping could faithfully reproduce the physics of transitional flows. It should be noted that there are several low-Re models where transition prediction was considered specifically during the model calibration (Wilcox, 1994, Langtry & Sjolander, 2002, Walters & Leylek, 2002). However, these model formulations still exhibit a close connection between the sublayer behaviour and the transition calibration. Re-calibration of one functionality also changes the performance of the other. It is therefore not possible to introduce additional experimental information without a substantial re-formulation of the entire model.

The engineering alternative to low-Re transition models are empirical correlations such as those of Abu-Ghannam & Shaw (1980), Mayle (1991) and Suzen et al. (2003). They typically correlate the transition momentum thickness Reynolds number to local freestream conditions such as the turbulence intensity and pressure gradient. These models are relatively easy to calibrate and are often sufficiently accurate to capture the major effects of transition. In addition, correlations can be developed for the different transition mechanisms, ranging from bypass to natural transition as well as crossflow instability or roughness. The main shortcoming of these models lies in their inherently non-local formulation. They typically require information on the integral thickness of the boundary layer and the state of the flow outside the boundary layer. While these models have been used successfully in special-purpose turbomachinery codes, the non-local operations involved with evaluating the boundary layer momentum thickness and determining the freestream conditions have precluded their implementation into general-purpose CFD codes.

Transition simulations based on linear stability analysis such as the e^n method are the lowest closure level available where the actual instability of the flow is simulated. In the simpler models described above, the physics are introduced through the calibration of the model constants. However, even the e^n method is not free from empiricism. This is because the transition n-factor is not universal and depends on the wind tunnel and freestream environment. The main obstacle to the use of the e^n model is that the required infrastructure needed to apply the model is very complicated. The stability analysis is typically based on velocity profiles obtained from highly resolved boundary layer codes that must be coupled to the pressure distribution of a RANS CFD code (Stock and Haase, 2000). The output of the boundary layer method is then transferred to a stability method,

which then provides information back to the turbulence model in the RANS solver. The complexity of this set-up is mainly justified for special applications where the flow is designed to remain close to the stability limit for drag reduction, such as laminar wing design.

Large Eddy Simulation (LES) and Direct Numerical Simulations (DNS) are suitable tools for transition prediction (e.g. Durbin et al. 2002), although the proper specification of the external disturbance level and structure poses substantial challenges. Unfortunately, these methods are far too costly for engineering applications. They are currently used mainly as research tools and substitutes for controlled experiments.

Despite its complexity, transition should not be viewed as outside the range of RANS methods. In many applications, transition is enforced within a narrow area of the flow due to geometric features, pressure gradients and/or flow separation. Even relatively simple models can capture these effects with sufficient engineering accuracy. The challenge to a proper engineering model is therefore mainly in the formulation of a model that can be implemented into a general RANS environment.

In this thesis a novel approach to simulating laminar to turbulent transition is described that can be implemented into a general RANS environment. The central idea behind the new approach is that Van Driest and Blumer's (1963) vorticity Reynolds number concept can be used to provide a link between the transition onset Reynolds number from an empirical correlation and the local boundary layer quantities. As a result the model avoids the need to integrate the boundary layer velocity profile in order to determine the onset of transition. This idea was first proposed by Menter et al. (2002) and is discussed in detail in Chapter 3 of this thesis.

The actual transition model formulation is based on two transport equations. The first is an intermittency equation used to trigger the transition process. The equation is similar to the model given by Menter et al (2002) with numerous enhancements and generalizations. The source terms of the intermittency equation (and thus the transition onset location) are controlled by the vorticity Reynolds number. In addition, a second transport equation was developed in order to avoid the additional non-local operations introduced by the quantities used in the experimental correlations. These correlations are typically based on freestream values such as the turbulence intensity or the pressure gradient outside the boundary layer. The additional transport equation is formulated in terms of the transition onset Reynolds number $Re_{\theta t}$. Outside the boundary layer, the transport variable is forced to follow the value of $Re_{\theta t}$ provided by the empirical correlation. This information is then diffused into the boundary layer by a standard diffusion term. By this mechanism, the strong variations of the turbulence intensity and the pressure gradient in the freestream can be taken into account.

The transition model described in this thesis satisfies all requirements given on page 2, except for the last one – coordinate independence. This is a consequence of the fact that transition correlations are based on non-Galilean invariant parameters such as the turbulence intensity (which is defined based on the local freestream velocity). As

boundary layer transition is always relative to walls, this is only an issue if multiple moving walls exist in a single computational domain.

The proposed transport equations do not attempt to model the physics of the transition process (unlike e.g. turbulence models), but form a framework for the implementation of correlation-based models into general-purpose CFD methods. The physics of the transition process are contained entirely in the empirical correlations provided to the model. The formulation is therefore not limited to one specific transition mechanism, like bypass transition, but can be used for all mechanisms as long as appropriate correlations can be provided. The current correlations used in this thesis have been formulated to cover standard bypass transition as well as flows in low free-stream turbulence environments (i.e. natural transition). There is a strong potential that the model will allow the first order effects of transition to be included in everyday industrial CFD simulations.

In Chapter 2 of this thesis a review of pertinent literature on boundary layer transition mechanisms is discussed. A detailed summary of the different methods that are currently used to predict transition is also included in this chapter. Chapter 3 describes in detail the development of the present transition model and gives an overview of how it has been calibrated. The new transition model has been validated against a large number of diverse and challenging test cases. In this thesis, an incremental approach was used to validate the model, first on simple flat plates, then 2D airfoils and then on to progressively more complicated 3D test cases. Chapter 4 details the results obtained for the ERCOFTAC (European Research Community on Flow Turbulence and Combustion) T3-series of transitional flat plate test cases. The results obtained for a number of 2D aeronautical and turbomachinery test cases are summarized in Chapter 5. Chapter 6 details the results obtained for challenging 3D cases, including a transonic wing, 3D helicopter, low-aspect ratio compressor and a wind turbine. Finally, conclusions and recommendations for future work are discussed in Chapter 7.

Chapter 2
Literature Review

2.1 Introduction

The purpose of this chapter is to review previous research that has been conducted on laminar to turbulent transition in boundary layers. The first section of this chapter will discuss the various modes by which transition is generally believed to occur. The primary modes are often referred to as natural, bypass and separated flow transition. Recently, the unsteady effects of an impinging wake have been found to have a significant effect on the transition process. The impinging wakes usually cause earlier transition and this mode is often referred to as wake induced transition. As well, it has been determined experimentally that if the boundary layer is strongly accelerated it can revert from turbulent flow back to laminar flow. This mode has been classified as reverse transition (Mayle, 1991).

The second section of this chapter will summarize the various methods that have been used to predict transition along with their advantages and disadvantages. The major emphasis will be on evaluating the methods for their suitability towards industrial applications in 3D, unstructured and parallelized CFD codes.

2.2 Transition Modes

2.2.1 Natural Transition

The early research on transition was based on inviscid stability theory, which suggested that all boundary layer flows were only unstable if there was an inflexion point in the velocity profile. It was later predicted physically by Prandtl and then proven mathematically by Tollmien that a laminar boundary layer can be destabilized by the presence of viscous instability waves, often referred to as Tollmien-Schlichting waves. However, the early experiments on transition had too large freestream disturbance levels and these findings were not well accepted until Schubauer and Skramstad (1947) were able to document the existence of Tollmien-Schlichting waves in a quiet wind tunnel.

It is now generally accepted that when the freestream turbulence level is low (<1%, Mayle, 1991) a laminar boundary layer becomes linearly unstable beyond a critical Reynolds number at which Tollmien-Schlichting waves start to grow. The instability is via a subtle mechanism whereby viscosity destabilizes the waves and they begin to grow

very slowly. Because the growth is so slow, transition to turbulence might not be complete until a streamwise distance which can be as large as 20 times farther downstream from the leading edge than the initial starting position of linear instability (Durbin et al., 2002). Orderly transition occurs only after the waves have become nonlinear and inviscid mechanisms have come into play which result in three-dimensional disturbances (Klebanoff et al., 1962). At this point turbulent spots are born (Emmons, 1951). The spots grow in the surrounding laminar layer until they eventually coalesce into a turbulent boundary layer. A schematic of the natural transition process is shown in Figure 2.1.

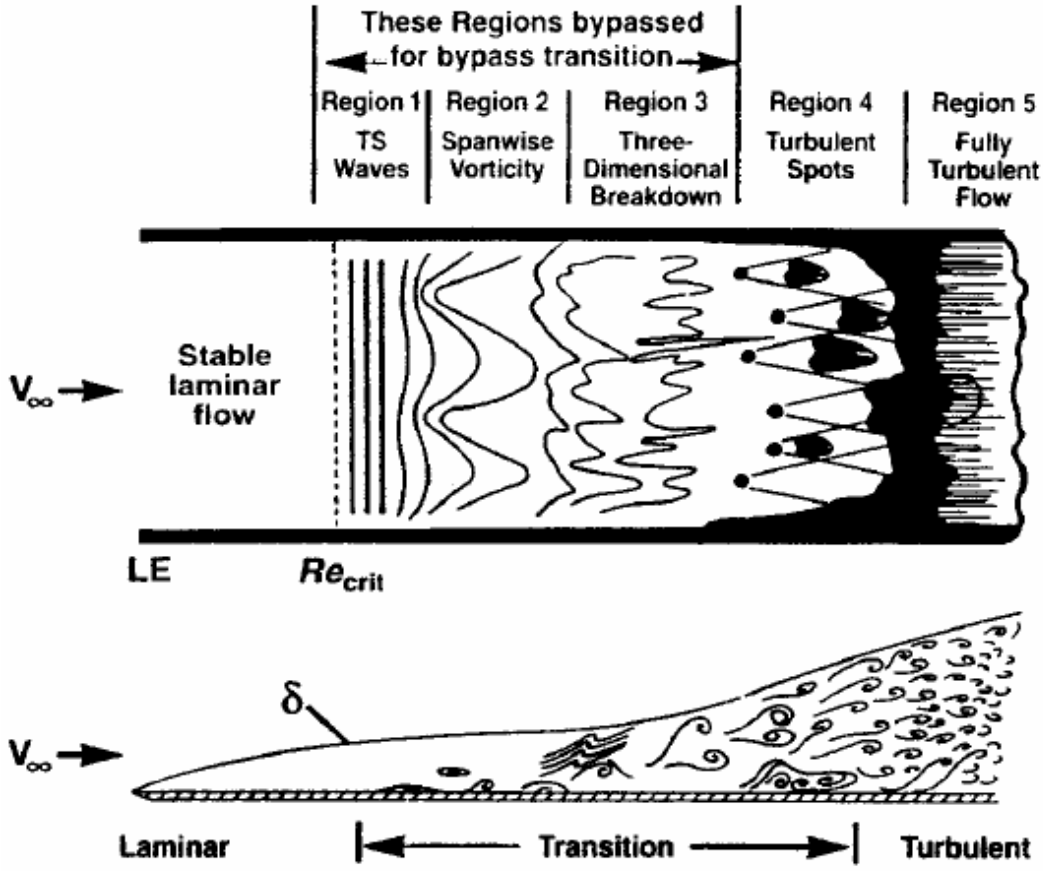

Figure 2.1 The natural transition process (from Schlichting, 1979)

For the case of a swept wing, Tollmien-Schlichting waves are not the only source of disturbances that can cause transition. When large sweep angles are present a 3D boundary layer develops near the wall that has a significant velocity component in the sweep direction. This is typically referred to as cross-flow and it can introduce an inflectional instability into the boundary layer which can cause transition to occur much earlier than would otherwise be the case due to pure Tollmien-Schlichting wave growth (Stock, 2006). At present it is thought that there are two types of cross-flow disturbances: stationary and traveling (Crouch, 1997). The stationary cross-flow instabilities are believed to be excited directly by steady surface roughness and the

traveling cross-flow instabilities require an unsteady source such as mild freestream turbulence to grow (Crouch and Ng, 2000). On an actual swept wing it is believed that all three disturbance sources (i.e. Tollmien-Schliching, stationary and traveling cross-flow disturbances) are present and can even interact with each other if they become large enough.

2.2.2 Bypass Transition

For transition at high freestream turbulence levels (>1%), the first and possibly second and third stages of the natural transition process are bypassed such that turbulent spots are directly produced within the boundary layer by the influence of freestream disturbances (Mayle, 1991). It is often argued that for bypass transition linear stability is irrelevant and to date no one has been able to detect Tollmien-Schlichting waves when the freestream turbulence level was greater than 1 percent (Mayle, 1991). For this reason, a freestream turbulence level of 1% is often taken as the boundary between natural transition and bypass transition. It should be noted that bypass transition can also occur due to surface roughness where the disturbances originate from the perturbations at the wall instead of from the freestream turbulence. As well, bypass transition can also occur when turbulent flow is injected directly into the boundary layer. An example of this type of bypass transition would occur due the cooling holes on a hot turbine blade or stator.

Bypass transition from a practical standpoint is often considered to start when the skin friction deviates from the laminar value. This has been shown to be the location where the first turbulent spots appear (Mayle and Schulz, 1997). As a result, everything that occurs before the spots are formed happens in a laminar boundary layer. However, measurements show that this pre-transitional flow is not steady-state and actually has significantly large levels of velocity fluctuations, often referred to as laminar fluctuations (Mayle and Schulz, 1997). This is illustrated for a flat plate in Figure 2.2, where transition did not start until a Reynolds number of 1.3×10^5.

The growth of the laminar fluctuations is believed to be caused by the pressure fluctuations in the turbulent freestream (Mayle and Schulz, 1997). These pressure waves propagate into the boundary layer and, similar to the Tollmien-Schlichting waves, cause the growth of velocity fluctuations until eventually they are large enough that turbulent spots form. The maximum growth of the laminar fluctuations for a flat plate is shown in Figure 2.3. Interestingly, the growth becomes almost linear once the freestream turbulence level decreases below 1%.

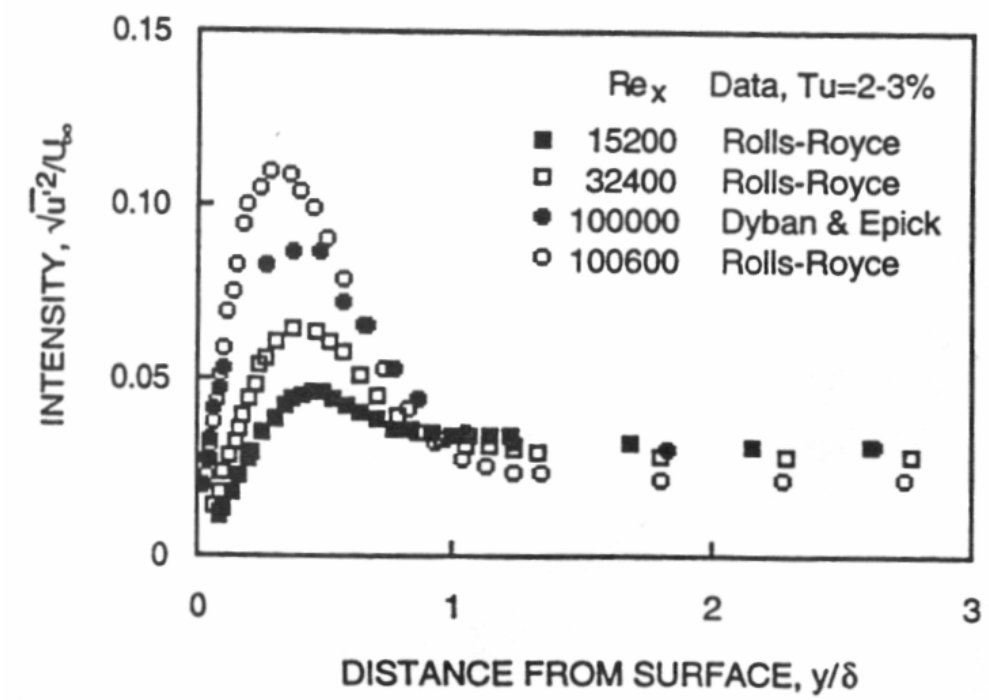

Figure 2.2 Fluctuations in a laminar boundary layer before the onset of transition (reproduced from Mayle and Schulz, 1997).

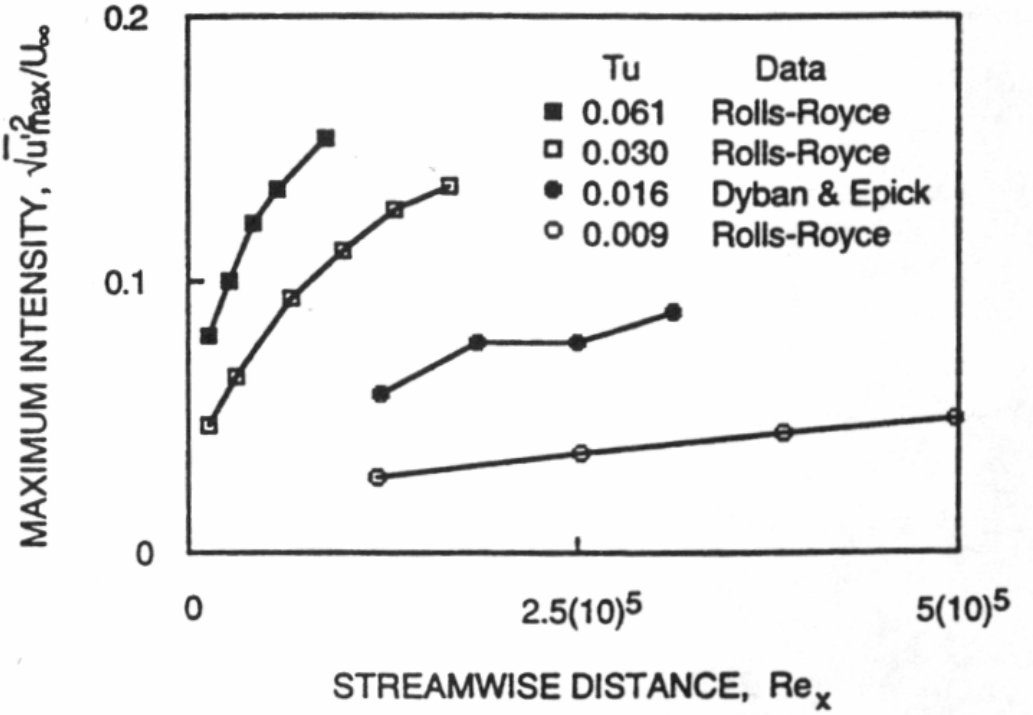

Figure 2.3 Maximum growth of fluctuations in a laminar boundary layer before transition (reproduced from Mayle and Schulz, 1997).

2.2.3 Separated Flow Transition

When a laminar boundary layer separates, transition may occur in the shear layer of the separated flow as a result of the inviscid instability mechanism. In this case, due to the enhanced mixing caused by the turbulent flow, the shear layer may reattach. This reattachment forms a laminar-separation / turbulent-reattachment bubble on the surface (Mayle, 1991). This type of transition can occur behind boundary layer trip wires and as a result of separation due to a strong adverse pressure gradient.

The bubble length depends on the transition process within the shear layer and may involve all of the stages listed for natural transition. Because of this, it is generally accepted that the freestream turbulence level plays a large role in determining the length of the separation bubble. Traditionally, separation bubbles have been classified as long or short based on their effect on the pressure distribution around an airfoil (Mayle, 1991). Short bubbles reattach shortly after separation and only have a local effect on the pressure distribution. Long bubbles can completely alter the pressure distribution around an airfoil (see Figure 2.4). Since long bubbles produce large losses and large deviations in exit flow angles, they should be avoided (Mayle, 1991). Short bubbles on the other hand, can be used to trip the boundary layer and thus allow larger adverse pressure gradients downstream of the reattachment point. One of the major challenges lies in determining whether or not a separation bubble will be long or short. This is aggravated by the fact that small changes in either Reynolds number or angle of attack of an airfoil can cause a

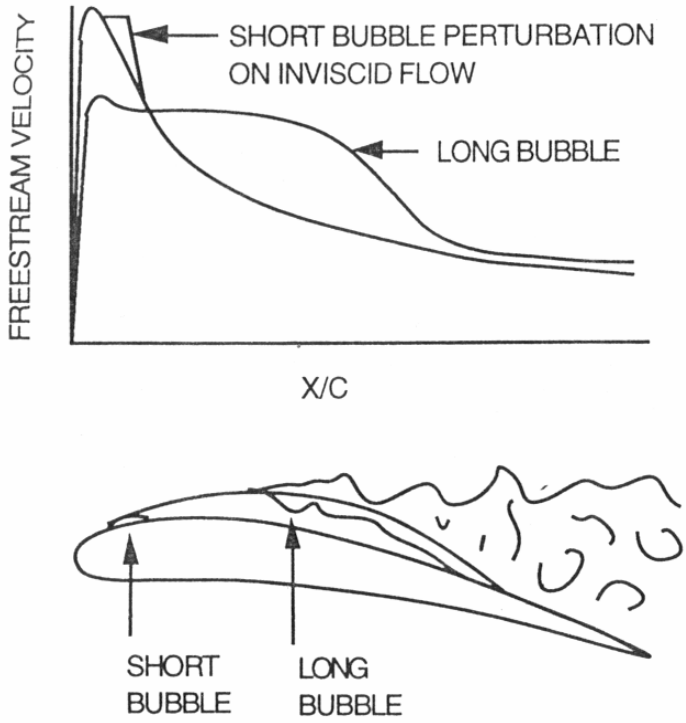

Figure 2.4 Separation bubble effects on suction side velocity distribution (reproduced from Malkiel and Mayle, 1996).

bubble to change dramatically from short to long (Mayle and Schulz, 1997). The sudden change in bubble length is often referred to as bursting. It can result in a dramatic loss of lift and could even cause the airfoil to stall if the bubble fails to reattach.

Separation induced transition can also occur around the leading edge of an airfoil if the leading edge radius is small enough. The size of the leading edge separation bubble is a strong function of the freestream turbulence intensity, the leading edge geometry, the angle of attack and to a lesser extent the Reynolds number (Walraevens and Cumpsty, 1995). Tain and Cumpsty (2000) found that the size of the leading edge bubble had a profound effect on the downstream boundary layer. They concluded that the larger the leading edge separation, the thicker the downstream boundary layer and thus the more likely it would separate due to an adverse pressure gradient. Consequently, compressor blade losses at off design conditions are thought to be strongly influenced by separation induced transition near the leading edge.

A schematic of a transitional separation bubble is shown in Figure 2.5. The forward portion of the bubble is a constant pressure region. It is comprised of a laminar shear layer that is inherently unstable due to the inflection point in the velocity profile and the large distance away from the region where the presence of the wall damps the velocity fluctuations. The inflection point promotes the growth of disturbances which eventually break down into turbulence at the location marked X_t. The transition process is usually complete before the shear layer reattaches.

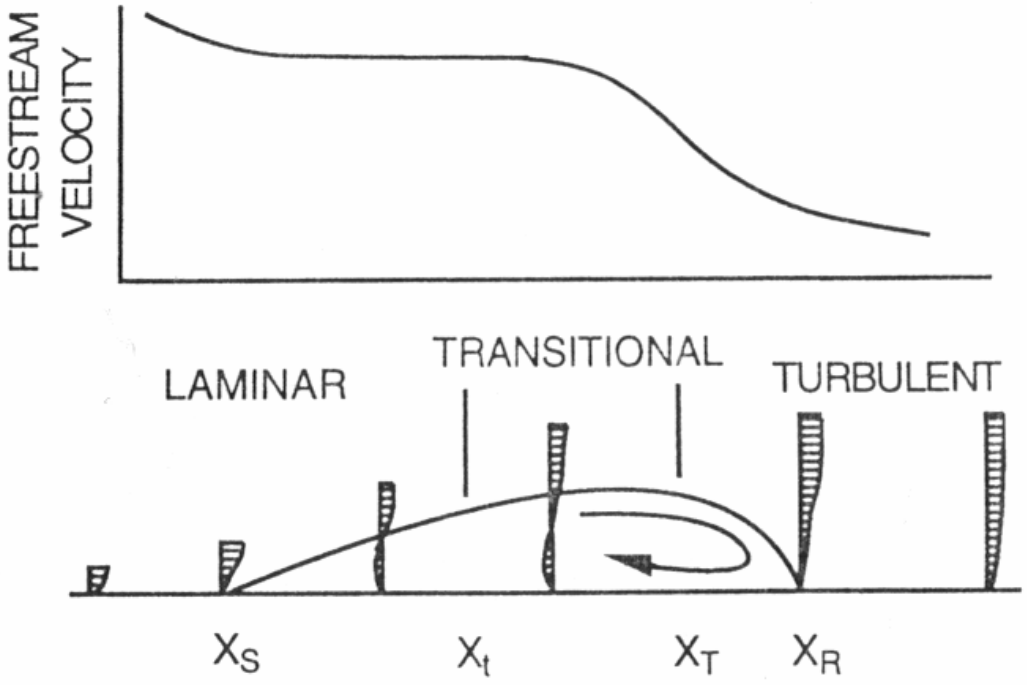

Figure 2.5 Velocity distribution over a separation bubble (reproduced from Malkiel Mayle, 1996).

2.2.4 Wake Induced Transition

One very important instance of bypass transition arises in turbomachinery flows where the blade rows are subjected to periodically passing turbulent wakes. It has been found experimentally that the wakes are so disruptive to the laminar boundary layer that turbulent spots often form in the location where the wake impinges on the surface. From the available literature it is not clear whether the transition is caused by the enhanced turbulence in the wake or the freestream momentum deficit and its interaction with the boundary layer. It is for this reason that this mode of transition is usually differentiated from bypass transition and is often referred to as wake induced transition.

If one subtracts the unsteady velocity field from the time average value to obtain a relative velocity field, the wake can be visualized as a negative jet that impinges on the surface (Durbin et al, 2002). This results in a backwards jet which is strongly destabilizing due to the inviscid instability mode. Shortly after the wake passes the flow breaks down and a turbulent spot is formed. A DNS computation illustrating this phenomena is shown in Figure 2.6.

In between the wakes transition can occur via any of the other possible modes and this has been detected experimentally (Mayle, 1991). As the wake passes, the boundary layer will slowly relax from turbulent flow to laminar flow. This region is often referred to as the calmed region and was first reported by Dong and Cumpsty (1990). The calmed region has a full velocity profile which is very stable and does not separate in adverse pressure gradients as easily as a laminar profile. Howell et al. (2001) have argued that it was this ability to withstand adverse pressure gradients that allowed the spots to keep the flow from separating.

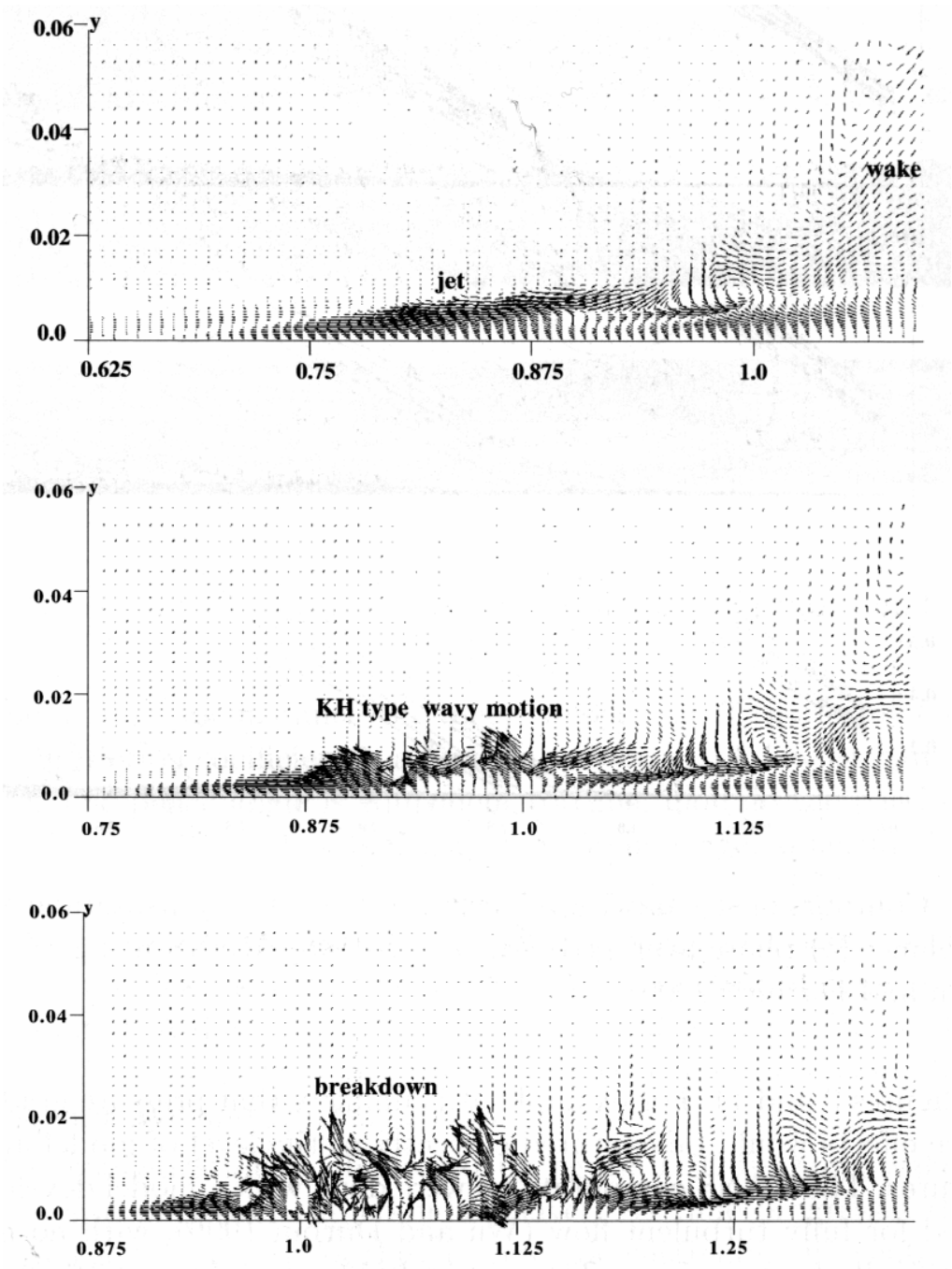

Figure 2.6 DNS simulation of the development of a backward jet in the relative velocity field and its breakdown to turbulence (reproduced from Durbin et al., 2002).

A space-time (ST) diagram can be very useful for illustrating the unsteady-state transition process because it places the variations of boundary layer skin friction in time and space on a single diagram. Halstead et al. (1997) were the first to use a space time diagram and to identify the calmed region. An idealized example of an ST diagram for a low-pressure turbine blade is show in Figure 2.7. The y-axis shows multiples of wake passing periods, the x-axis indicates the position along the airfoil chord and the colour flood shows the surface skin friction. Transitional flows caused by wakes are labeled W, turbulent flow caused by separated flow transition is marked T, and calmed flow is marked C. The diagram illustrates two cases of wake induced transition each one with a different wake-passing frequency. At the lower wake-passing frequency (Figure 2.7a), the flow at the trailing edge of the blade is turbulent because of the wakes, then calmed and then turbulent again due to separated flow transition. If the time between wake-passing periods is sufficiently short (Figure 2.7b) then the separation bubble will not have time to reestablish itself and thus the losses associated with the bubble will be diminished (Howell et al., 2001).

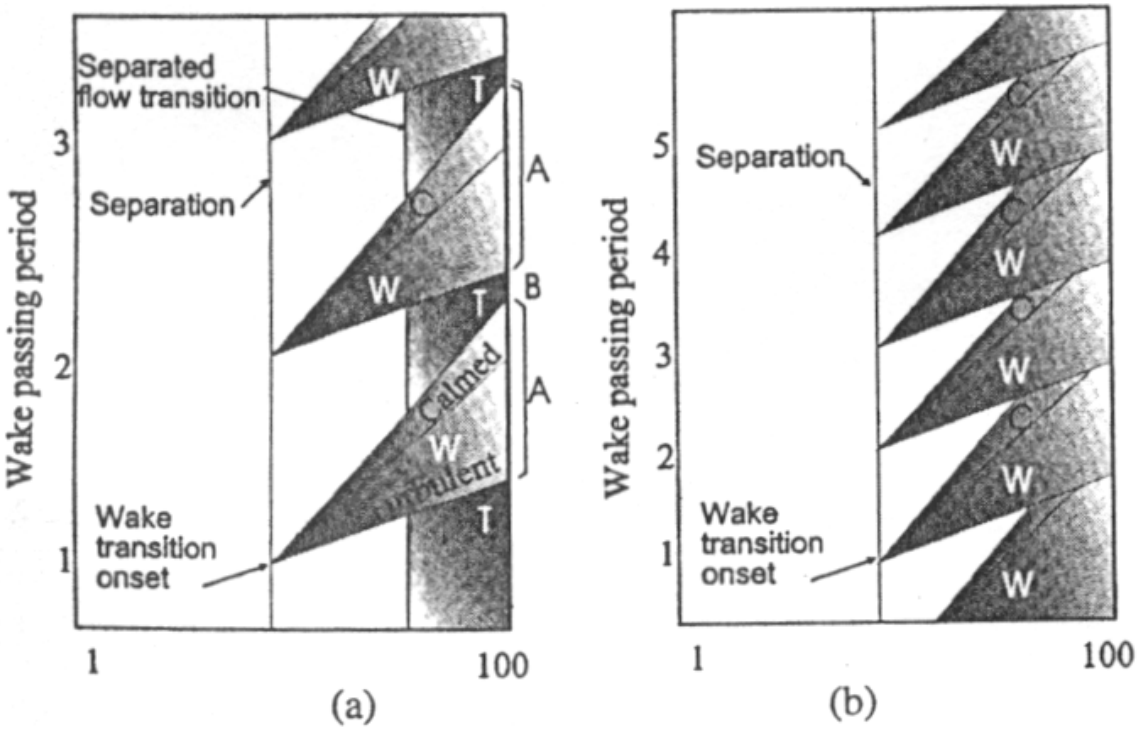

Figure 2.7 Idealized ST diagram of wake-induced transition showing two different wake passing frequencies (reproduced from Howell et al., 2001).

2.2.5 Reverse Transition

Transition from turbulent to laminar flow is possible if the flow is strongly accelerated. This is often referred to as either "reverse" transition or "relaminarization". The acceleration on the trailing edge pressure side of most airfoils and on the leading edge suction side of most turbines is large enough to cause reverse transition (Mayle, 1991). There is not a lot of experimental data on reverse transition but it is known to occur when

the acceleration parameter, $K = \upsilon/U^2(dU/dx)$, is greater than about 3×10^{-6} (Mayle, 1991). In addition, it is possible for a relaminarized boundary layer to transition back to turbulent flow if the acceleration becomes small enough (i.e. $K < 3\times10^{-6}$). An example of relaminarisation and then retransition once the acceleration diminishes is shown in Figure 2.8.

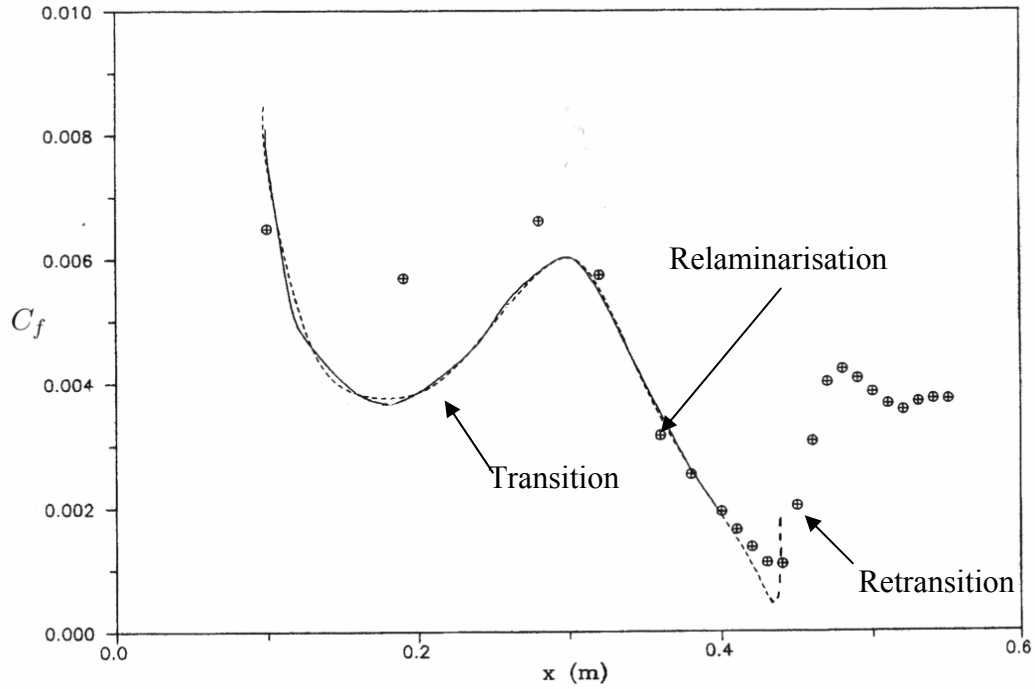

Figure 2.8 Relaminarisation and retransition on a flat plate with a freestream turbulence level of 0.1% (reproduced from Savill, 2002).

2.3 Transition Prediction

The following sections will summarize the various methods that have been used to predict transition along with their advantages and disadvantages. The major emphasis will be on evaluating the various methods for their suitability towards industrial design calculations in 3D, unstructured and parallelized CFD codes.

2.3.1 Direct Numerical Simulation and Large Eddy Simulation

In principle, laminar flow break down, the development of turbulent spots and transition to fully turbulent flow can be simulated very accurately using DNS (Zheng et al., 1998). A DNS computation is performed by solving the full unsteady-state Navier-Stokes equations. Since there is no Reynolds averaging there is no requirement for turbulence closure by a turbulence model. In order to capture the small scales of turbulence a DNS computation requires an extremely fine grid. A DNS of transition on a flatplate is shown in Figures 2.9 and 2.10. The skin friction, velocity profiles and the laminar fluctuations (e.g. Figure 2.11, $Re_\theta = 177$) that eventually become turbulence are predicted very well. This simulation had approximately 50 million grid points and was performed in about four weeks on a supercomputer with 64 processors.

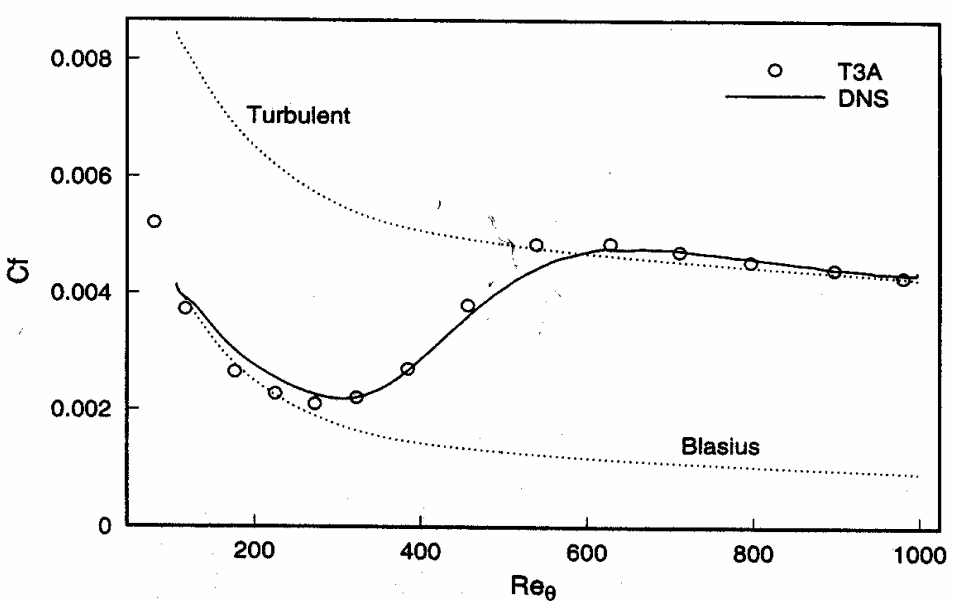

Figure 2.9 Direct Numerical Simulation of transition on a flatplate (reproduced from Durbin et al., 2002)

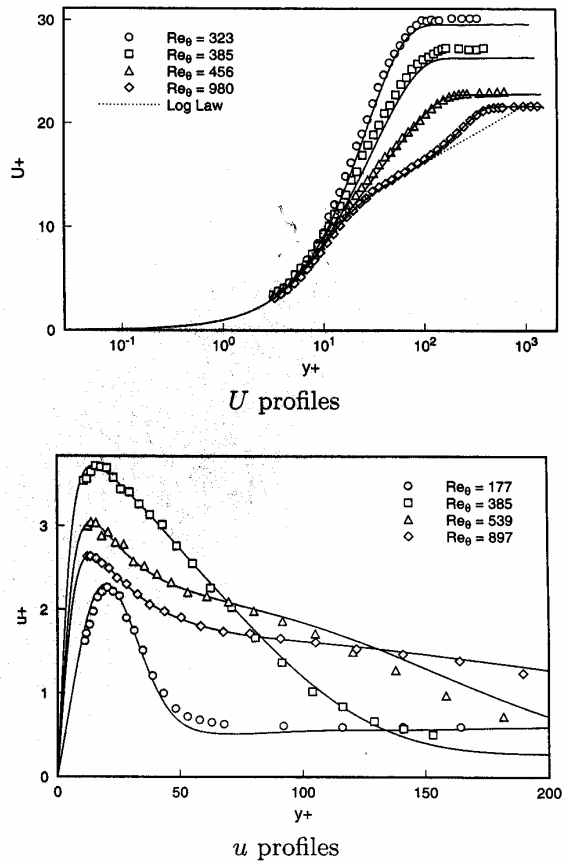

Figure 2.10 DNS (solid lines) and experimental (symbols) profiles of mean (U) and fluctuating (u) velocities at various streamwise locations for the T3A test case (reproduced from Durbin et al., 2002).

With the increasing speed of modern and cost effective CPU's and the advent of cluster computing DNS computations have moved beyond simple flat plates and it is now possible to perform a DNS of a 2D low-pressure turbine blade at Reynolds numbers up to 1.5×10^5 (Wu and Durbin, 2001). This is illustrated in Figure 2.11 for a turbine blade without and with upstream impinging wakes. The wakes cause wake-induced transition and a turbulent spot can be seen in the DNS computation convecting downstream on the suction side of the blade.

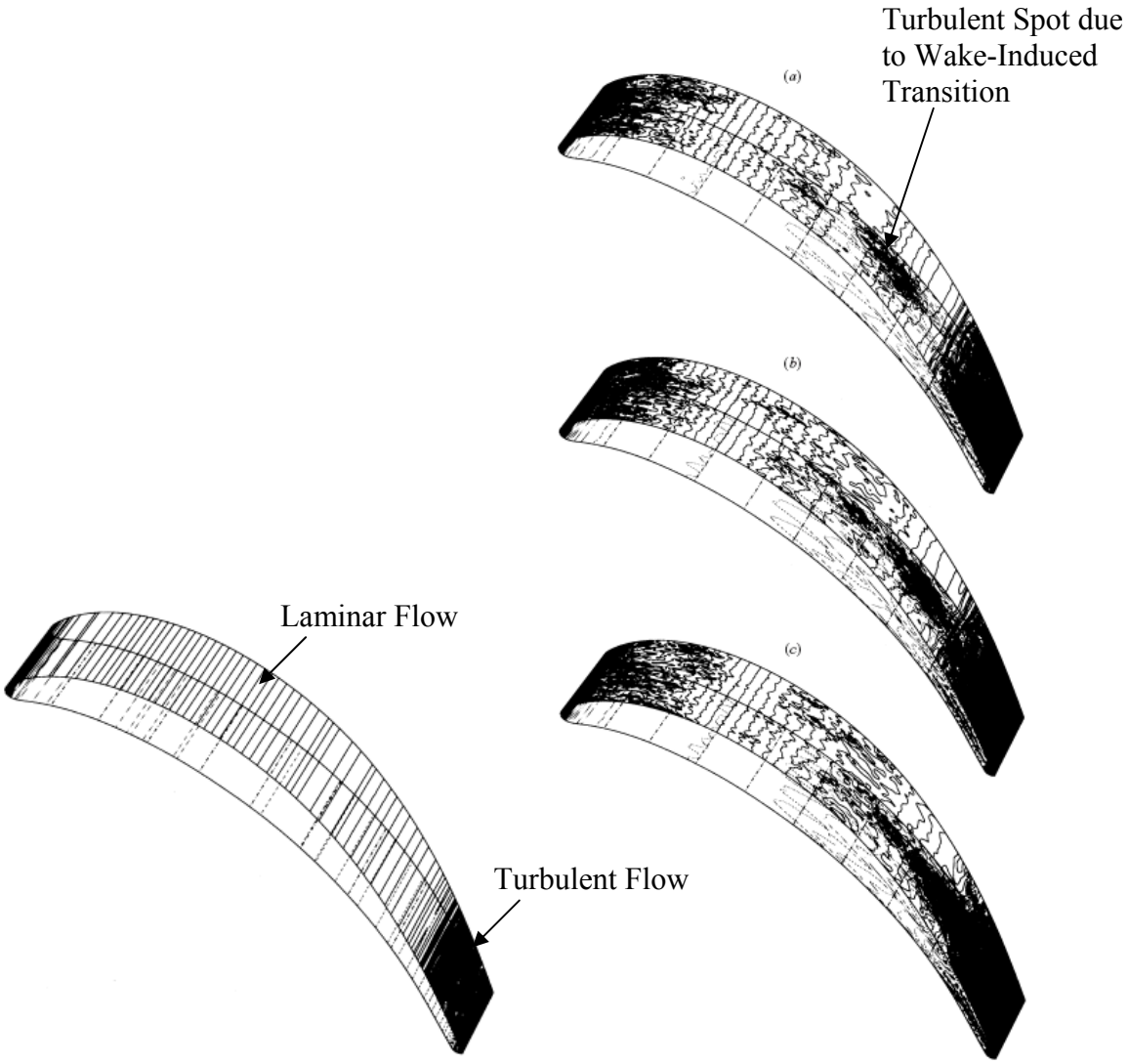

Figure 2.11 DNS computation of a turbine blade without (left) and with upstream impinging wakes at three different wake positions (right). Contour lines of wall normal velocity where straight lines (i.e. zero normal velocity hence parallel flow) indicate laminar flow and dark regions represent turbulent flow. Reproduced from Wu and Durbine (2001).

Due to the extraordinary large computational requirements, DNS is clearly not yet at the stage where it can serve as a practical tool for engineering design applications. This will be the case for a long time as additional computing resources in industry are usually used to simulate larger and more complicated geometry, not for improved modeling. The strength of DNS lies in the wealth of full-field instantaneous and ensemble averaged data that is provided as well as the ability to prescribe precise inflow conditions (Durbin et al., 2002). DNS databases are quickly becoming an invaluable tool for developing and testing turbulence models as well as improving our understanding of fluid dynamics. However, it will be a very long time before DNS itself can replace turbulence and transition modelling.

Because of the significant computational costs associated with DNS, a number of researchers have applied the concept of Large Eddy Simulation (LES) to transitional flows. In LES computations only the large scale eddies are resolved, the small scale eddies are modeled using an eddy viscosity approach such as that proposed by Smagorinsky (1963). One of the main problems with LES is that the predicted transition location is very sensitive to the choice of Smagorinsky constant that is used to calibrate the subgrid eddy viscosity (Germano et al. 1991). Germano et al. (1991) have since proposed the dynamic subgrid-scale model which computes the Smagorinsky constant locally. The dynamic model has the advantage that in laminar boundary layers the subgrid eddy viscosity is automatically reduced to zero. Consequently, it is believed that this model should be more appropriate for predicting transitional flows. The time development of the plane-averaged wall shear stress for a transitional channel flow computed with DNS, LES and the Dynamic LES model is shown in Figure 2.12 where the Dynamic LES model appears to be in good agreement with DNS results.

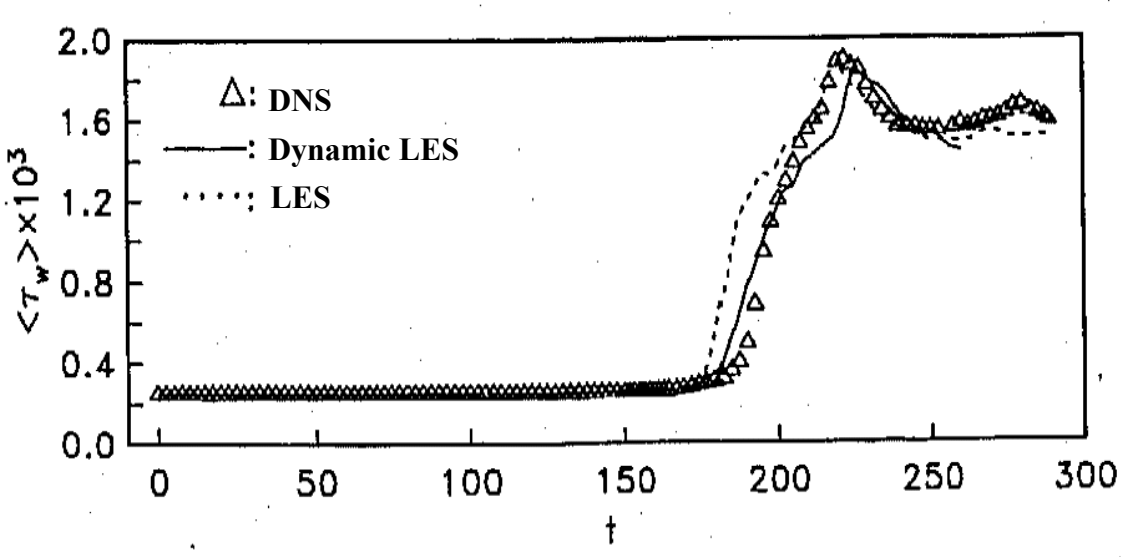

Figure 2.12 Time (t) development of the plane-averaged wall shear stress (τ_w) for a transitional channel flow. Reproduced from Germano et al. (1991).

Nevertheless, the Dynamic LES model is not a complete solution to the issues associated with applying LES to predict transitional flows. LES computations performed by

Michelassi et al. (2003) on a low-pressure turbine blade with periodically impinging wakes have indicated that while the Dynamic LES model was in good qualitative agreement with DNS results, noticeable differences were observed in the quantitative comparison. This is illustrated in Figure 2.13 where the time-averaged skin friction from a DNS is compared to that of an LES. The LES results predict transition too far downstream by about 10% chord.

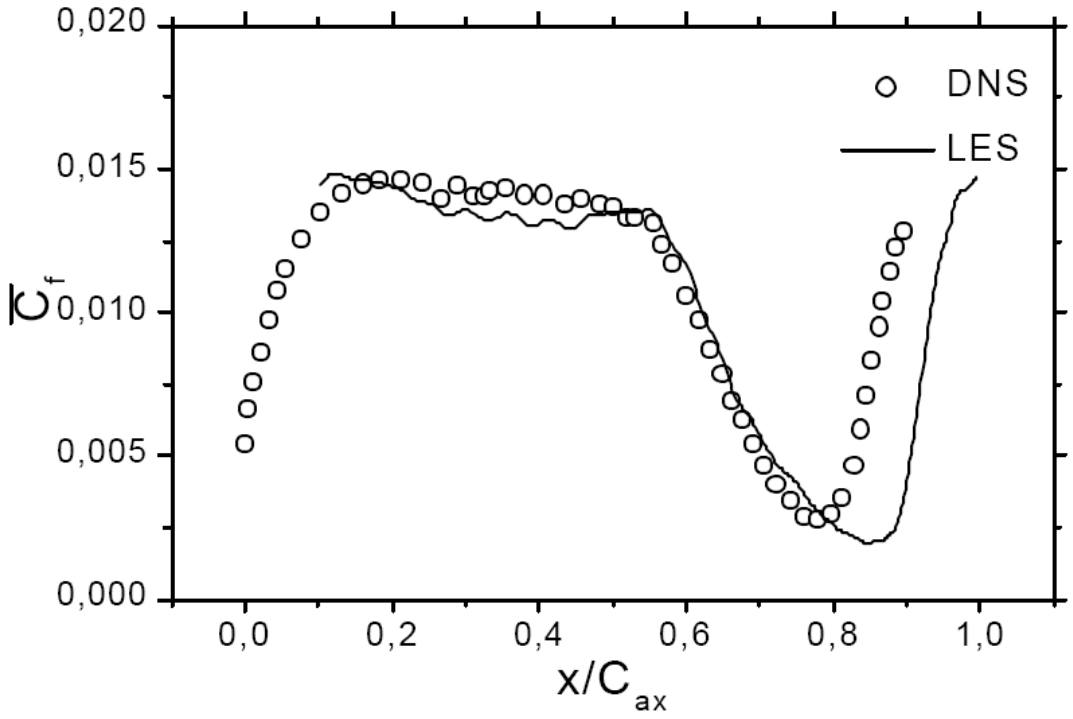

Figure 2.13 Time averaged skin friction (Cf ×10) on the suction side of a low-pressure turbine blade subjected to periodic impinging wakes for the DNS results of Wu and Durbin (2001) and the LES results of Michelassi et al. (2003). Reproduced from Michelassi et al. (2003).

2.3.2 e^n Method and Parabolized Stability Equations for Predicting Onset

One of the more widely used methods for predicting transition is the so-called e^n method. For predicting natural transition on airfoils, this approach is considered the state of the art by the aircraft industry This method is based on the local linear stability theory and the parallel flow assumption in order to calculate the growth of disturbance amplitudes from the boundary layer neutral point to the transition location (Smith and Gamberoni, 1956 and van Ingen, 1956). It requires three successive steps: The first step consists of the calculation of the laminar velocity and temperature profiles along the body of interest. In the second step, the local growth rates of the unstable waves are computed for each of these profiles. This can be accomplished by solving either the local stability equations or

the Parabolized Stability Equations (PSE). In the third step, the local growth rates are integrated along each streamline in order to determine the *n* factor. Once the disturbance amplitude ratio (e^n) exceeds the limiting *n* factor transition is assumed to start.

The major problem with the e^n method is that the *n* factor does not represent the amplitude of a disturbance in the boundary layer but rather the amplification factor from an initial unknown amplitude (Warren and Hassan, 1997). The initial amplitude of the disturbance in the boundary layer is related to the external disturbance environment through a generally unknown receptivity process. For this reason the *n* factor at the onset of transition is not universal and must be determined by calibration to wind tunnel or flight tests. Hence the e^n approach is considered a semi-empirical method. Typical values for *n* can vary from 7 to 9.

For isolated airfoils the e^n method has been shown to produce very good transition predictions compared to wind tunnel measurements (Stock and Haase, 2000). Figure 2.14 details the measured transition onset location for a wind turbine airfoil and the position predicted by the e^n method (assuming a transition *n* factor of 9) for various angles of attack. For this case the e^n method is in very good agreement with the experimental data.

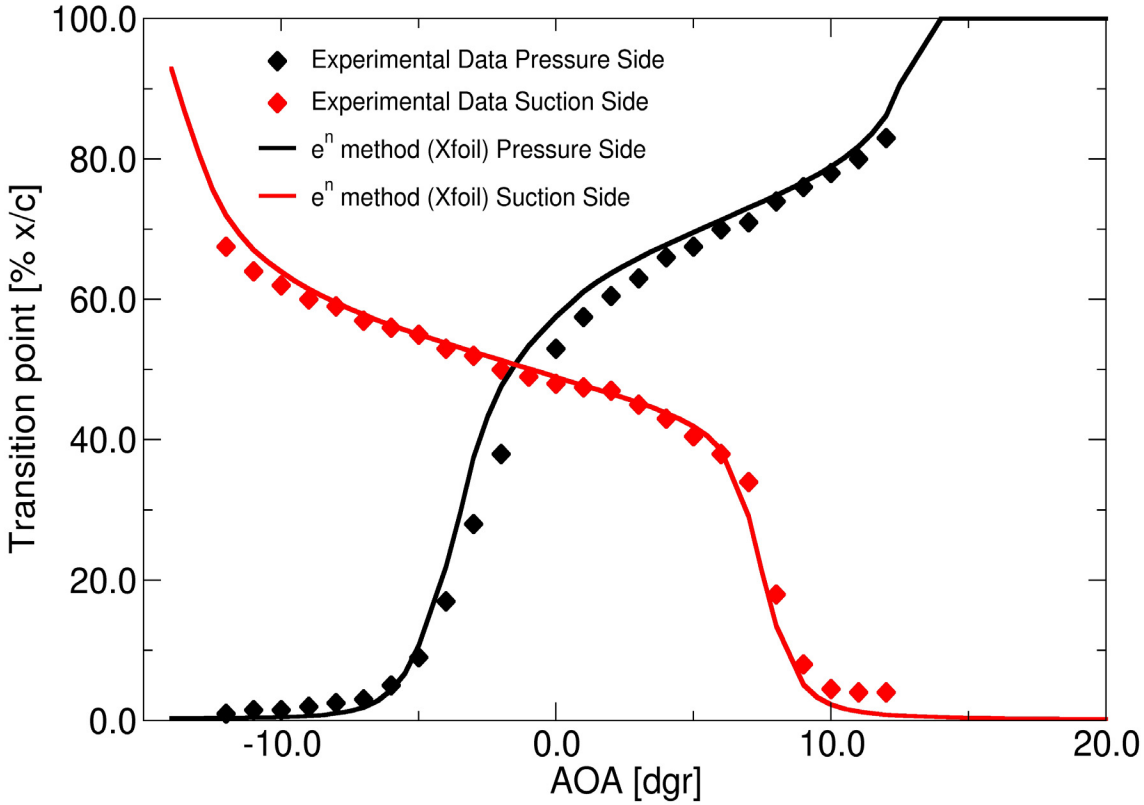

Figure 2.14 Experimentally measured transition onset location for a wind turbine airfoil and the position predicted by the e^n method (using the airfoil design code Xfoil) for various angles of attack.

Another major problem with the e^n method occurs for separated flow transition where the onset of transition causes the boundary layer to reattach. In this case, often the purely laminar solution is massively separated and exhibits unsteady vortex shedding (Zheng et al., 1998). Since the steady-state solution is not available, the local growth rates cannot be computed using the local stability equations or PSE and the e^n method is inappropriate for predicting these types of flows.

As well, the e^n method can only be used to predict the onset of transition; it can not be used to predict the subsequent transitional region. For this reason there is now growing interest in approaches that solve the non-linear Parabolized Stability Equations (PSE) because the development of the unstable waves up to the weakly non-linear regime can be simulated (Savill, 2002). An example of this is shown in Figure 2.15. However, this approach is still not appropriate for solving problems with separation induced transition.

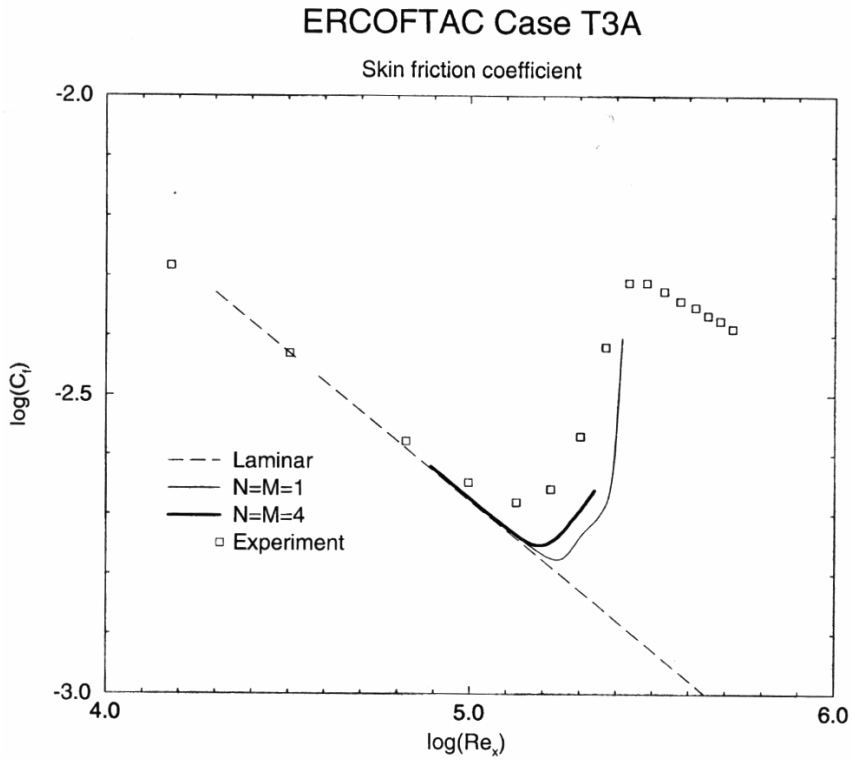

Figure 2.15 PSE predictions of skin friction (Cf) versus experimental data for a freestream turbulence of 3% (reproduced from Savill, 2002).

Finally, there remain some formidable barriers towards applying the e^n method to general aerospace applications. The first is that since the e^n method is based on linear stability theory it cannot predict transition due to non-linear effects such as bypass or surface roughness induced transition. As well, while the grids and subsequent CFD solutions obtained from typical industrial Navier-Stokes solvers can accurately compute both laminar and turbulent skin friction, the solutions are not accurate enough to evaluate the stability equations. As a result, the Navier-Stokes solution must be coupled to an accurate boundary layer code (Stock and Haase, 2000). Finally, the need to track the growth of the disturbance amplitude ratio along the streamline results in a significant

issue for 3D flows where the streamline direction is not aligned with the grid. Because of this limitation, the present author is not aware of any published instance were the e^n method has been successfully applied to predict transition on a complex configuration such as a full 3-dimensional aircraft configuration. For all of these reasons methods based on linear stability are not favoured as a means for general prediction of transition.

2.3.3 Empirical Correlations for Transition Onset

One of the most common ways of predicting the boundary layer transition onset location in industrial CFD codes (particularly in turbomachinery codes) is to employ empirical correlations. The empirical correlations usually relate the freestream turbulence intensity (Tu) to the transition Reynolds number based on the momentum thickness Reynolds number ($Re_{\theta t}$). A typical example is the Mayle (1991) correlation which is shown in Figure 2.16. This correlation is based on fairly recent high-quality experimental data for transition onset. Another popular correlation is that of Abu-Ghannam and Shaw (1980). This correlation is shown in Figure 2.17. It is based on older data but it can account for the effect of pressure gradient on the transition onset location. Empirical correlations are also attractive because they have been used with great success for many years now (particularly in design codes such as MISES) and give consistent results even when used in 3D structured Navier-Stokes codes.

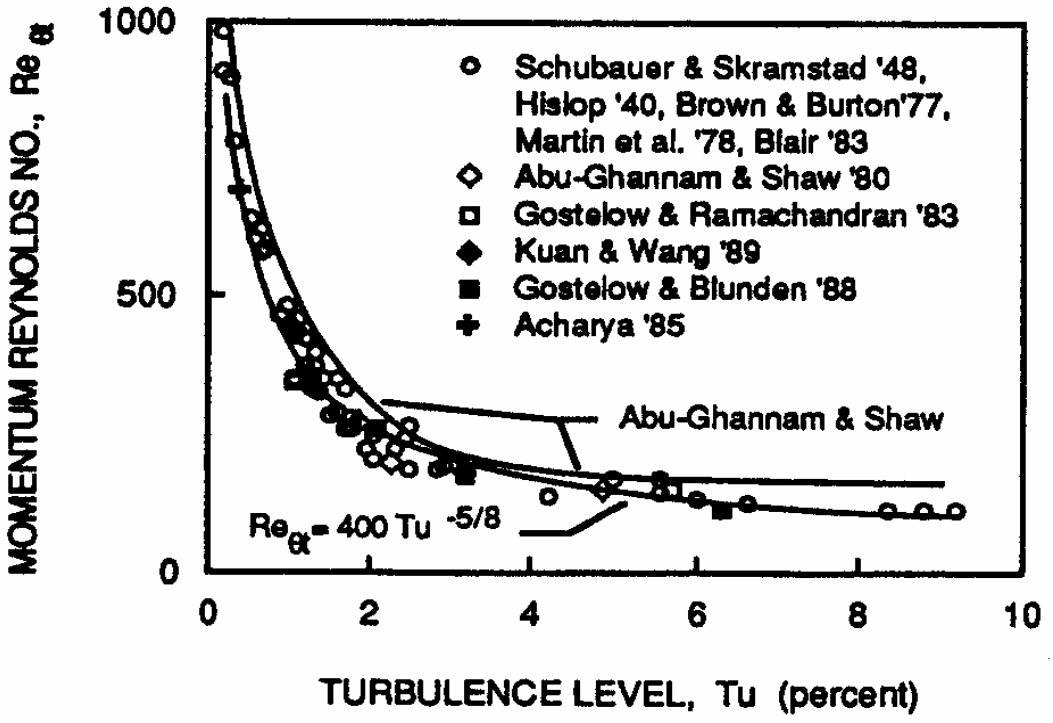

Figure 2.16 The Mayle (1991) correlation for transition momentum thickness Reynolds number (reproduced from Mayle, 1991).

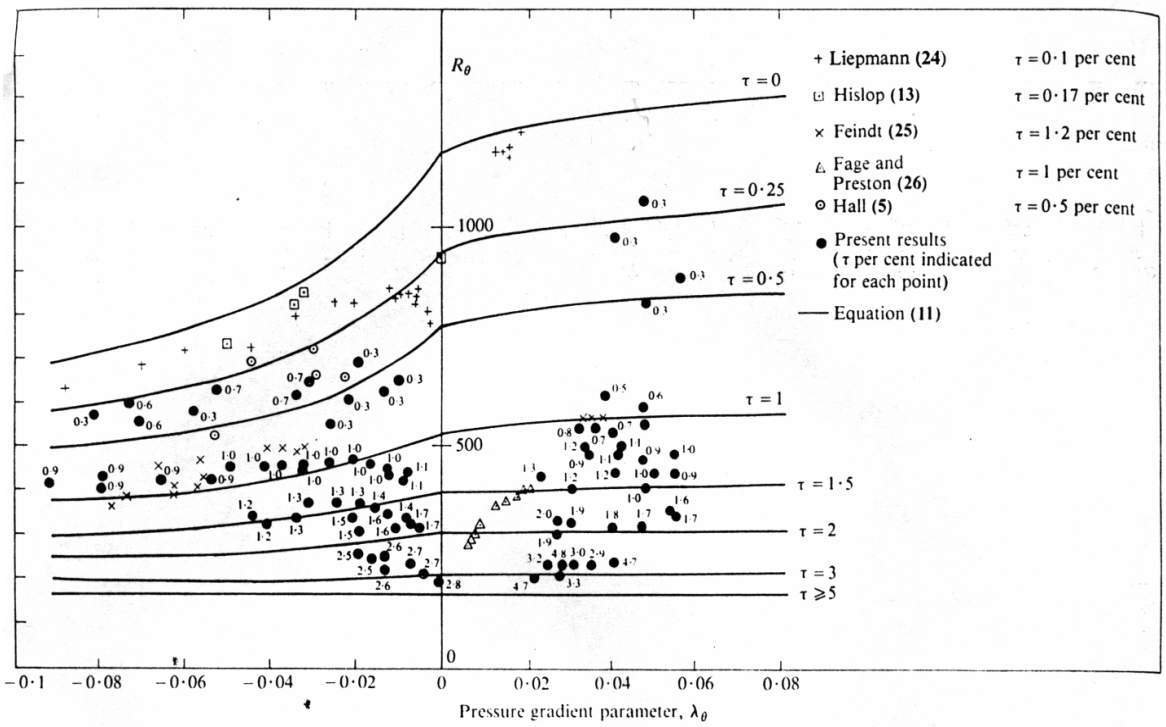

Figure 2.17 The correlation of Abu-Ghannam and Shaw (1980) (reproduced from Abu-Ghannam and Shaw, 1980).

In order to employ an empirical correlation for transition onset the laminar solution around the body of interest must first be calculated. After this has been accomplished the boundary layer quantities are integrated to obtain the momentum thickness Reynolds number (Re_θ) along every point on the body. Transition onset is then assumed to occur at the position where the local value of the momentum thickness Reynolds number exceeds that predicted by the correlation. Once the starting location of transition has been determined a turbulence model is turned on and the subsequent flow development is calculated. Although only as reliable as the underlying correlations, this approach can give fairly satisfactory results. It should also be noted that correlations can also be found not only for the onset location of transition, but also for the length of transition (e.g. Abu Ghannam and Shaw, 1980). There are various ways to interface transition length correlations with a turbulence model. The most common approach is to use the concept of intermittency to slowly ramp up the turbulence production instead of simply switching on the turbulence model. Intermittency methods are discussed in more detail in section 2.3.4.

Cho et al. (1993) used the correlation of Abu Ghannam and Shaw (1980) coupled with a two-layer low-Reynolds number turbulence model in order to predict unsteady blade-wake interactions on a turbine blade. They adapted this correlation for unsteady flows by using a Lagrangian approach and following fluid parcels in the boundary layer under

disturbed and undisturbed free streams. In this work, the empirical correlation was used to modify one of the turbulence model viscous damping functions in order to predict a smooth transition zone. In a similar approach, Eulitz and Engel (1998) used an empirical correlation proposed by Drela (1995) and coupled this to the one-equation Spalart-Allmaras turbulence model. This model was subsequently implemented in the DLR TRACE CFD code (Nuernberger and Greza, 2002), which is used in many different industrial applications. The pressure distribution on a low-pressure turbine undergoing separation-induced transition predicted by Nuernberger and Greza (2002) is shown in Figure 2.18. Finally, Schiele (1999) proposed new empirical correlations for transition onset and investigated a number of different turbulence model/empirical correlation coupling strategies. Schiele (1999) also performed an extensive validation of these approaches on a large number of test cases including flat plates under the influence of different turbulence intensities and pressure gradients as well as three different turbine blade geometries under the influence of different freestream turbulence levels and Reynolds numbers. In most cases relatively good agreement with the experimental measurements was obtained.

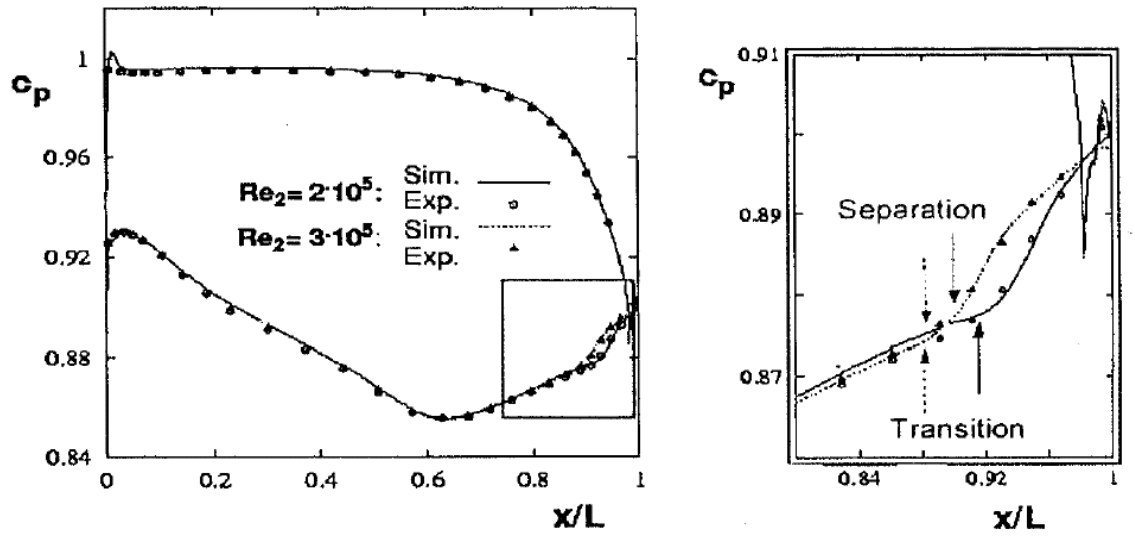

Figure 2.18 Predicted and measured pressure coefficient (Cp) distribution on a low-pressure turbine blade for two different Reynolds numbers using an empirical correlation coupled to a one-equation turbulence model. Reproduced from Nuernberger and Greza (2002).

While the empirical correlation method proves sufficiently accurate, it poses numerical and programming challenges in Navier-Stokes codes. As mentioned previously, for classical correlation based transition models, it is necessary to compare the actual momentum-thickness Reynolds number (Re_θ) to the transition value from the correlation, $Re_{\theta t}$. This is not an easy task in a Navier-Stokes environment because the boundary layer edge is not well defined and the integration will therefore depend on the implementation of a search algorithm. All of the previously mentioned examples were based on structured CFD codes and had some substantial search algorithms implemented for

integrating the boundary layers and tracking the location where the onset criteria was satisfied. The difficulties associated with non-local formulations are exaggerated by modern CFD methods that are based on unstructured grids and massive parallel execution. Unstructured grids do not easily provide the infrastructure needed to integrate global boundary layer parameters because the grid lines normal to the surface cannot be easily identified. In the case of a general parallelised CFD code, the boundary layer can be split between different CPU domains making the integration impossible to perform in parallel. The use of correlation-based transition criteria is therefore incompatible with modern CFD codes. As a result, one has to either abandon the correlation based transition methods, or to develop correlation-based transition models, which use only local information.

Finally, the current correlation-based methods are inherently two-dimensional. Important effects like end-wall boundary layers or leakage flows cannot be included. On the other hand, the correlation-based methods are very attractive, as they allow the inclusion of experimental evidence and additional parameters that are believed to affect transition (e.g. surface roughness, freestream length scale, etc). As a result of this, the accuracy of the empirical correlations will improve as better experimental data on transition becomes available and for these reasons empirical correlations are still a very promising method for predicting transition.

2.3.4 Intermittency Models for Predicting the Transition Length

As mentioned earlier, Emmons (1951) first characterized transition as an eruption of turbulent spots. Since then, subsequent studies have investigated the intermittent behaviour of the flow across the transitional region as the turbulent spots convect downstream in the boundary layer. This has led to the concept of "intermittency" which is a measure of the probability that a given point is located inside the turbulent region. Based on this idea Dhawan and Narasimha (1958) developed an algebraic function that described the streamwise evolution of the intermittency factor. Over the years there have been many intermittency models that have been proposed. They can be categorized into two main approaches: Algebraic (prescribed) intermittency or transport equations for intermittency. Whenever an intermittency model is used, the transition onset location must be obtained from another model (usually an empirical correlation).

The algebraic or prescribed intermittency models appear to be widely used in the structured-grid CFD codes when the transition length is believed to be important. The transition onset location is usually based on an empirical correlation of which the most common is that of Abu-Ghannam and Shaw (1980). The algebraic intermittency is usually implemented by multiplying the eddy viscosity of a turbulence model by the value of intermittency. Upstream of transition the intermittency is zero and as a result the eddy viscosity is zero and a laminar boundary layer develops. Once the transition onset occurs, the intermittency is slowly ramped up from zero to one until the fully turbulent boundary is achieved. There are many algebraic models for intermittency and these are usually based on experiments where properties like the spot spreading rate have been measured (see for example Gostelow et al., 1994). Another approach proposed by Sieger

et al. (1995) is to base the intermittency on the ratio of the local boundary layer momentum thickness Reynolds number to the starting and ending transition Reynolds numbers. In the case of Sieger et al. (1995) the start and ending transition Reynolds numbers were based on empirical correlations.

A relatively new approach to intermittency modelling is to propose a transport equation for the intermittency factor where the source terms are designed to mimic the behaviour of some of the algebraic intermittency models. The main advantages of this approach is that it is possible to model the transition process not only in the flow direction but also across the boundary-layer and thus provide a more realistic prediction of the transition process (Pecnik et al. 2003). Notable efforts in this area have been made by Steelant and Dick (2001), Suzen and Huang (2004) and Menter et al. (2002). The first two models required the integration of the boundary layer quantities in order to determine the momentum thickness and hence the transition onset location. As well, the intermittency equation source terms required non-local information such as the freestream velocity. As a result, their applicability was limited to boundary layer codes or structured-grid Navier-Stokes codes where the grid lines were aligned normal to the wall and the required quantities could be obtain by searching in the grid j coordinate (i.e. in the wall normal direction by assuming the grid is perfectly aligned with the wall). Pecnik et al (2003) compared both of these models on two flat plate and three turbine blade test cases (see for example Figure 2.19).

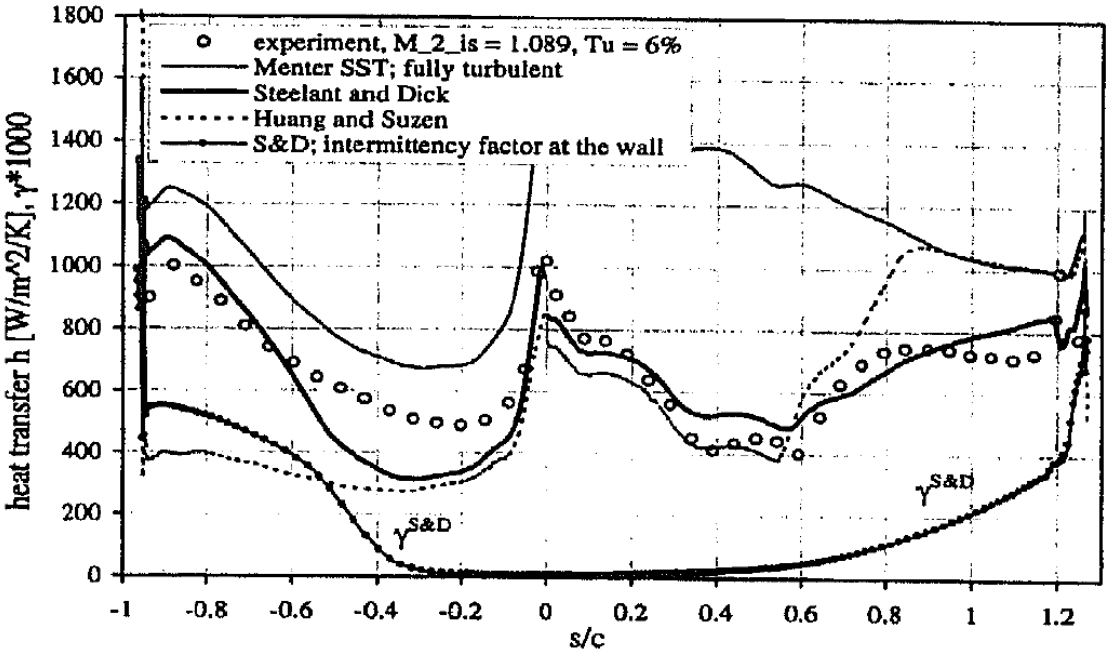

Figure 2.19 Heat transfer distribution on a transonic turbine blade predicted by the Steelant and Dick (2001) and Suzen and Huang (2004) intermittency models. Reproduced from Pecnik et al (2003).

They concluded that the Steeland and Dick (2001) model was slightly better than the Suzen and Huang (2004) model because it allowed the freestream intermmitency to be equal to one and as a result the model could predict the effects of large freestream turbulence levels on the buffeted laminar boundary layer. The third intermittency model was based strictly on local variables and was the "proof of concept" model for the present thesis. The main disadvantage with the Menter et al. (2002) model was that the source terms were far too large (this was needed in order to recover the fully turbulent solution at the boundary layer edge) and as a result the model could only predict point transition in practice. As well, the user had to manually specify the transition onset Reynolds number as it was not determined automatically.

2.3.5 Low-Re Turbulence Models

The preferred method for predicting transition with unstructured/parallelized CFD codes is to use a low-Reynolds number two-equation turbulence model without any subsequent coupling to an empirical correlation. This is because these models are relatively easy to implement (they don't require any search algorithms) and in some cases are capable of predicting transition even in 3D flows. Low-Reynolds number turbulence models employ damping functions that are designed to predict viscous sublayer behaviour so that wall functions are not required. In order to predict transition they rely on the diffusion of turbulence from the freestream into the boundary layer and the interaction of this freestream turbulence with the model source terms.

A large number of low-Reynolds number turbulence models have been developed since the concept was first proposed by Jones and Launder (1973). A few of these models were found to predict transition at reasonable Reynolds numbers when the freestream turbulence level was sufficiently high. However, the ability of these models to predict transition is coincidental and is due to the similarities between the viscous sublayer and the developing laminar boundary layer where the production of turbulence is damped (Schmidt and Patankar, 1991). The transition predicted by a number of low-Reynolds number turbulence models on a flat plate is shown in Figures 2.20 and 2.21.

Clearly, none of the models are very good at predicting the onset location or the subsequent transitional region. According to Zheng et al. (1998), without further modifications low-Reynolds number turbulence models tend to predict the onset of transition far too early, do not have the proper sensitivity to strong pressure gradients and do not predict transition well in separated shear layers.

One notable exception is the low Reynolds number k-ε model developed by Biswas and Fukuyama (1994). This model has been shown to predict attached transition quite accurately when the freestream turbulence level was greater than 1%. Biswas and Fukuyama successfully applied their model to a variety of test cases which included transition on flat plates as well as a nozzle guide vane. The results for a flat plate are shown in Figures 2.22 and 2.23.

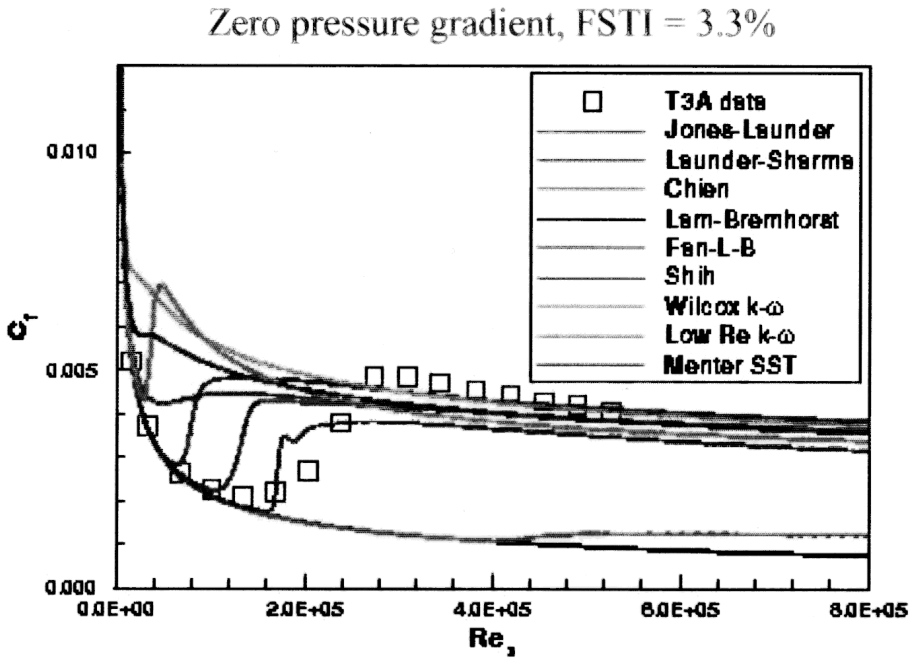

Figure 2.20 Transition in zero pressure gradient predicted by a variety of low-Reynolds number turbulence models (courtesy of Suzen and Huang, personal correspondence).

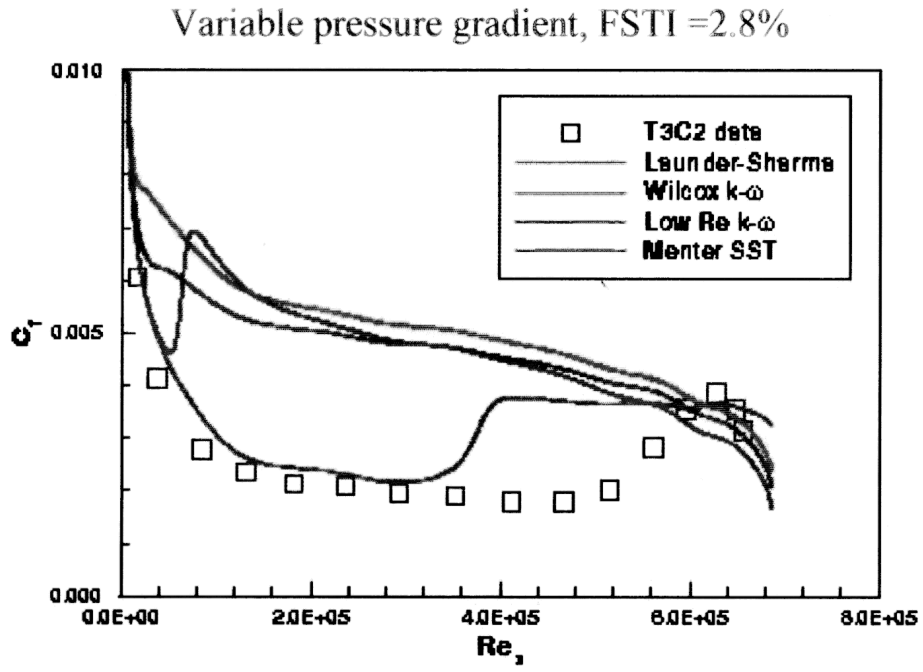

Figure 2.21 Transition in variable pressure gradient predicted by a variety of low-Reynolds number turbulence models (courtesy of Suzen and Huang, personal correspondance).

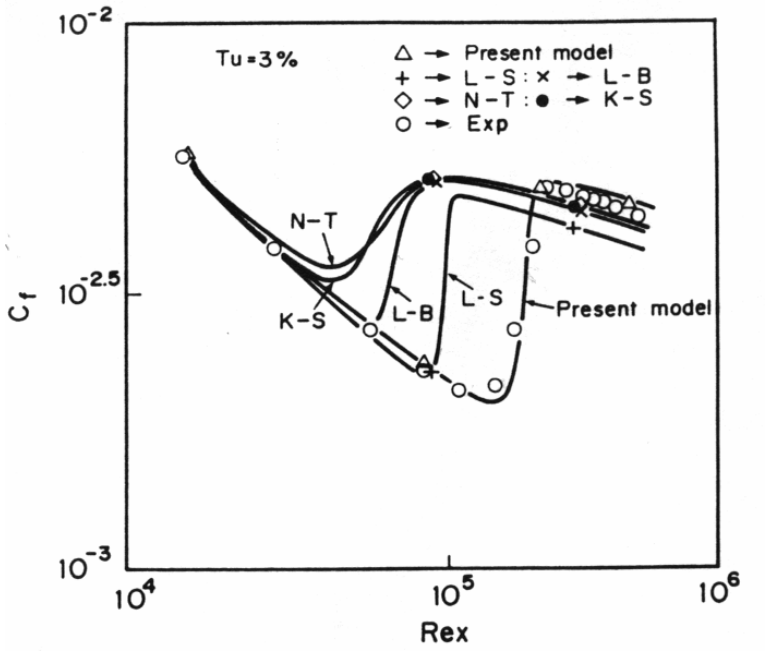

Figure 2.22 Skin friction (Cf) predicted by the low-Reynolds number turbulence model of Biswas and Fukuyama (1994, present model) and various other low-Reynolds number turbulence models (reproduced from Biswas and Fukuyama, 1994).

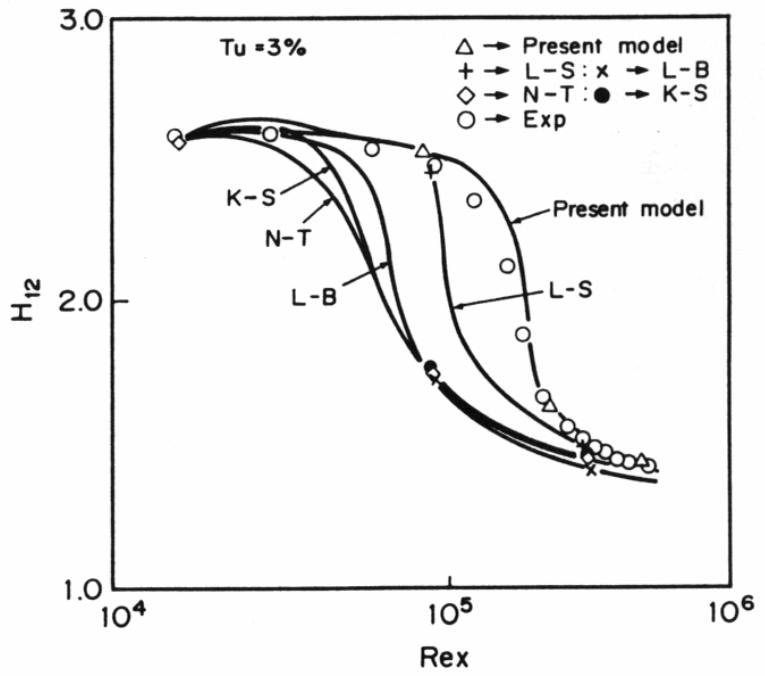

Figure 2.23 Shape factor (H) predicted by the low-Reynolds number turbulence model of Biswas and Fukuyama (1994, present model) and various other low-Reynolds number turbulence models (reproduced from Biswas and Fukuyama, 1994).

The model of Biswas and Fukuyama model was implemented by Langtry (2002) into a Navier-Stokes code. While the predictions of attached transition onset and length were reasonable, the model had poor numerical robustness. In order to converge a solution the equations for k and ε had to be under-relaxed by factors of 0.1. This resulted in a solution time that was approximately ten times longer then what would be required for a fully turbulent computation.

For the case of separation-induced transition on a flat plate a steady-state converged solution could not be obtained. Robustness and accuracy are two of the main requirements of an industrial turbulence model and the fact that many low-Reynolds number turbulence models are not robust or cannot be trusted to predict transition accurately appears to be what has limited their usefulness in industrial computations.

It should be noted that since the predictive failure of the low-Reynolds number turbulence models has become widely accepted a number of researchers have moved on to start developing low-Reynolds number Reynolds Stress or Algebraic Stress models that can predict transition. The hope is that by accounting for the production of the different Reynolds stresses separately the accuracy of the transition model could be improved. The basis for this is that the flat plate experiments and also the DNS computations have indicated that the developing Reynolds stress balances in the laminar boundary layer before transition behave quite differently from each other and from those in a turbulent boundary layer. Notable efforts in this area include Savill (2002) and Lardeau et al. (2004).

2.3.6 Transport Equation for Laminar Kinetic Energy

A very interesting transition modeling approach that has recently been proposed is based on modelling the development of the pre-transitional laminar fluctuations all the way up to the onset of transition and then into the turbulent region. The idea was originated by Mayle and Schulz (1997) who proposed a transport equation for the kinetic energy of the laminar fluctuations upstream of transition. The onset of transition was judged to occur once the laminar fluctuations in the boundary layer reached a certain level. Again the main problem with the Mayle and Schulz (1997) model was that the source term in the transport equation was based on non-local values such as the freestream velocity. Walters and Leylek (2003) used Mayle and Schulz's (1997) ideas to develop a locally formulated transport equation for the laminar kinetic energy which represents the magnitude of non-turbulent streamwise fluctuations in the pre-transitional boundary layer. This laminar kinetic energy equation was then coupled to a turbulent kinetic energy (k) and a turbulent eddy frequency (ω) equation. The model automatically predicts the onset of transition without any intervention from the user and is based strictly on local variables. It has not been extensively validated except for a few flat plate test cases and a turbine blade. However, the initial results of this model were promising and indicate that the model appears to have the correct sensitivity to freestream turbulence. The predicted laminar fluctuations and Stanton number of a flat plate subjected to two different freestream turbulence levels are shown in Figures 2.24 and 2.25.

It remains to be seen how accurately the model can predict the effects of pressure gradient and separation on transition, particularly at lower (< 1%) turbulence intensities where natural transition is present. It is also an open question as to whether this model can be extended to predict additional effects such as roughness or freestream length scale. It should be noted that Lardeau et al. (2004) are also investigating the development of a laminar kinetic energy equation. It is expected that the concept of a laminar kinetic energy equation will be a very active area of transition research in the near future.

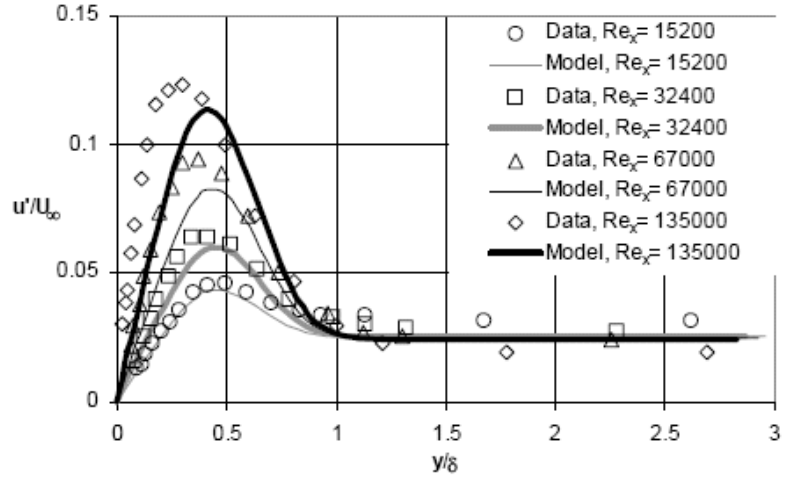

(a)

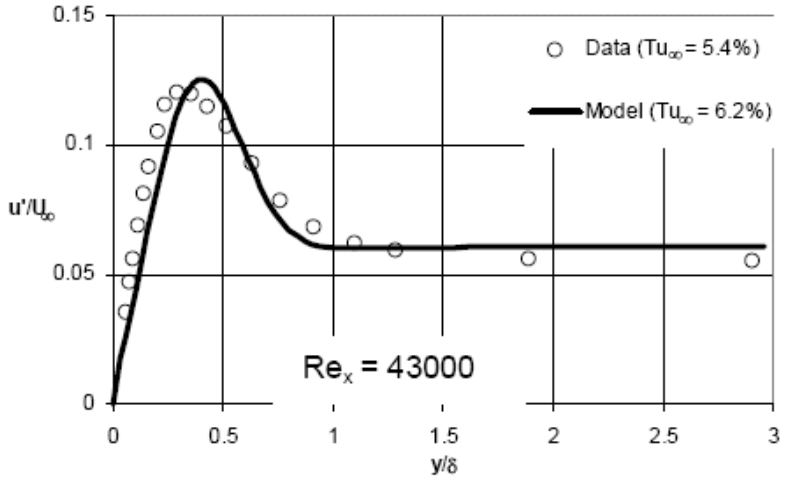

(b)

Figure 2.24 Profiles of total fluctuation intensity in the pre-transitional region for FSTI = 2.6% (a) and FSTI = 6.2% (b). The model appears to predict the fluctuation levels in relatively good agreement with the experimental data (reproduced from Walters and Leylek, 2002).

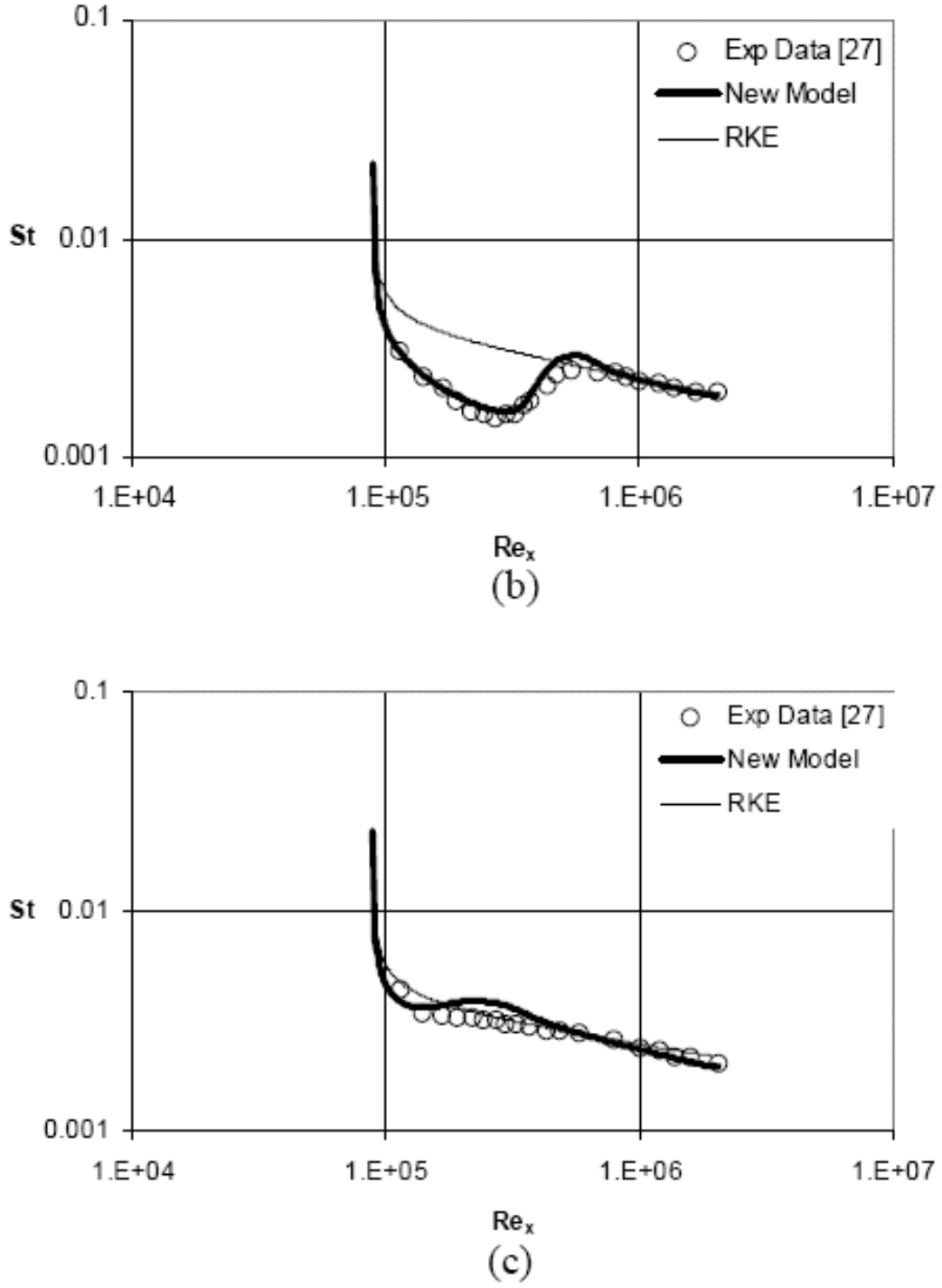

Figure 2.25 Stanton number versus downstream Reynolds number for each of the three flat plate cases: Tu = 2.6% (b), and Tu = 6.2% (c) (reproduced from Walters and Leylek, 2002).

In order for a transition model to be useful for industrial predictions of transition not only must it be accurate but it must also be robust, and must be based on a local formulation that is applicable to unstructured and massively parallelized CFD codes. To date, none of the transition models has been shown to satisfy all of these requirements and there is clearly a need in industry for such an accurate, robust and locally formulated model. It is for these reasons that the present thesis was undertaken. The next chapter will detail the development of a transition model that satisfies the above requirements. The remainder of this thesis will be concerned with validating the new model against a variety of test cases that include transition under the influence of freestream turbulence intensity, pressure gradients, separation and unsteady-state impinging wakes.

Chapter 3
Development of the Transition Model

3.1 Introduction

A novel approach to avoid the need for non-local information in correlation-based models has been introduced by Menter et al. (2002). In this formulation, only local information is used to activate the production term in the intermittency equation. The link between the correlation and the intermittency equation is achieved through the use of the vorticity Reynolds number. The model given by Menter et al. (2002) did not satisfy the requirements of an industrial-strength transition model, both in terms of its numerical behaviour and in terms of its calibration. It is the goal of the present thesis to develop a transition model built on the same concepts, which avoids the deficiencies of the original formulation, and is calibrated over a wide range of flow conditions.

The proposed formulation is based on two transport equations. The first is an intermittency equation used to trigger the transition process. The equation is similar to the model given by Menter et al. (2002), with numerous enhancements and generalizations. This intermittency equation is used to control the production of turbulent kinetic energy in the boundary layer. In addition, a second transport equation is developed in order to avoid the additional non-local operations introduced by the quantities used in the experimental correlations. These correlations are typically based on freestream values, like the turbulence intensity or the pressure gradient outside the boundary layer. The additional transport equation is formulated in terms of the transition onset Reynolds number $Re_{\theta t}$. Outside the boundary layer, the transport variable is forced to follow the value of $Re_{\theta t}$ provided by the experimental correlation. This information is then diffused into the boundary layer by a standard diffusion term. By this mechanism, the strong variations of the turbulence intensity and the pressure gradient in the freestream (which are typically observed in industrial flows) can be taken into account. This transport equation essentially takes a non-local empirical correlation and transforms it into a local quantity, which can then be compared to the local vorticity Reynolds number in order to determine where in the flow the transition criteria has been satisfied. At every location in the flow where the vorticity Reynolds number exceeds the local transition Reynolds number, a source term in the intermittency equation is activated and turbulence is produced. This is the central mechanism by which the transition model operates and the details are given in the following sections.

It should be stressed that the proposed transport equations do not attempt to model the physics of the transition process (unlike e.g. turbulence models), but form a framework for the implementation of correlation-based models into general-purpose CFD methods. The physics of the transition process is contained entirely in the experimental correlations

provided to the model. The formulation is therefore not limited to one specific transition mechanism, like bypass transition, but can be used for all mechanisms, as long as appropriate correlations can be provided. The current correlations have been formulated to cover standard bypass transition as well as flows in low free-stream turbulence environments. In the present thesis, all details of the formulation of the model framework will be given. Some of the empirical correlations used in the simulations are based on internal information and are therefore proprietary. However, the framework is generally applicable and can be combined with standard (e.g. Mayle 1991, Abu-Ghannam and Shaw 1980) or in-house correlations. The basic model framework (transport equations without the correlations) will be called γ-Re_θ model.

3.2 Vorticity Reynolds Number

Instead of using the momentum thickness Reynolds number to trigger the onset of transition, the current model is based on the vorticity Reynolds number, Re_v, (van Driest and Blumer 1963, Menter et al. 2002):

$$\mathrm{Re}_v = \frac{\rho y^2}{\mu}\frac{\partial u}{\partial y} = \frac{\rho y^2}{\mu}\Omega \tag{3.1}$$

where y is the distance from the nearest wall. Since the vorticity Reynolds number depends only on density, viscosity, wall distance and the vorticity (or shear strain rate) it is a local property and can be easily computed at each grid point in an unstructured, parallel Navier-Stokes code.

A scaled profile of the vorticity Reynolds number is shown in Figure 3.1 for a Blasius boundary layer. The scaling is chosen in order to have a maximum of one inside the boundary layer. This is achieved by dividing the Blasius velocity profile by the corresponding momentum thickness Reynolds number and a calibration constant of 2.193. In other words, the maximum of the profile is proportional to the momentum thickness Reynolds number and can therefore be related to the transition correlations (Menter et al., 2002) as follows:

$$\mathrm{Re}_\theta = \frac{\max\left(\mathrm{Re}_v\right)}{2.193} \tag{3.2}$$

Based on this observation, a general framework can be built, which can serve as a local environment for correlation based transition models.

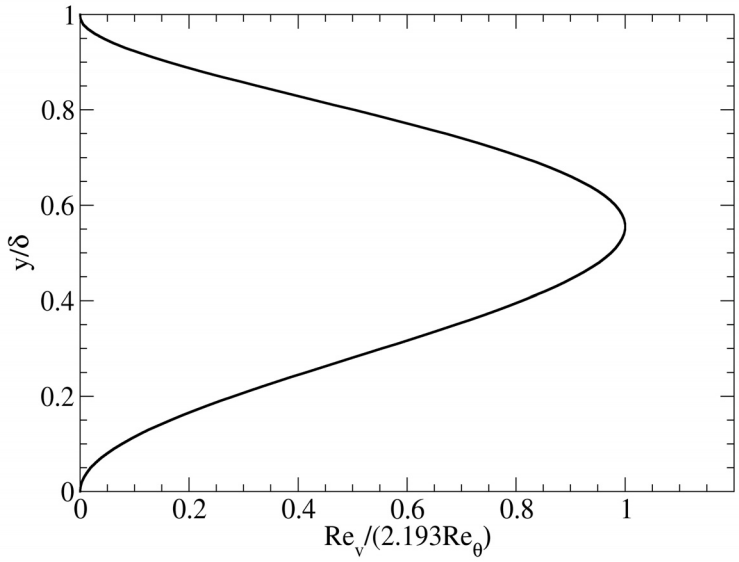

Figure 3.1 Scaled vorticity Reynolds number (Re_v) profile in a Blasius boundary layer.

When the laminar boundary layer is subjected to strong pressure gradients, the relationship betwee momentum thickness and vorticity Reynolds number described by Equation (3.2) changes due to the change in the shape of the profile. The relative difference between momentum thickness and vorticity Reynolds number, as a function of shape factor (H), is shown in Figure 3.2. For moderate pressure gradients ($2.3 < H < 2.9$) the difference between the actual momentum thickness Reynolds number and the maximum of the vorticity Reynolds number is less than 10%. Based on boundary layer analysis a shape factor of 2.3 corresponds to a pressure gradient parameter (λ_θ) of approximately 0.06. Since the majority of experimental data on transition in favourable pressure gradients falls within that range (see for example Abu-Ghannam and Shaw, 1980) the relative error between momentum thickness and vorticity Reynolds number is not of great concern under those conditions.

For strong adverse pressure gradients the difference between the momentum thickness and vorticity Reynolds number can become significant, particularly near separation (H = 3.5). However, the trend with experiments is that adverse pressure gradients reduce the transition momentum thickness Reynolds number. In practice, if a constant transition momentum thickness Reynolds number is specified, the transition model is not very sensitive to adverse pressure gradients and an empirical correlation such as that of Abu-Ghannam and Shaw (1980) is necessary in order to predict adverse pressure gradient transition accurately. It will also be shown in this thesis that the increase in vorticity Reynolds number with increasing shape factor can actually be used to predict separation induced transition. This is one of the main advantages of the present approach because the standard definition of momentum thickness Reynolds number is not suitable in separated flows.

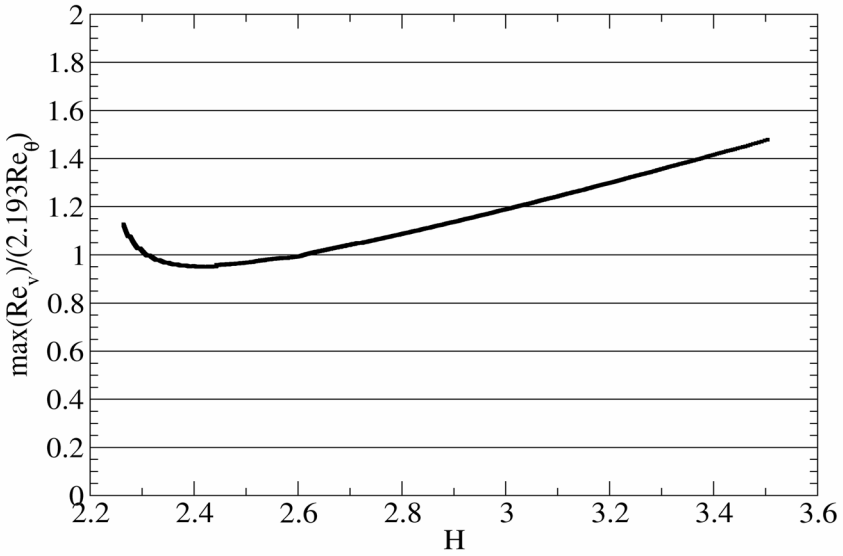

Figure 3.2 Relative error between the maximum value of vorticity Reynolds number (Re_v) and the momentum thickness Reynolds number (Re_θ) as a function of boundary layer shape factor (H).

3.3 Transition Model Formulation

The main requirement for the transition model development was that only local variables and gradients, as well as the wall distance should be used in the equations. The wall distance can be computed from a Poisson equation and does therefore not break the paradigm of modern CFD methods. The present formulation avoids another very severe shortcoming of the correlation-based models, namely their limitation to 2D flows. Already the definition of a momentum-thickness is strictly a 2D concept. It cannot be computed in general 3D flows such as a turbine blade sidewall boundary layer. The current formulation avoids this shortcoming, and allows the simulation of 3D flows originating from different walls.

In the following section, a transport equation for the intermittency, γ, will be described in detail, which can be used to trigger transition locally. The intermittency function is coupled with the SST k-ω turbulence model (Menter, 1994). It is used to turn on the production term of the turbulent kinetic energy downstream of the transition point in the boundary layer. This differs from the typical definition of intermittency (e.g. Suzen et al., 2003) where the intermittency is often used to modify the eddy viscosity. However, from a modeling standpoint the present approach has certain advantages (e.g. capturing the effect of large freestream turbulence levels and the subsequent increase in the laminar skin friction and heat transfer).

In addition to the transport equation for the intermittency, a second transport equation is solved in terms of the transition onset momentum-thickness Reynolds number ($\overline{\mathrm{Re}_{\theta t}}$). This is necessary in order to capture the non-local influence of the turbulence intensity, which changes due to the decay of the turbulence kinetic energy in the freestream, as well as due to changes in the freestream velocity outside the boundary layer. This additional transport equation is an essential part of the model as it ties the empirical correlation to the onset criteria in the intermittency equation and allows the model's use in general geometries and over multiple blades, without interaction from the user.

The formulation of the intermittency equation has been extended to account for the rapid onset of transition caused by separation of the laminar boundary layer. In addition, the model can be fully calibrated with in-house transition onset and transition length correlations. The correlations can also be extended to flows at low free-stream turbulence intensity or to flows with cross-flow instability. The model formulation therefore offers a flexible environment for engineering transition predictions that is fully compatible with the infrastructure of modern CFD methods.

The present transition model formulation is described in six sections. The first section details the formulation of the intermittency transport equation used to trigger the transition onset. The second section describes the new transport equation for the transition momentum thickness Reynolds number $\overline{\mathrm{Re}_{\theta t}}$, which is used to capture the non-local effect of freestream turbulence intensity and pressure gradient at the boundary layer edge. The third section describes a modification that is used to improve the predictions for separated flow transition. The fourth section describes a new empirical correlation that has been developed by the present author to improve on the standard Abu-Ghannam and Shaw (1980) correlation. The fifth section describes the SST model along with the numerical method used to solve the Navier-Stokes and Energy equations and the sixth section describes the link between the transition model and the SST model

3.3.1 Transport Equation for Intermittency

A new transport equation for the intermittency γ has been developed that corrects most of the deficiencies that were observed with the baseline intermittency equation proposed by Menter et al. (2002). The principle deficiencies with this equation were that the transition length was too short and the distance between the specified critical momentum thickness Reynolds number, $\mathrm{Re}_{\theta c}$, and the actual transition Reynolds number, $\mathrm{Re}_{\theta t}$, was too large. In addition, since the source term for the production of intermittency was based on the strain rate, the model suffered from excessive production of intermittency in stagnation regions. As a result, for a turbine blade, the large values of intermittency produced in the stagnation region convected around the blade and resulted in a fully turbulent boundary layer on the surface of the blade. The intermittency equation described in this thesis has been modified specifically to allow for a good prediction of the transitional region while avoiding the problem of early transition due to a stagnation point.

A significant change to the formulation given by Menter et al. (2002) is that the intermittency is now set to be equal to one in the freestream, instead of a small value as in the original model. This differs from the usual definition of intermittency where the freestream intermittency is usually zero and is only equal to one in turbulent boundary layers. However, the present approach has several advantages, especially in stagnation regions and near the boundary layer edge, where the original formulation did interfere with the turbulence model. The concept of a non-zero freestream intermittency is not new and has been employed by Steelant and Dick (2001) in their intermittency transport equation. Although physics arguments can be made for this modification (at least for bypass transition, where the turbulence is diffused into the boundary layer from high freestream levels) it is mainly used here to extend the applicability and robustness of the current method. As well, the empirical correlations for transition onset are applicable only for predicting boundary layer transition, not free shear transition (i.e. a laminar jet transitioning to a turbulent jet). As a result, in the freestream the transition model should enforce the fully turbulent behaviour of the turbulence model. In principle, a laminar freestream can be modeled by selecting a freestream turbulent length scale that results in small (i.e. <1) eddy viscosity ratios (μ_t/μ).

The intermittency equation is formulated as follows:

$$\frac{\partial(\rho\gamma)}{\partial t} + \frac{\partial(\rho U_j \gamma)}{\partial x_j} = P_\gamma - E_\gamma + \frac{\partial}{\partial x_j}\left[\left(\mu + \frac{\mu_t}{\sigma_f}\right)\frac{\partial \gamma}{\partial x_j}\right] \tag{3.3}$$

The transition source term is defined as:

$$P_{\gamma 1} = F_{length}\, c_{a1} \rho S \left[\gamma F_{onset}\right]^{0.5} \left(1 - c_{e1}\gamma\right) \tag{3.4}$$

where S is the strain rate magnitude. This term is designed to be equal to zero (due to the F_{onset} function) in the laminar boundary layer upstream of transition and active everywhere the local vorticity Reynolds number exceeds the local transition onset criteria. The magnitude of this source term is controlled by the transition length function (F_{length}). The density and strain rate are present in order to have the correct units for the source term.

The last term in Eq. 3.4 is used to limit the maximum value of the intermittency so that it cannot exceed a value of one. This limiting value is controlled by the constant c_{e1} (which is set to one in this case).

One of the main differences to other intermittency models lies in the formulation of the function F_{onset}, which is used to trigger the intermittency production (i.e. activate Equ 3.4). It is designed to switch rapidly from a value of zero in a laminar boundary layer to a value of one at every location in the flow field where the local vorticity Reynolds number exceeds the local transition onset criteria. It is formulated as a function of the local vorticity (in this case strain rate) Reynolds number:

$$\mathrm{Re}_V = \frac{\rho y^2 S}{\mu} \tag{3.5}$$

$$F_{onset\,1} = \frac{\mathrm{Re}_v}{2.193 \cdot \mathrm{Re}_{\theta c}} \tag{3.6}$$

$$F_{onset\,2} = \min\left(\max\left(F_{onset\,1}, {F_{onset\,1}}^4\right), 2.0\right) \tag{3.7}$$

$$R_T = \frac{\rho k}{\mu \omega} \tag{3.8}$$

$$F_{onset\,3} = \max\left(1 - \left(\frac{R_T}{2.5}\right)^3, 0\right) \tag{3.9}$$

$$F_{onset} = \max\left(F_{onset\,2} - F_{onset\,3}, 0\right) \tag{3.10}$$

One of the problems that was observed with the F_{onset2} function was that during the transition process, due to the change in the velocity profile, the vorticity Reynolds number would actually decrease and this could cause the transition process to stall. As a result, the viscosity ratio was introduced in Eq. 3.9 in order to help ensure that the F_{onset} function was active throughout the transitional region. The rational behind this equation is given in more detail in Menter et al. (2002). $Re_{\theta c}$ in Eq. (3.6) is the critical Reynolds number where the intermittency first starts to increase in the boundary layer. This occurs upstream of the transition Reynolds number, $Re_{\theta t}$ (see Figure 3.3) because there is a delay due to the fact that the turbulence must first build up to appreciable levels in the boundary layer before any change in the laminar profile can occur. As a result, $Re_{\theta c}$ can be thought of as the location where turbulence starts to grow while $Re_{\theta t}$ is the location where the velocity profile first starts to deviate from the purely laminar profile. The connection between the two must be obtained from an empirical correlation where:

$$\mathrm{Re}_{\theta c} = f\left(\overline{\mathrm{Re}_{\theta t}}\right) \tag{3.11}$$

and $\overline{\mathrm{Re}_{\theta t}}$ comes from the transport equation given by Eq. (3.17). This correlation is determined based on a series of numerical experiments on a flat plate where the critical Reynolds number was varied along with the freestream turbulence intensity and the subsequent transition Reynolds number was measured based on the most upstream location where the skin friction started to increase.

F_{length} in Eq. (3.4) is an empirical correlation that controls the length of the transition region. It is based on a significant amount of numerical experimentation whereby a series of flat plate experiments were reproduced and a curve fitting program was used to develop a correlation that resulted in the correct prediction of the transition length as compared to experimental data. The effect of different values of F_{length} is shown Figure 3.4. Once the correct values for F_{length} were determined (as a function of transition

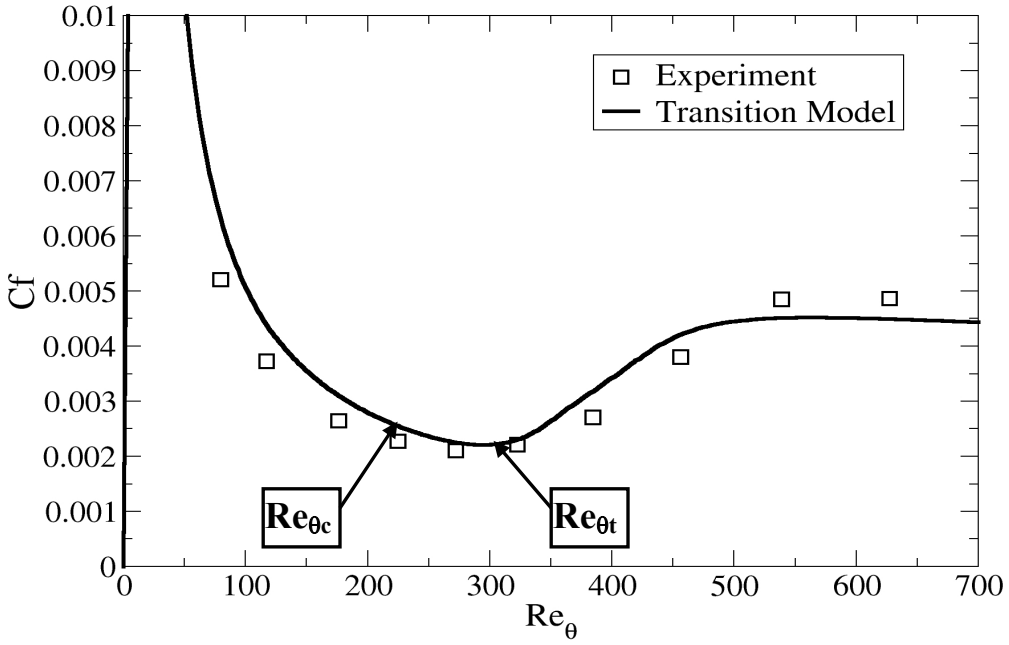

Figure 3.3 Difference between critical momentum thickness Reynolds ($Re_{\theta c}$) number where the intermittency first starts to grow and transition momentum thickness Reynolds number ($Re_{\theta t}$) where the skin friction starts to increase.

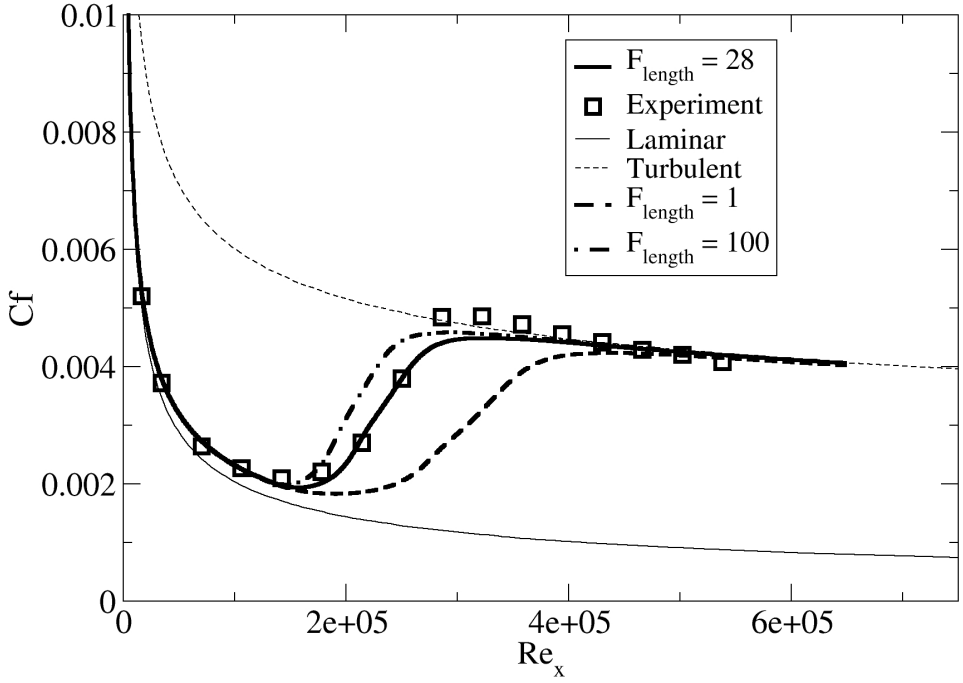

Figure 3.4 Influence of different values of F_{length} on the predicted transition length.

Reynolds number) these values where used to develop a correlation so that the transition length could be correctly reproduced over the whole range of Reynolds numbers. It

should be noted that the $Re_{\theta c}$ and F_{length} correlations are strong functions of each other and there was a significant amount of iteration required in order to obtain good agreement between both correlations. The F_{length} correlation is also defined as a function of $\overline{\mathrm{Re}_{\theta t}}$:

$$F_{length} = f\left(\overline{\mathrm{Re}_{\theta t}}\right) \tag{3.12}$$

The destruction/relaminarization source is defined as follows:

$$E_{\gamma} = c_{a2}\rho\Omega\gamma F_{turb}\left(c_{e2}\gamma - 1\right) \tag{3.13}$$

where Ω is the vorticity magnitude. This term acts like a sink term and ensures that the intermittency remains close to zero in the laminar boundary layer (it is one in the freestream due to the inlet boundary condition and also due the presence of wall distance in Eq. 3.6). It also enables the model to predict relaminarisation because it provides a means for the intermittency to return to zero once the transition criteria in the F_{onset} function is no longer satisfied (e.g. an accelerated boundary layer that becomes thin enough to relaminarize) . The constant c_{a2} controls the strength of the destruction term and ensures that this term is smaller then the transition source term P_{γ}. This allows the transition source term to overwhelm the destruction term once the onset criteria is satisfied. The constant c_{e2} controls the lower limit of intermittency, where the term changes sign. The value of 50 results in a lower limit of 0.02, which is small enough to keep the boundary layer laminar. The vorticity was used in the destruction term in order to avoid the destruction of intermittency in the freestream due to freestream strain rates. This is illustrated in Figure 3.5.

F_{turb} is used to disable the destruction/relaminarization source outside of a laminar boundary layer or in the viscous sublayer and is defined as follows:

$$F_{turb} = e^{-\left(\frac{R_T}{4}\right)^4} \tag{3.14}$$

The constants for the intermittency equation are:

$$\begin{aligned} c_{e1} &= 1.0; \quad c_{a1} = 2.0; \\ c_{e2} &= 50; \quad c_{a2} = 0.06; \quad \sigma_f = 1.0; \end{aligned} \tag{3.15}$$

The boundary condition for γ at a wall is zero normal flux while at an inlet the value of γ is equal to 1. In order to capture the laminar and transitional boundary layers correctly, the grid must have a y^+ of approximately 1. If the y^+ is too large (i.e. > 5) than the transition onset location moves upstream with increasing y^+ (see for example Figure A.1 in the Appendix). It has also been determined that the transition onset location is

sensitive to the advection scheme used for the turbulence and transition model equations. For this reason all equations were solved with a bounded high resolution (i.e. approx. 2nd order) upwind scheme. This resulted in grid independent solutions on reasonable sized grids (e.g. for a turbine blade, 200 nodes around the blade, y^+ of 1 with a wall normal grid expansion ratio of 1.1 – 1.15).

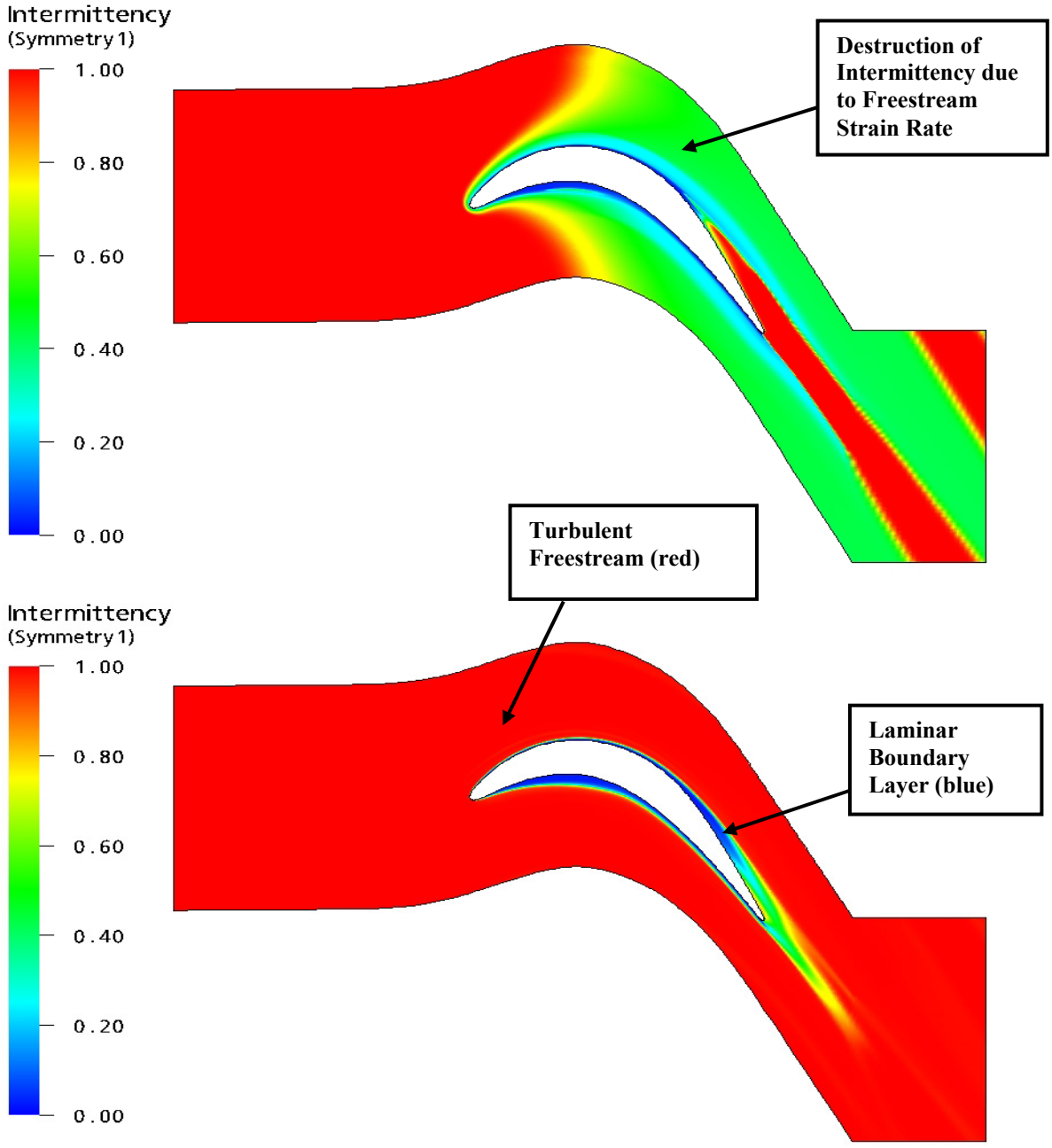

Figure 3.5 Contour of Intermittency using strain rate based destruction terms (top) and vorticity based destruction terms (bottom).

3.3.2 Transport Equation for Transition Momentum Thickness Reynolds Number

The experimental transition correlations relate the Reynolds number of transition onset, $Re_{\theta t,}$ to the turbulence intensity, *Tu*, and other quantities in the freestream where:

$$\mathrm{Re}_{\theta t} = f(Tu,...)_{freestream} \tag{3.16}$$

This is a non-local operation, as the value of $Re_{\theta t}$ is required by the intermittency equation inside the boundary layer, and not only in the freestream. It should also be noted that the turbulence intensity can change strongly in a domain and that one global value over the entire flowfield is therefore not acceptable. Examples of such flows are highly loaded transonic turbomachinery or unsteady-state rotor-stator interactions. Since the main requirement for the current transition model is that only local quantities can be used, there must be a means of passing the information about the freestream conditions into the boundary layer.

The following transport equation can be used to resolve this issue using a local formulation. The basic concept is to treat the transition momentum thickness Reynolds number, $Re_{\theta t}$, as a transported scalar quantity. The idea is then to use an empirical correlation to calculate $Re_{\theta t}$ in the freestream and to allow the freestream value to diffuse into the boundary layer. This is possible because the empirical correlations are defined as $Re_{\theta t}$ = f(Tu, dp/ds), and since Tu and dp/ds (streamwise pressure gradient) are defined in the freestream, $Re_{\theta t}$ is the only unknown quantity in the equation. This transport equation essentially takes a non-local empirical correlation (i.e. Eq. 3.34) and transforms it into a local quantity, which can then be used to compute the transition length (F_{length}, Eq. 3.11) and critical Reynolds number ($Re_{\theta c}$, Eq. 3.12) at every location in the flow field. The intermittency equation (Eq. 3.3) can then be solved like a normal transport equation because the source terms are now local.

The transport equation for the transition momentum thickness Reynolds number ($\overline{\mathrm{Re}_{\theta t}}$) is defined as follows:

$$\frac{\partial\left(\rho\,\overline{\mathrm{Re}_{\theta t}}\right)}{\partial t} + \frac{\partial\left(\rho U_j\,\overline{\mathrm{Re}_{\theta t}}\right)}{\partial x_j} = P_{\theta t} + \frac{\partial}{\partial x_j}\left[\sigma_{\theta t}\left(\mu + \mu_t\right)\frac{\partial\,\overline{\mathrm{Re}_{\theta t}}}{\partial x_j}\right] \tag{3.17}$$

Outside the boundary layer, the source term $P_{\theta t}$ is designed to force the transported scalar $\overline{\mathrm{Re}_{\theta t}}$ to match the local value of $Re_{\theta t}$ calculated from an empirical correlation. The source term is defined as follows:

$$P_{\theta t} = c_{\theta t}\frac{\rho}{t}\left(\mathrm{Re}_{\theta t} - \overline{\mathrm{Re}_{\theta t}}\right)\left(1.0 - F_{\theta t}\right) \tag{3.18}$$

$$t = \frac{500\ \mu}{\rho U^2} \tag{3.19}$$

where t is a time scale, which is present for dimensional reasons. The time scale was determined based on dimensional analysis with the main criteria being that it had to scale with the convective and diffusive terms in the transport equation. The blending function $F_{\theta t}$ is used to turn off the source term in the boundary layer and allow the transported scalar $\overline{\mathrm{Re}_{\theta t}}$ to diffuse in from the freestream. $F_{\theta t}$ is equal to zero in the freestream and one in the boundary layer. An example of the $F_{\theta t}$ blending function for a transonic turbine blade is shown in Figure 3.6 and it can be seen that the blending function does a good job covering the boundary layer. The $F_{\theta t}$ blending function is defined as follows:

$$F_{\theta t} = \min\left(\max\left(F_{wake}\cdot e^{-\left(\frac{y}{\delta}\right)^4}, 1.0 - \left(\frac{\gamma - 1/c_{e2}}{1.0 - 1/c_{e2}}\right)^2\right), 1.0\right) \tag{3.20}$$

$$\theta_{BL} = \frac{\overline{\mathrm{Re}_{\theta t}}\mu}{\rho U} \qquad \delta_{BL} = \frac{15}{2}\theta_{BL} \qquad \delta = \frac{50\Omega y}{U}\cdot\delta_{BL} \tag{3.21}$$

$$\mathrm{Re}_{\omega} = \frac{\rho\omega y^2}{\mu} \tag{3.22}$$

$$F_{wake} = e^{-\left(\frac{\mathrm{Re}_{\omega}}{1\times10^5}\right)^2} \tag{3.23}$$

The F_{wake} function ensures that the blending function is not active in the wake regions downstream of an airfoil/blade. The boundary condition for $\overline{\mathrm{Re}_{\theta t}}$ at a wall is zero flux. The boundary condition for $\overline{\mathrm{Re}_{\theta t}}$ at an inlet is calculated from the empirical correlation based on the inlet turbulence intensity.

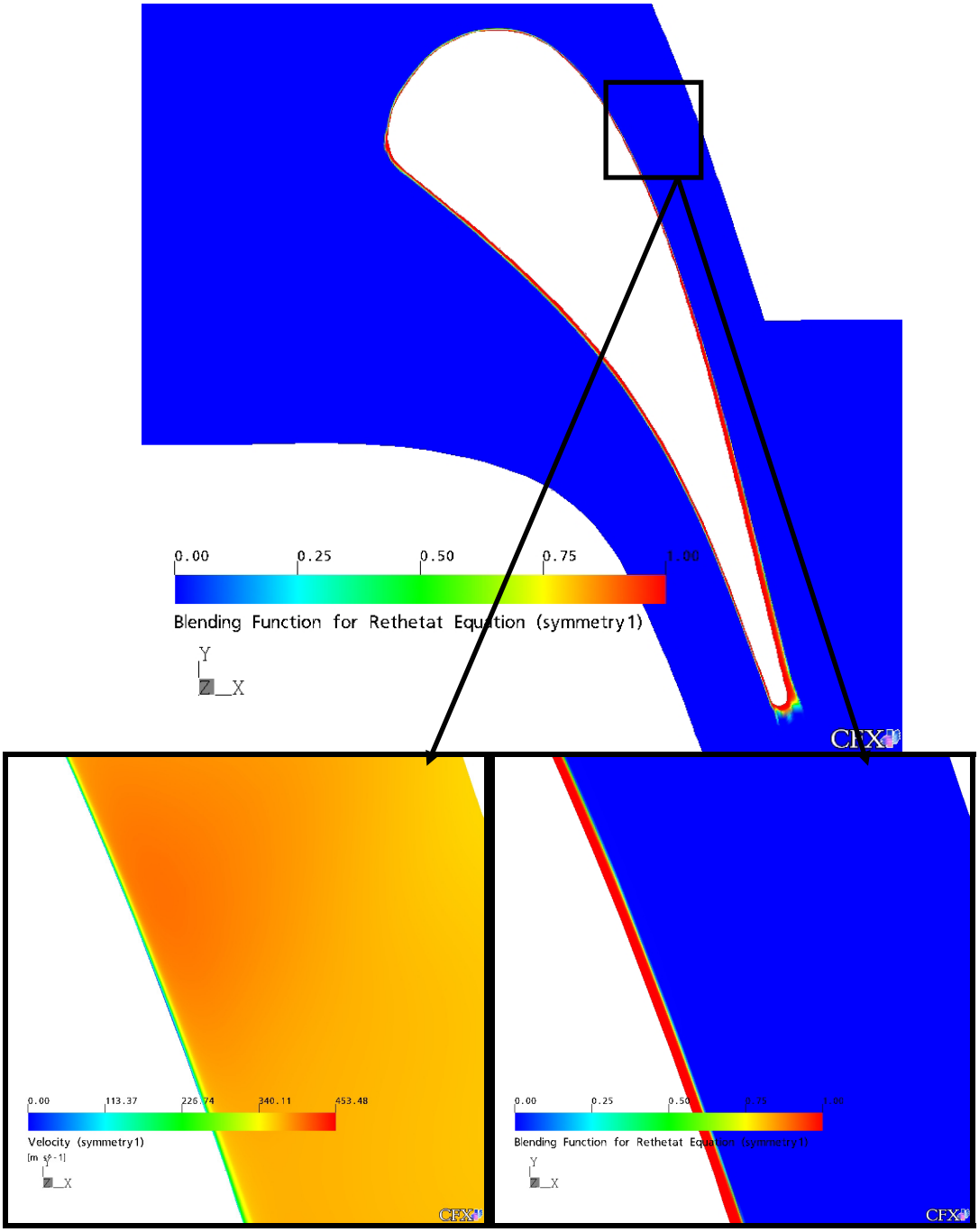

Figure 3.6 Velocity contours (bottom, left) and $F_{\theta t}$ blending function (top and bottom, right) for \the VKI transonic turbine cascade.

The model constants for the transport equation are as follows, where $c_{\theta t}$ controls the magnitude of the source term and $\sigma_{\theta t}$ controls the diffusion coefficient:

$$c_{\theta t} = 0.03$$
$$\sigma_{\theta t} = 2.0$$

The profiles of the transported scalar $\overline{\mathrm{Re}_{\theta t}}$ for a flat plate case with rapidly decreasing freestream turbulence intensity (and hence increasing $\overline{\mathrm{Re}_{\theta t}}$) are shown in Figure 3.7. There is a lag between changes in the freestream value of $\overline{\mathrm{Re}_{\theta t}}$ and that inside the boundary layer. The lag is desirable, as according to Abu-Ghannam and Shaw (1980) the onset of transition is primarily affected by the past history of pressure gradient and turbulence intensity and not the local value at transition. The lag between the local value of $\overline{\mathrm{Re}_{\theta t}}$ in the boundary layer and that in the freestream can be controlled by the diffusion coefficient $\sigma_{\theta t}$. The larger the value of $\sigma_{\theta t}$ the less sensitive the transition model is to history effects. The present value of $\sigma_{\theta t} = 2$ was obtained based on the T3 series of flat plate transition experiments (see Chapter 4) were the freestream turbulence intensity and pressure gradient were rapidly changing and flow history effects are believed to be significant.

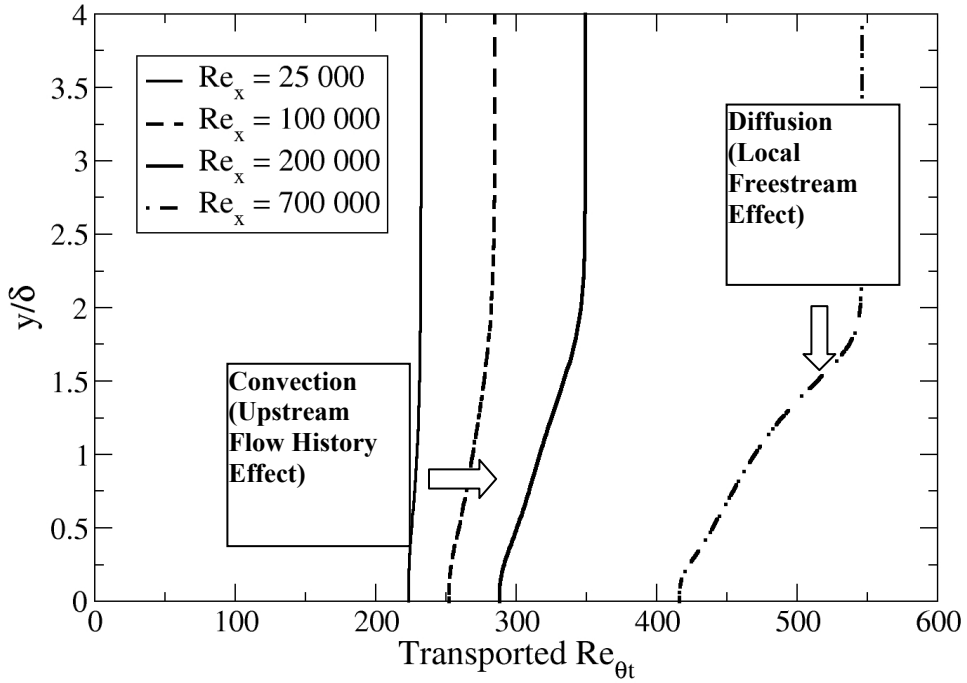

Figure 3.7 Profiles of the transported scalar for a flat plate with a rapidly decaying freestream turbulence intensity (T3A test case).

A contour plot of the local value of the transition momentum thickness Reynolds number from the new empirical correlation ($Re_{\theta t}$) and from the solution of the transport equation ($\overline{Re_{\theta t}}$) is shown in Figure 3.8. The two are virtually identical except in the boundary layer regions as desired. This illustrates that the source term in Eq. 3.17 does indeed force the transported scalar ($\overline{Re_{\theta t}}$) to match the local freestream value from the empirical correlation ($Re_{\theta t}$). Of particular interest is the large increase in $Re_{\theta t}$ near the blade leading edge due to the strong acceleration and the large decrease in the wake region due to the large levels of local turbulence intensity. It should be emphasized that the pressure gradient far from the boundary layer edge is really not relevant to the transition onset criteria. However, this is not of concern because the source term in Eq. 3.17 will ensure that at the boundary layer edge, the correct pressure gradient value is present. This value is what is actually diffused into the boundary layer and used in the transition prediction.

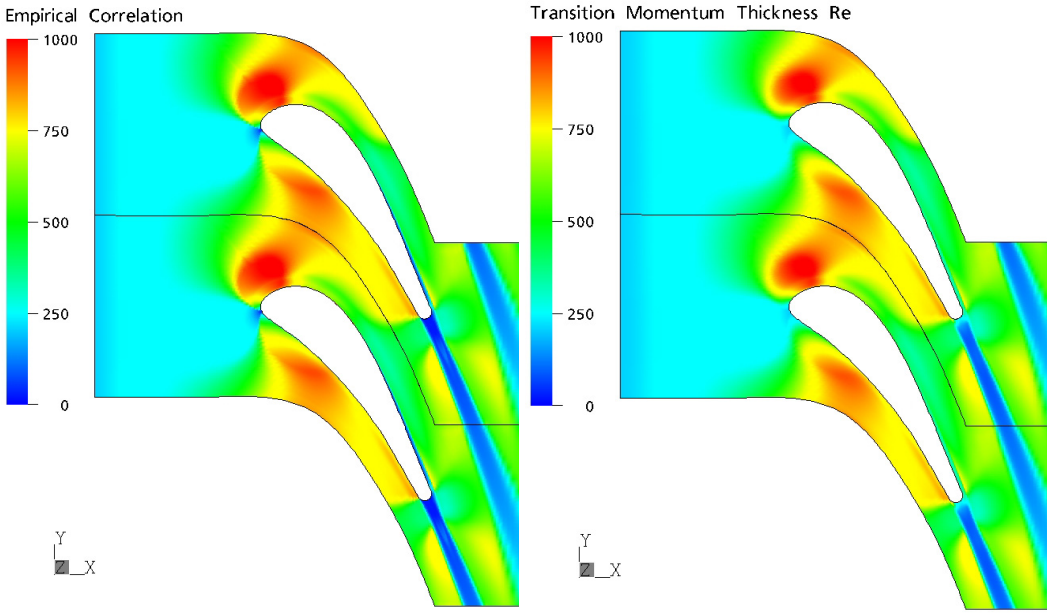

Figure 3.8 Contours of transition onset momentum thickness Reynolds number from the empirical correlation ($Re_{\theta t}$, left) and the transport equation ($\overline{Re_{\theta t}}$, right) for a turbine blade.

3.3.3 Separation Induced Transition

It became apparent during the development of the present transition model that whenever a laminar boundary layer separation occurred, the model consistently predicted the turbulent reattachment location too far downstream. Based on experimental results for a low-pressure turbine blade the agreement with experimental data tended to decrease as the freestream turbulence intensity was lowered. Presumably this is because the turbulent kinetic energy, k, in the separating shear layer is smaller at lower freestream turbulence

intensities. As a result, it takes longer for k to grow to large enough values that would cause the boundary layer to reattach. This is the case even if the onset of transition is predicted at or near the separation point.

To correct this deficiency, a modification to the transition model was introduced that allows k to grow rapidly once the laminar boundary layer separates. The modification has been formulated so that it has a negligible effect on the predictions for attached transition or fully turbulent flow. The main idea behind the separation-induced transition correction is to allow the local intermittency to exceed 1 whenever the laminar boundary layer separates. This will result in a large production of k, which in turn will cause earlier reattachment. The means for accomplishing this is based on the fact that for a laminar separation the vorticity Reynolds number Re_v significantly exceeds the critical momentum thickness Reynolds number $Re_{\theta c}$. As a result, the ratio between the two (when $Re_v > Re_{\theta c}$) can be thought of as a measure of the size of the laminar separation and can therefore be used to increase the production of turbulent kinetic energy. The modification for separation-induced transition is given by:

$$\gamma_{sep} = \min\left(s_1 \max\left[0, \left(\frac{\mathrm{Re}_v}{3.235\,\mathrm{Re}_{\theta c}} \right) - 1 \right] F_{reattach}, 2 \right) F_{\theta t} \tag{3.24}$$

$$F_{reattach} = e^{-\left(\frac{R_T}{20}\right)^4} \tag{3.25}$$

$$\gamma_{eff} = \max\left(\gamma, \gamma_{sep}\right) \tag{3.26}$$

$$s_1 = 2$$

The size of the separation bubble can be controlled with the constant s_1. $F_{reattach}$ disables the modification once the viscosity ratio is large enough to cause reattachment. $F_{\theta t}$ is the blending function from the $\overline{\mathrm{Re}_{\theta t}}$ equation (Eq. 3.17) and confines the modification to boundary layer type flows. The constant 3.235 is the relation between Re_v and Re_θ for a shape factor (H) equal to 3.5 (i.e. at the separation point, see Figure 3.2). The destruction term in the k-equation is limited so that it can never exceed the fully turbulent value, only the production term can be larger than the fully turbulent value (see Eq. 3.27). The ability to include such a complex effect in such a simple way into the model shows the flexibility of the current approach.

Figure 3.9 illustrates the contours of intermittency (γ), effective intermittency (γ_{eff} – Eq. 3.24) and turbulence intensity (Tu) for the T3C4 test case (see Chapter 4) near the laminar separation bubble. The effective intermittency is equal to the intermittency from the transport equation everywhere except in the laminar separation bubble where it is allowed to increase beyond one. This in turn results in excess production of turbulent kinetic energy, which forces the boundary layer to reattach. Through the s_1 constant, the reattachment location can be controlled. The larger the value of s_1 the shorter the reattachment length.

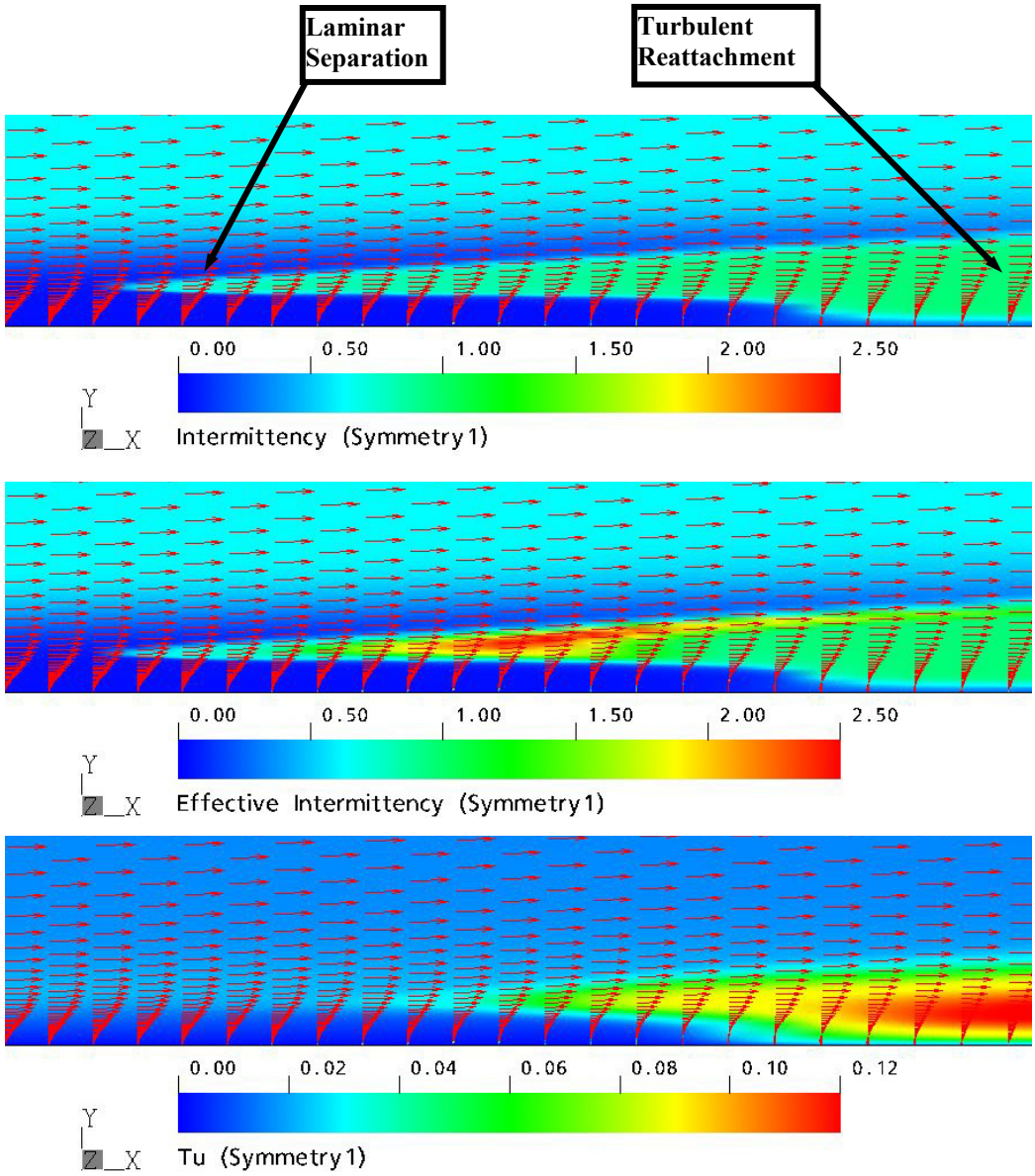

Figure 3.9 Intermittency (γ, top), Effective Intermittency (γ_{eff}, middle) and turbulence intensity (Tu, bottom) for the T3C4 test case.

3.3.4 New Empirical Correlation

In the present thesis some improvements have been made to the empirical correlation for transition onset that was first published in Menter et al (2004). This was done in order to improve the results at lower freestream turbulence intensities (Tu < 1 percent) when natural transition occurs.

The new empirical correlation is based on the following parameters:

$$\lambda_\theta = \frac{\rho\theta^2}{\mu}\frac{dU}{ds} \tag{3.27}$$

$$Tu = 100\frac{\sqrt{2k/3}}{U} \tag{3.28}$$

Where dU/ds is the acceleration along the streamwise direction and can be computed by taking the derivative of the velocity (U) in the x, y and z directions and then summing the contribution of these derivatives along the streamwise flow direction:

$$U = \left(u^2 + v^2 + w^2\right)^{\frac{1}{2}} \tag{3.29}$$

$$\frac{dU}{dx} = \frac{1}{2}\left(u^2 + v^2 + w^2\right)^{-\frac{1}{2}} \cdot \left[2u\frac{du}{dx} + 2v\frac{dv}{dx} + 2w\frac{dw}{dx}\right] \tag{3.30}$$

$$\frac{dU}{dy} = \frac{1}{2}\left(u^2 + v^2 + w^2\right)^{-\frac{1}{2}} \cdot \left[2u\frac{du}{dy} + 2v\frac{dv}{dy} + 2w\frac{dw}{dy}\right] \tag{3.31}$$

$$\frac{dU}{dz} = \frac{1}{2}\left(u^2 + v^2 + w^2\right)^{-\frac{1}{2}} \cdot \left[2u\frac{du}{dz} + 2v\frac{dv}{dz} + 2w\frac{dw}{dz}\right] \tag{3.32}$$

$$\frac{dU}{ds} = \left[\left(u/U\right)\frac{dU}{dx} + \left(v/U\right)\frac{dU}{dy} + \left(w/U\right)\frac{dU}{dz}\right] \tag{3.33}$$

The use of the streamline direction is not Galilean invariant. However, this deficiency is inherent to all correlation-based models, as their main variable, the turbulence intensity is already based on the local freestream velocity and does therefore violate Galilean invariance. This is not problematic, as the correlations are defined with respect to a wall boundary layer and all velocities are therefore relative to the wall. Nevertheless, multiple moving walls in one domain will require additional information.

The empirical correlation has been modified from Menter et al. (2004) to improve the predictions of natural transition. The predicted transition Reynolds number as a function

of turbulence intensity is shown in Figure 3.11. For pressure gradient flows the model predictions are similar to the Abu-Ghannam and Shaw (1980) correlation. The empirical correlation is defined as follows:

$$\mathrm{Re}_{\theta t} = \left[1173.51 - 589.428Tu + \frac{0.2196}{Tu^2}\right] F(\lambda_\theta), Tu \le 1.3 \tag{3.34}$$

$$\mathrm{Re}_{\theta t} = 331.50\left[Tu - 0.5658\right]^{-0.671} F(\lambda_\theta), Tu > 1.3 \tag{3.35}$$

$$F(\lambda_\theta) = 1 - \left[-12.986\lambda_\theta - 123.66\lambda_\theta^{\,2} - 405.689\lambda_\theta^{\,3}\right] e^{-\left[\frac{Tu}{1.5}\right]^{1.5}}, \lambda_\theta \le 0 \tag{3.36}$$

$$F(\lambda_\theta) = 1 + 0.275\left[1 - e^{[-35.0\lambda_\theta]}\right] e^{\left[\frac{-Tu}{0.5}\right]}, \lambda_\theta > 0 \tag{3.37}$$

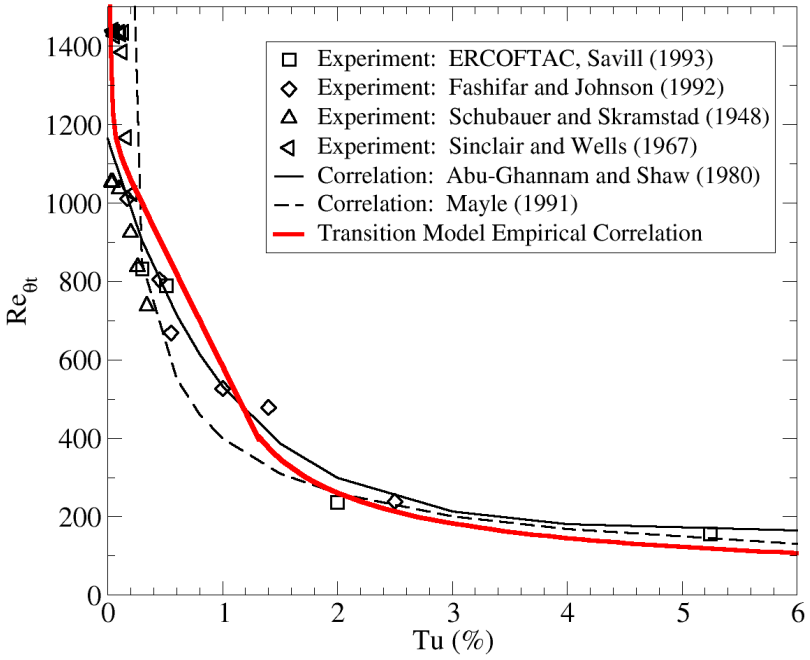

Figure 3.11 Transition onset momentum thickness Reynolds number ($\mathrm{Re}_{\theta t}$) predicted by the new correlation as a function of turbulence intensity (Tu) for a flat plate with zero pressure gradient.

For numerical robustness the acceleration parameters, the turbulence intensity and the empirical correlation should be limited as follows:

$$-0.1 \le \lambda_\theta \le 0.1$$
$$Tu \ge 0.027$$
$$\mathrm{Re}_{\theta t} \ge 20$$

A minimum turbulence intensity of 0.027 percent results in a transition momentum thickness Reynolds number of 1450, which is the largest experimentally observed flat plate transition Reynolds number based on the Sinclair and Wells (1967) data. For cases where larger transition Reynolds are believed to occur (e.g. aircraft in flight) this limiter may need to be adjusted downwards.

The empirical correlation is used only in the source term (Eq. 3.18) of the transport equation for the transition onset momentum thickness Reynolds number. Equations 3.34 to 3.37 must be solved iteratively because the momentum thickness (θ_t) is present in the left hand side of the equation and also in the right hand side in the pressure gradient parameter (λ_θ). In the present work an initial guess for the local value of θ_t was obtained based on the zero pressure gradient solution of Eq. 3.34, 3.35 and the local values of U, ρ and μ. With this initial guess, equations 3.34 to 3.37 were solved by iterating on the value of θ_t and convergence was obtained in less then ten iterations using a shooting method.

3.3.5 Navier-Stokes, Energy and Turbulence Model Equations

The Navier-Stokes, Energy and the turbulence model equations are briefly summarized in the following pages. The Reynolds Averaged Navier-Stokes equations in a stationary frame and using the Boussinesq eddy-viscosity assumption to relate the Reynolds stress and turbulent flux terms to the mean flow variables are defined below (Note: in the case of high speed compressible flow, Favre averaging is used instead of Reynolds averaging):

The conservation of mass equation:

$$\frac{\partial \rho}{\partial t} + \frac{\partial}{\partial x_j}\left(\rho \overline{U}_j\right) = 0 \tag{3.38}$$

The conservation of momentum equation:

$$\frac{\partial}{\partial t}\left(\rho \overline{U}_i\right) + \frac{\partial}{\partial x_j}\left(\rho \overline{U}_j \overline{U}_i\right) = -\frac{\partial P^*}{\partial x_i} + \frac{\partial}{\partial x_j}\left\{\mu_{eff}\left(\frac{\partial \overline{U}_i}{\partial x_j} + \frac{\partial \overline{U}_j}{\partial x_i}\right) - \frac{2}{3}\mu_{eff}\frac{\partial \overline{U}_l}{\partial x_l}\delta_{ij}\right\} \tag{3.39}$$

where P^* is the sum of the pressure (P) and the $\frac{2}{3}\rho\delta_{ij}k$ term which comes from the eddy viscosity Boussinesq assumption. The two are grouped together because they are both scalar normal stresses.

The effective viscosity is the sum of the laminar and turbulent viscosities:

$$\mu_{eff} = \mu + \mu_t \tag{3.40}$$

The conservation of energy equation:

$$\frac{\partial}{\partial t}(\rho H)-\frac{\partial P}{\partial t}+\frac{\partial}{\partial x_j}\left(\rho \overline{U}_j H\right)=\frac{\partial}{\partial x_j}\left(\lambda\frac{\partial T}{\partial x_j}+\frac{\mu_t}{\mathrm{Pr}_t}\frac{\partial h}{\partial x_j}\right)$$
$$+\frac{\partial}{\partial x_j}\left\{\overline{U}_i\left[\mu_{eff}\left(\frac{\partial \overline{U}_i}{\partial x_j}+\frac{\partial \overline{U}_j}{\partial x_i}\right)-\frac{2}{3}\mu_{eff}\frac{\partial \overline{U}_l}{\partial x_l}\delta_{ij}\right]+\mu\frac{\partial k}{\partial x_j}\right\} \tag{3.41}$$

where H is the total energy ($H=h+\frac{1}{2}\overline{U}_i\overline{U}_i+k$), k is the turbulent kinetic energy and the $\frac{2}{3}\rho\delta_{ij}k$ term is grouped with the pressure portion of the static enthalpy (h). The turbulent Prandtl number (Pr_t) is treated as a constant equal to 0.9.

The SST turbulence model (Menter, 1994) has been used to compute the turbulent viscosity (μ_t) that is present in the momentum and energy equations in order to model the effects of turbulence on the flow. The SST model combines the advantages of the k-ε and the k-ω model to achieve an optimal model formulation for a wide range of applications (Menter, 1994). For this a blending function F1 is introduced which is equal to one near the solid surface and equal to zero for the flow domain away from the wall. It activates the k-ω model in the near wall region and the k-ε model for the rest of the flow. By this approach the attractive near-wall performance of the k-ω model can be used without the potential errors resulting from the free stream sensitivity of that model. In addition, the SST model also features a modification of the definition of the eddy viscosity, which can be interpreted as a variable c_μ, where c_μ in the k-ε model is constant. This modification is required to accurately capture the onset of separation under pressure gradients. The modelled equations for the turbulent kinetic energy k and the turbulence frequency ω are as follows:

$$\frac{\partial \rho k}{\partial t}+\frac{\partial \rho U_j k}{\partial x_j}=P_k-D_k+\frac{\partial}{\partial x_j}\left(\Gamma_k\frac{\partial k}{\partial x_j}\right) \tag{3.42}$$

$$\frac{\partial \rho\omega}{\partial t}+\frac{\partial \rho U_j \omega}{\partial x_j}=\frac{\gamma}{\nu_t}P_k-\beta\rho\omega^2+\frac{\partial}{\partial x_j}\left(\Gamma_\omega\frac{\partial \omega}{\partial x_j}\right)$$
$$+(1-F_1)2\rho\sigma_{\omega 2}\frac{1}{\omega}\frac{\partial k}{\partial x_j}\frac{\partial \omega}{\partial x_j} \tag{3.43}$$

where the production and destruction terms for the turbulence kinetic energy equation are defined as:

$$P_k=\min\left(\mu_t S^2, 10D_k\right) \tag{3.44}$$

$$D_k = \beta^* \rho \omega k \tag{3.45}$$

and the blending function F_1 is calculated from

$$F_1 = \tanh(\arg_1^4) \tag{3.46}$$

$$\arg_1 = \min\left(\max\left(\frac{\sqrt{k}}{\beta^* \omega y}; \frac{500\upsilon}{y^2 \omega} \right); \frac{4\rho\sigma_{\omega 2} k}{CD_{k\omega} y^2} \right) \tag{3.47}$$

$$CD_{k\omega} = \max\left(2\rho\sigma_{\omega 2} \frac{1}{\omega} \frac{\partial k}{\partial x_j} \frac{\partial \omega}{\partial x_j}; 1.0e^{-10} \right) \tag{3.48}$$

The turbulent viscosity is then calculated by

$$\mu_t = \min\left[\frac{\rho k}{\omega}; \frac{a_1 \rho k}{SF_2} \right] \tag{3.49}$$

with the constant $a_1 = 0.31$ and the blending function F_2 obtained from

$$F_2 = \tanh(\arg_2^2) \tag{3.50}$$

$$\arg_2 = \max\left(2\frac{\sqrt{k}}{\beta^* \omega y}; \frac{500\upsilon}{y^2 \omega} \right) \tag{3.51}$$

The coefficients, φ of the model are functions of F_1: $\varphi = F_1\varphi_1 + (1-F_1)\varphi_2$, where φ_1, φ_2 stand for the coefficients of the k-ω and the k-ε model respectively:

$\sigma_{k1}=1.176$, $\sigma_{\omega 1}=2.000$, $\kappa=0.41$, $\gamma_1=0.5532$, $\beta_i=0.0750$,
$\beta^*=0.09$, $c_l=10$

$\sigma_{k2}=1.000$, $\sigma_{\omega 2}=1.168$, $\kappa=0.41$, $\gamma_2=0.4403$, $\beta_i=0.0828$, $\beta^*=0.09$

The CFD results shown in this thesis have been obtained with the commercial CFD code CFX-5. In CFX-5 the Reynolds-Averaged Navier-Stokes (RANS) equations are discretised using a vertex-based finite volume method, which is conservative and time-implicit (Raw (1996), Schneider and Raw (1987)). The computational hybrid and unstructured mesh can consist of different element types such as hexahedrals, prisms, wedges, and tetrahedrals. A control volume is constructed around each nodal point of the mesh and the fluxes are computed at the integration points located at the sub faces between two control volumes. The discrete equations are evaluated using a bounded

high-resolution advection scheme similar to that of Barth and Jesperson (1989). The mass flow is evaluated such that a pressure-velocity coupling is achieved by the Rhie and Chow (1983) algorithm.

The discrete systems of equations are solved by the coupled algebraic multi-grid method developed by Raw (1996). The numerical effort of this method scales linearly with the number of grid nodes, which is selected to resolve the computational domain. Steady state applications are computed by time step iteration until a user defined convergence level is reached. For a transient computation an iterative procedure updates the non-linear coefficients within each time step (coefficient loop) while the outer loop advances the solution in time.

3.3.6 Coupling the Transition Model with the Turbulence Model

The present transition model has been calibrated for use with the SST turbulence model Menter (1994). The coupling between the transition model and the turbulence model as accomplished by modifying equations 3.42 and 3.43 in the turbulence model as follows:

$$\frac{\partial}{\partial t}(\rho k)+\frac{\partial}{\partial x_j}(\rho u_j k)=\widetilde{P}_k-\widetilde{D}_k+\frac{\partial}{\partial x_j}\left((\mu+\sigma_k\mu_t)\frac{\partial k}{\partial x_j}\right) \tag{3.52}$$

$$\frac{\partial}{\partial t}(\rho\omega)+\frac{\partial}{\partial x_j}(\rho u_j \omega)=\alpha\frac{P_k}{\nu_t}-D_\omega+Cd_\omega+\frac{\partial}{\partial x_j}\left((\mu+\sigma_k\mu_t)\frac{\partial \omega}{\partial x_j}\right) \tag{3.53}$$

$$\widetilde{P}_k=\gamma_{eff}P_k \tag{3.54}$$

$$\widetilde{D}_k=\min\left(\max(\gamma_{eff},0.1),1.0\right)D_k \tag{3.55}$$

where P_k and D_k are the production and destruction terms from the turbulent kinetic energy equation in the original SST turbulence model (see Eq. 3.44 and 3.45). γ_{eff} is the effective intermittency obtained from Eq. 3.26. It should be stressed that the intermittency is used only to control the source terms in the k-equation, it is not used to multiply the eddy viscosity. In this way the present concept of intermittency is somewhat different than the standard definition used by Steelant and Dick (2001) or Suzen and Huang (2004). However, the present approach has two main advantages. The first is that it improves the robustness of the model because the intermittency (which is difficult to linearize due to the empirical correlations in the source terms) does not enter directly into the momentum equations. The second advantage is that it allows the model to predict the effects of high freestream turbulence levels on the buffeted laminar boundary layer. This is because when the freestream eddy viscosity is large, the small values of intermittency in the boundary layer do not cancel out the local eddy viscosity. Consequently, the increase in the laminar shear stress and heat transfer that has been observed experimentally in buffeted laminar boundary layers can, in principle, be captured by the present model.

The final modification to the SST model is a change in the blending function F_1 responsible for switching between the *k*-ω and *k*-ε models. It was found that in the center of the laminar boundary layer F_1 could potentially switch from 1.0 to 0.0. This is not desirable, as the *k*-ω model must be active in the laminar and transitional boundary layers. The deficiency in the blending function is not surprising as the equations used to define F_1 were intended solely for use in turbulent boundary layers. The solution is to redefine F_1 in terms of a blending function that will always be equal to 1.0 in a laminar boundary layer. The modified blending function is defined as follows:

$$R_y = \frac{\rho y \sqrt{k}}{\mu} \tag{3.56}$$

$$F_3 = e^{-\left(\frac{R_y}{120}\right)^8} \tag{3.57}$$

$$F_1 = \max\left(F_{1orig}, F_3\right) \tag{3.58}$$

where F_{1orig} is the original blending function from the SST turbulence model (see Eq. 3.46).

This concludes the development chapter of the new transition model. The transition model has been validated against a large number of diverse and challenging test cases. The next four chapters will present the results from these test cases. Chapter 4 will summarize the results for a number of flat plate test cases, which include the ERCOFTAC T3-series and the Schubauer and Klebanof (1955) experiments. Chapter 5 will detail a number of 2D test cases including a compressor blade, high and low pressure turbine blades, a wind turbine airfoil and a multi-element flap. Chapter 6 will summarize the results for a number of 3D test cases including a transonic wing, a 3D compressor blade and a full helicopter configuration.

Due to the large number of test cases and limitations in computational resources it was not possible to perform a grid independence study for every single test case in this thesis. Instead, a number of sensitivity studies were performed with the transition model on the effect of y^+, wall normal expansion ratio and streamwise grid refinement in order to determine some best practice guidelines for the grid generation. A summary of these best practice guidelines along with the various studies is included in the Appendix of this thesis. It was found that in order for grid independent results to be achieved the maximum y^+ had to be 1 or less, the wall-normal expansion ratio had to be between 1.1 and 1.2 and at least 100 streamwise nodes along the length of the boundary layer were needed to properly capture the laminar, transitional and turbulent boundary layer development. These best practice guidelines have been followed for all the test cases presented in this thesis and in many cases, particularly in the streamwise direction, the grids were even finer then the minimum requirements.

Chapter 4
Flat Plate Test Cases

4.1 Introduction

The transition model developed in the previous chapter has been used to predict the ERCOFTAC (European Reseach Community on Flow, Turbulence and Combustion) T3 series of experimental flat plate test cases. These experiments were performed by researchers at Rolls Royce in the early 1990's (Savill, 1992). The wind tunnel geometry consisted of a flat plate mounted in a test section with a very small rounded leading edge. The radius of the rounded leading edge was 0.75 mm and the flat plate had a length of 1.5 m. The T3 series of test cases (T3A, T3B, T3AM, T3C5, T3C2, T3C3, T3C4) have often been used to evaluate the ability of transition models to predict the onset and length of transition. They have become the standard test cases against which most transition models are compared. All the T3 series of test cases had freestream turbulence intensities of 1% or greater, and as a result bypass transition was the dominant transition mode. In order to test the new transition model's ability to predict natural transition the Schubauer and Klebanoff (1955) flat plate experiment has also been computed. This chapter will conclude with a test case for relaminarisation and also a test for hysteresis in the predicted transition location. It will be shown that if the acceleration parameter is high enough the present transition model can in fact predict relaminarisation. It will also be shown that the present transition model does not suffer from any hysteresis in the predicted transition location when subject to different initial starting conditions. This is an important requirement for a general transition model because if there is any hysteresis in the predicted transition location the model will not be able to predict unsteady-state transition effects (e.g. periodic wake passing in a blade row) correctly.

The T3 measurements were performed on a flat plate subjected to different levels of freestream turbulence and pressure gradient. Test cases T3A, T3B and T3AM had a zero streamwise pressure gradient with freestream turbulence intensities of 3%, 6% and 1% respectively. The different freestream turbulence levels were imposed by inserting different turbulence grids into the wind tunnel test section upstream of the flat plate. The Schubauer and Klebanoff (1955) zero pressure gradient flat plate experiment was performed in a relatively quiet wind tunnel and had a freestream turbulence intensity of only about 0.1 percent near the transition location.

The T3C test cases had a streamwise pressure gradient that is representative of an aft-loaded turbine blade and freestream turbulence levels of 2.5 percent. The wind tunnel geometry was identical to the T3A, T3B and T3AM cases except the tunnel wall opposite of the flat plate was contoured in order to impose a streamwise pressure gradient on the

flat plate and thus alter the development of the flat plate boundary layer. The main difference between the various T3C test cases was that the wind tunnel velocity, U_o, (and hence the tunnel Reynolds number) was progressively lowered so that the transition onset location moved from the favourable pressure gradient region at the leading edge to the adverse pressure gradient at the end of the plate (see Figure 4.1). The T3C test cases are therefore excellent tests for the combined effect of pressure gradient and boundary layer history on the predicted onset and length of transition.

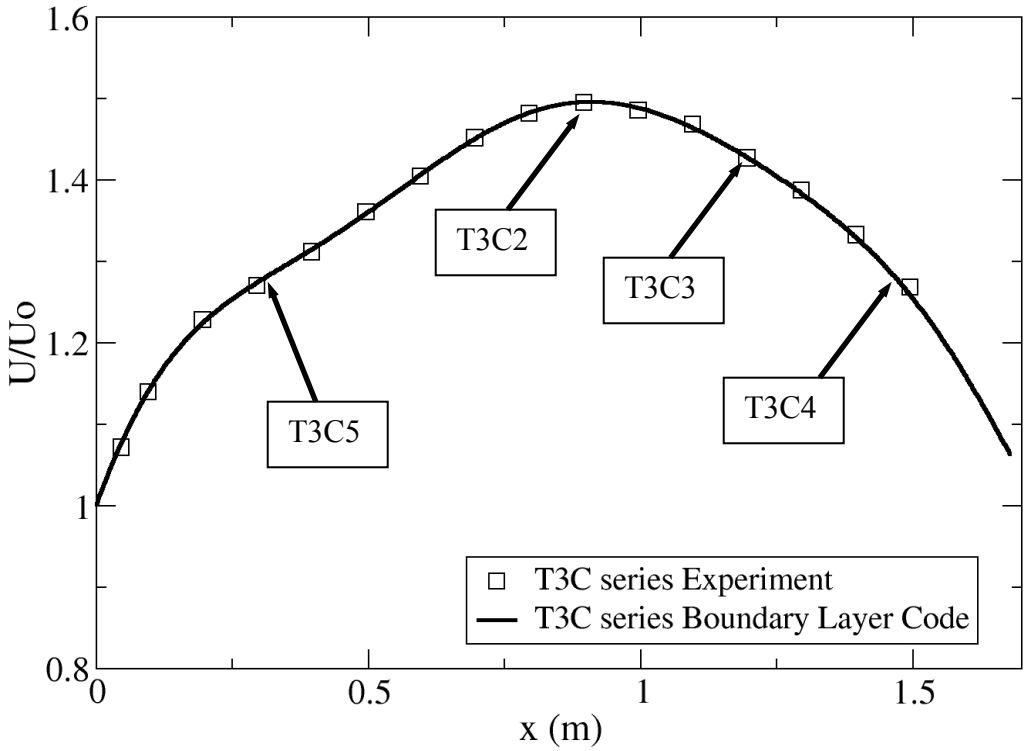

Figure 4.1 Non-dimensional freestream velocity distribution (U/Uo) vs distance from the flat plate leading edge for the T3C series of test cases. The transition onset location for each T3C test case is also indicated.

A summary of the inlet conditions used for each test case in this chapter is shown in Table 4.1. The inlet turbulent quantities were specified in order to match the experimentally measured decay of freestream turbulence. This is illustrated in Figure 4.2.

All the computations in this chapter, with the exception of the T3C4 and the hysteresis cases, were computed with a parabolic finite difference boundary layer code that was provided by Suzen and Huang (2004). The computational grid for the boundary layer code consisted of 1000 streamwise nodes and 200 normal nodes with the first grid point y^+ value below 1. The large number of streamwise nodes was required to obtain grid independence because the boundary layer code used only first order upwinding for the advection terms. For the T3C cases the freestream velocity from the experiment (see Figure 4.1) was enforced at the upper boundary condition (i.e. the 200^{th} normal node) and allowed to propagate by diffusion down to the wall, thus enforcing the pressure

Case	Inlet Velocity (m/s)	Turbulence Intensity (%) Inlet / Leading Edge value	μ_t / μ	Density (kg/m^3)	Dynamic Viscosity (kg/ms)
T3A	5.4	3.3	12.0	1.2	1.8×10^{-5}
T3B	9.4	6.5	100.0	1.2	1.8×10^{-5}
T3A-	19.8	0.874	8.72	1.2	1.8×10^{-5}
Schubauer and Klebanof	50.1	0.3	1.0	1.2	1.8×10^{-5}
T3C2	5.29	3.0	11.0	1.2	1.8×10^{-5}
T3C3	4.0	3.0	6.0	1.2	1.8×10^{-5}
T3C4	1.37	3.0	8.0	1.2	1.8×10^{-5}
T3C5	9.0	4.0	15.0	1.2	1.8×10^{-5}

Table 4.1 Inlet condition for the flat plate test cases.

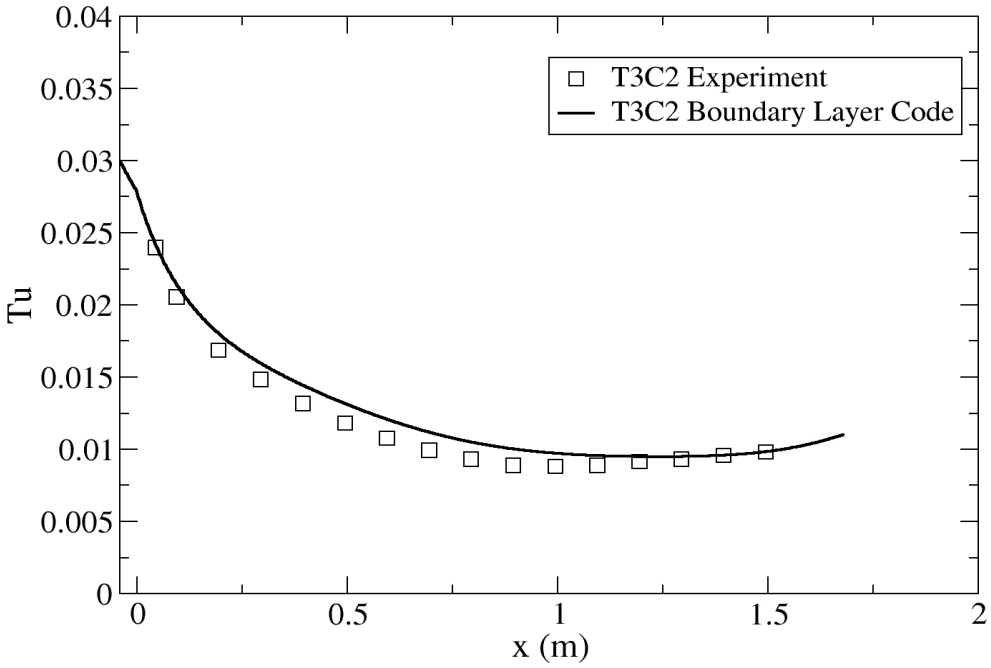

Figure 4.2 Freestream turbulence intensity vs distance from the leading edge of the flat plate for the T3C2 test case.

distribution from the experiment. The freestream turbulence quantities were not enforced at the upper boundary conditions (here a zero flux boundary condition is applied), rather the inlet viscosity ratio was varied in order to match the experimentally measured turbulence levels. The calculations for the boundary layer code were started just downstream of the circular leading edge (i.e. the effect of the leading edge is omitted). As well, because the boundary layer code is a parabolic (i.e. information only travels

downstream) initial conditions are not required in order to run the computation. For attached flow at the grid independent limit, the transition model solutions obtained with a parabolic boundary layer code are identical to those of a full Navier-Stokes code (Menter et al., 2004). The main advantage towards using the boundary layer code is that the determination of the inlet viscosity ratio needed to match the experimentally measured decay of freestream turbulence is a trial and error process, which would have taken a lot longer to do using a Navier-Stokes code.

The T3C4 case had a small laminar separation and as a result could not be computed by the parabolic boundary layer code. Consequently, this computation was performed with the Navier-Stokes code CFX-5. The hysteresis case was also performed with CFX-5 due to the requirement of having to specify different initial conditions and also to capture elliptic effects such as the transition location moving upstream or downstream with time (neither of which was possible to do with the parabolic boundary layer code). Both the T3C4 and hysteresis flat plate cases were performed with a C-mesh that consisted of 236×90 cells. The best practice grid guidelines (see Appendix) were used to generate these grids. As was mentioned earlier, the experimental flat plate had a circular leading edge with a radius of 0.75 mm and this has also been included in the CFX-5 computations. The mesh used for the hysteresis (zero pressure gradient) test cases is shown in Figure 4.3. The distance between the first cell center and the wall was specified

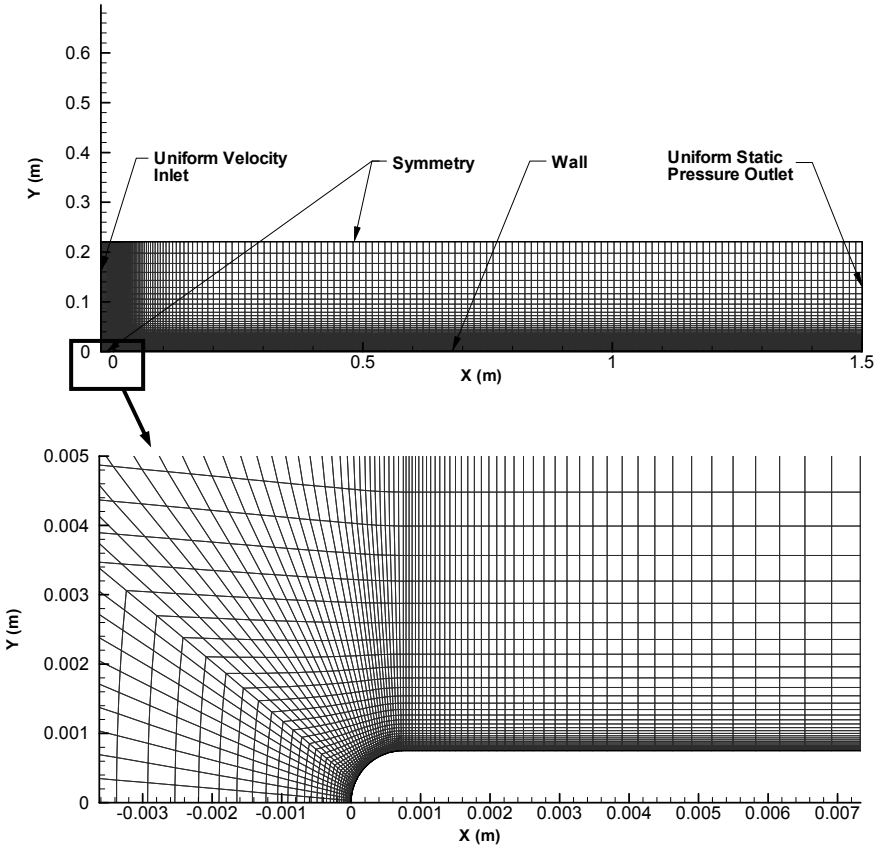

Figure 4.3 Flat plate mesh used to compute the hysteresis test case (top) along with a close up of the leading region (bottom).

so that a y^+ of 1.0 or less was present at all times. There were at least 25 cells in the laminar boundary layer at all stream-wise locations. For the T3C4 test case the pressure gradient was imposed by varying the contour shape of the upper slip wall. The required area variation between the flat plate and the upper slip wall was computed from the experimental freestream velocity distribution shown in Figure 4.1. The mesh used for the T3C4 pressure gradient case is shown in Figure 4.4.

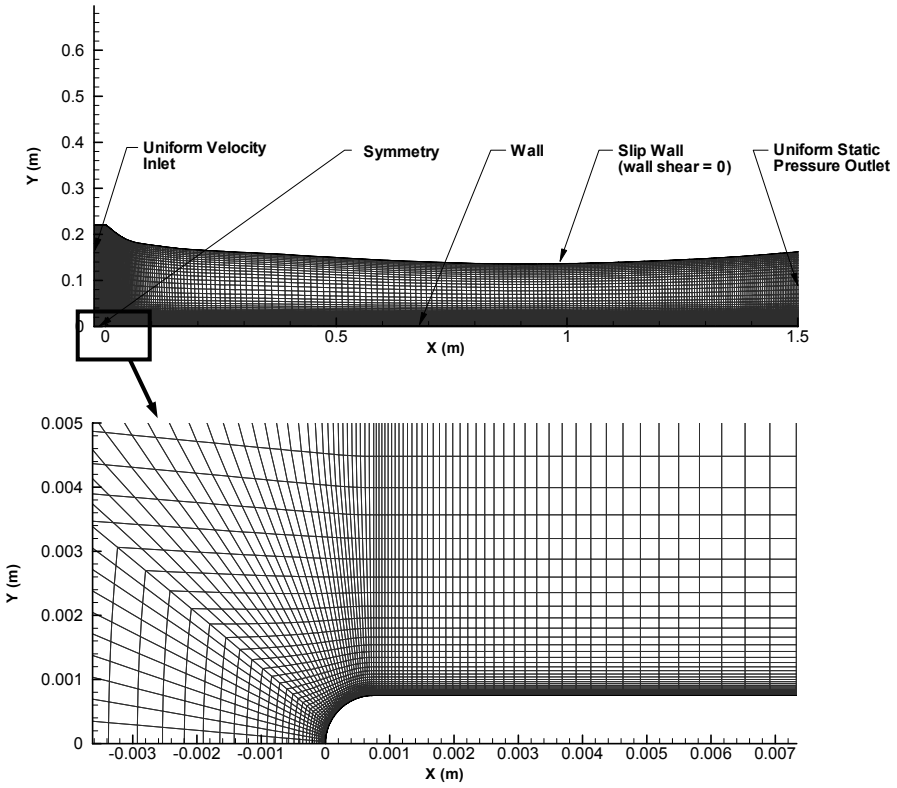

Figure 4.4 Flat plate mesh used to compute the T3C4 test case (top) along with a close up of the leading edge region (bottom).

4.2 Results: Zero Pressure Gradient Test Cases

The skin friction computed by the boundary layer code for the ERCOFTAC T3B, T3A, T3A- and the Schubauer and Klebanoff test cases is shown in Figures 4.5-4.8. These test cases had leading edge freestream turbulence intensities of 6.5%, 3.3%, 0.87% and 0.3% percent respectively. As a result the transition location moves downstream for lower freestream turbulence intensities. In general, the agreement with the experimentally measured skin friction and transition locations is good. The model was able to predict transition from a Reynolds number of 50,000 all the way out to 3 million as the freestream turbulence was lowered.

The T3 cases are particularly difficult because the freesteam turbulence is not constant and varies rapidly along the length of the flat plate. For the high turbulence intensity case (T3B) the laminar skin friction tends to be over-predicted. This is due to the large values of freestream eddy viscosity that had to be specified in order to obtain the correct decay rate of turbulence intensity with streamwise distance.

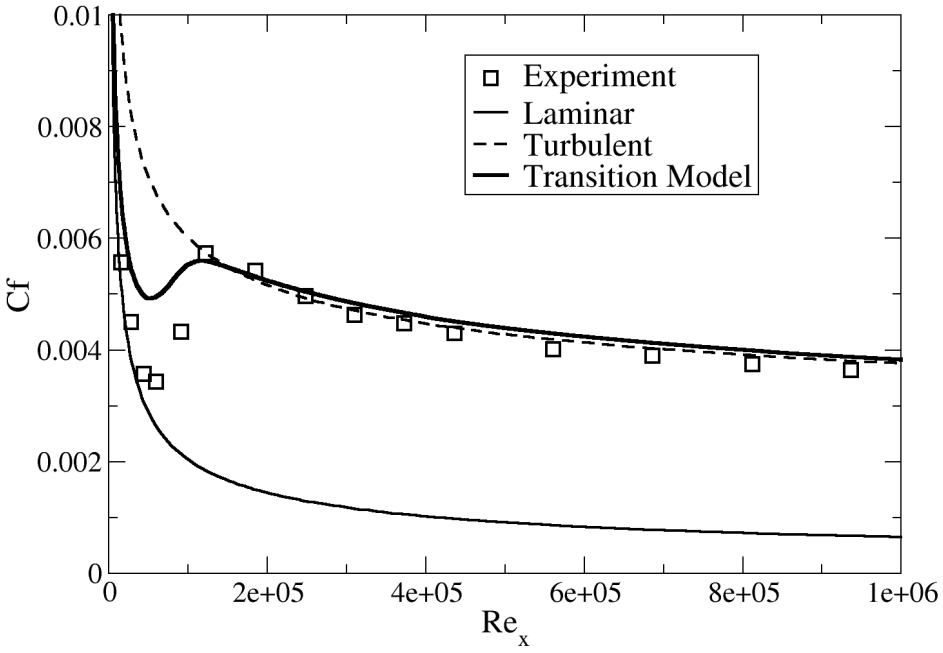

Figure 4.5 T3B test Case (FSTI = 6.5 percent)

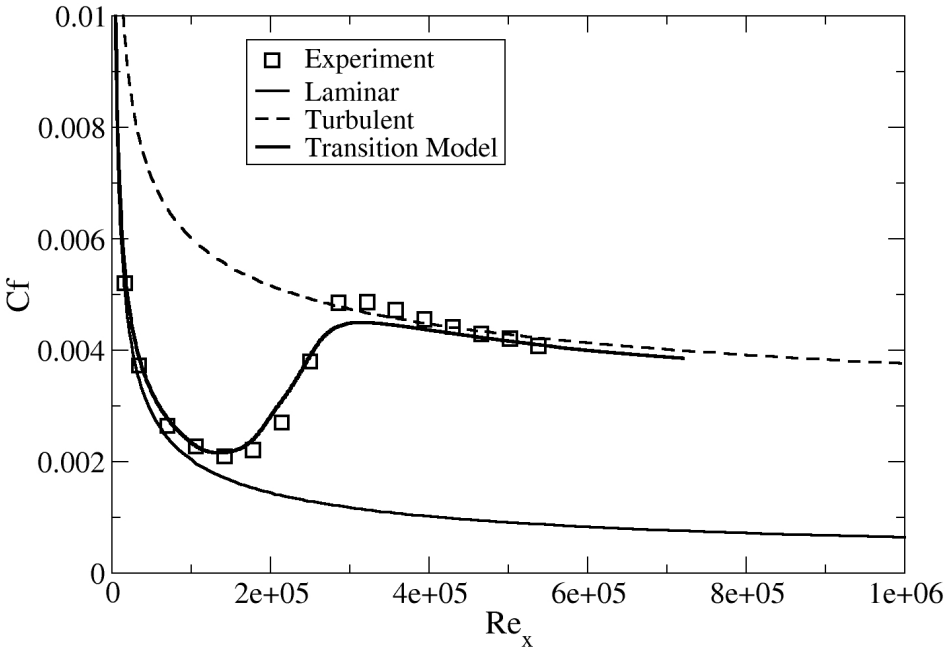

Figure 4.6 T3A test case (FSTI = 3.3 percent)

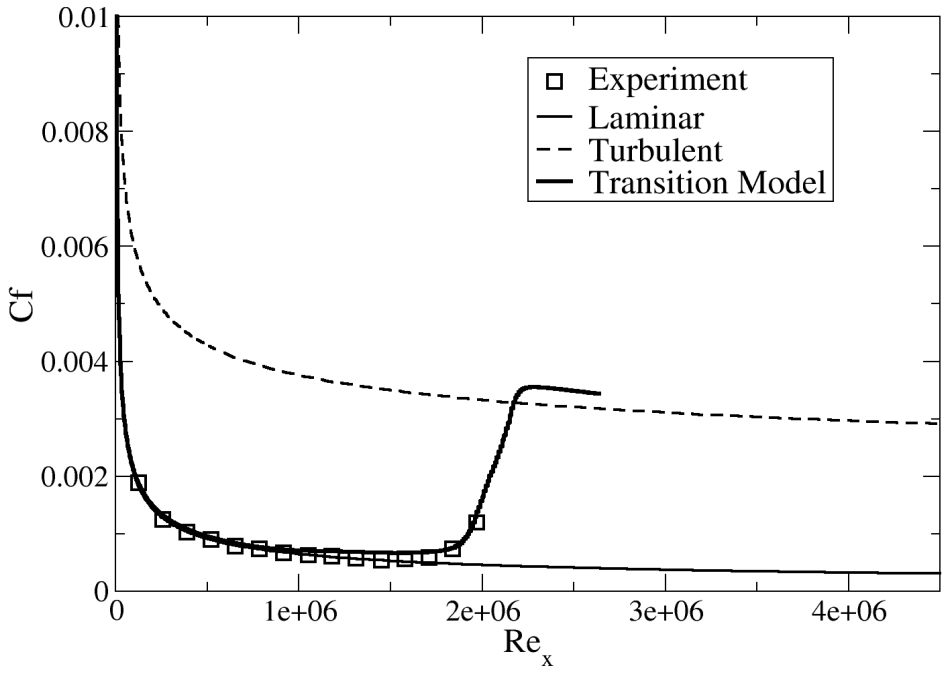

Figure 4.7 T3A- test case (FSTI = 0.874 percent)

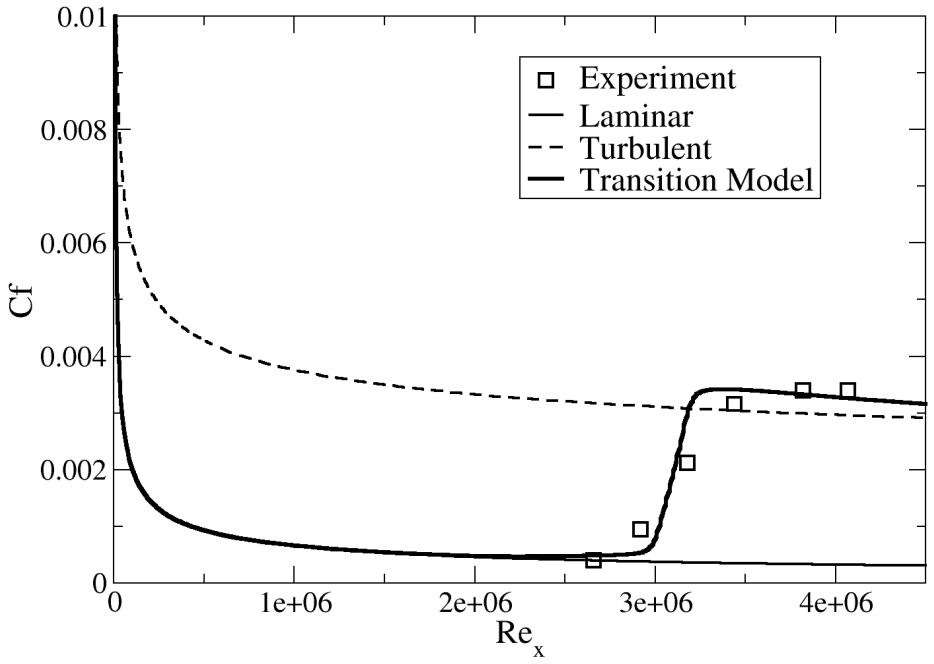

Figure 4.8 Schubauer and Klebanoff test case (FSTI = 0.3 percent)

The results of the hysteresis check are shown in Figure 4.9. The check was performed for the T3A case using CFX-5 and the grid shown in Figure 4.3 and was done by initializing the flow quantities based on the laminar solution, the fully turbulent solution and also by specifying the inlet conditions (i.e. velocity = 5.4 m/s, Tu = 3.3 and μ_t/μ = 12) as uniform values everywhere in the starting flow field. The final converged solutions were then compared to see if there were any differences that would indicate a sensitivity to the initial starting conditions (see Figure 4.9). The transition model does not appear to have any significant hysteresis and is therefore independent of the initial conditions. This check was performed with an older version of the transition model and as a result the predicted skin friction is slightly different than the results obtained with the present version for the T3A test case (see Figure 4.6).

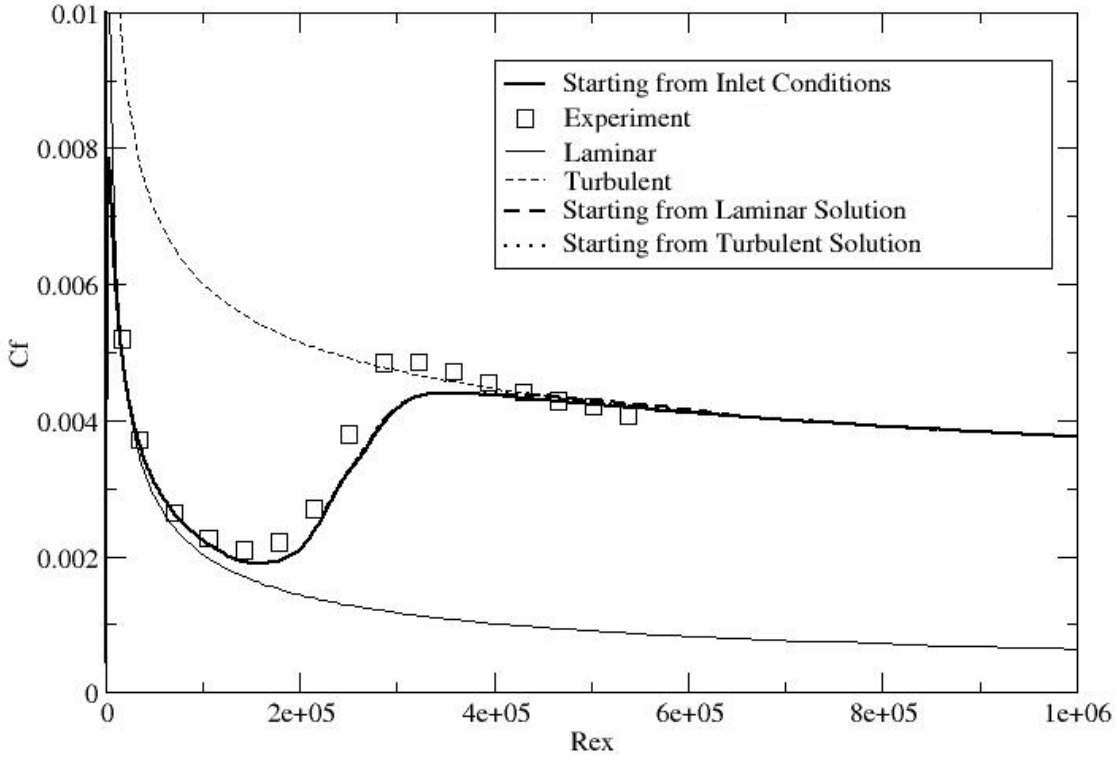

Figure 4.9 Hysteresis check using different initial conditions for the turbulence field.

4.3 Results: Pressure Gradient Test Cases

The computed skin friction coefficient for the T3C5 test case is compared to the experimental data in Figure 4.10. Also shown for comparison is the fully laminar solution. For the T3C5 test case, the Reynolds number is high enough that the transition occurs in a favourable pressure gradient near the beginning of the flat plate. The onset of transition was predicted slightly downstream of the experimental location. Because of the strong favourable pressure gradient the transition length is somewhat elongated and the model captures this effect in reasonably satisfactory agreement with the experiment.

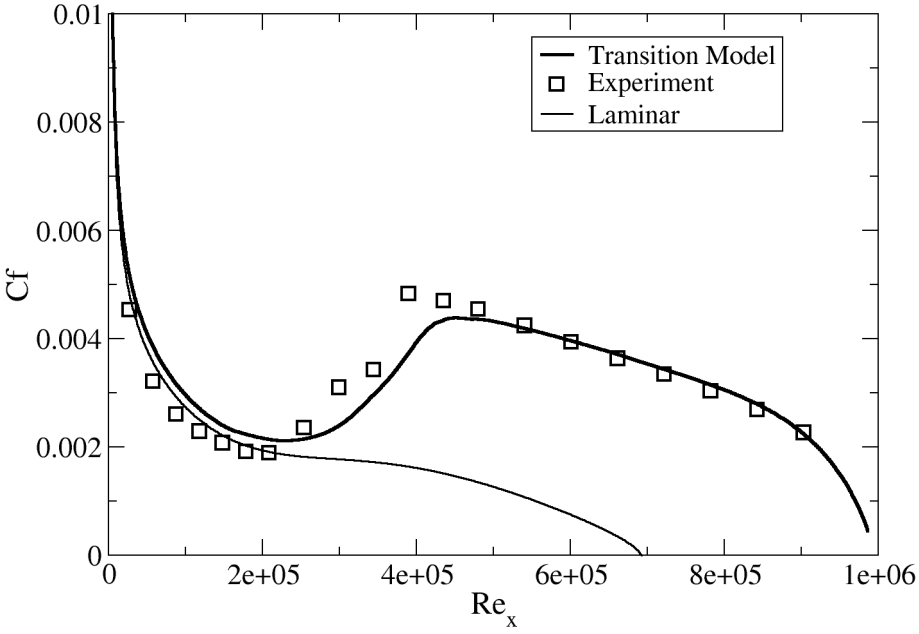

Figure 4.10 Predicted skin friction (Cf) for the T3C5 test case (transition in a favorable pressure gradient).

The results for the T3C2 test case are shown in Figure 4.11. The Reynolds number for this case is lower than T3C5 and as a result the transition location moves downstream. The experimental start of transition in the T3C2 case occurs near the suction peak imposed by the opposite wall (approximately 0.9 m downstream of the leading edge) and the end of transition occurs in an adverse pressure gradient. Again the onset of transition was predicted slightly downstream of the experimental location. However, in the adverse pressure gradient region the predicted transition length is shorter and as a result the model predicts the end of transition in the same location as in the experimental data.

The Reynolds number for the T3C3 case was even lower than the T3C2 case. As a result, the experimental start and end of transition occurs in an adverse pressure gradient. The predicted skin friction is compared to experiment in Figure 4.12. Both the predicted onset and length of transition are in excellent agreement with the experiment.

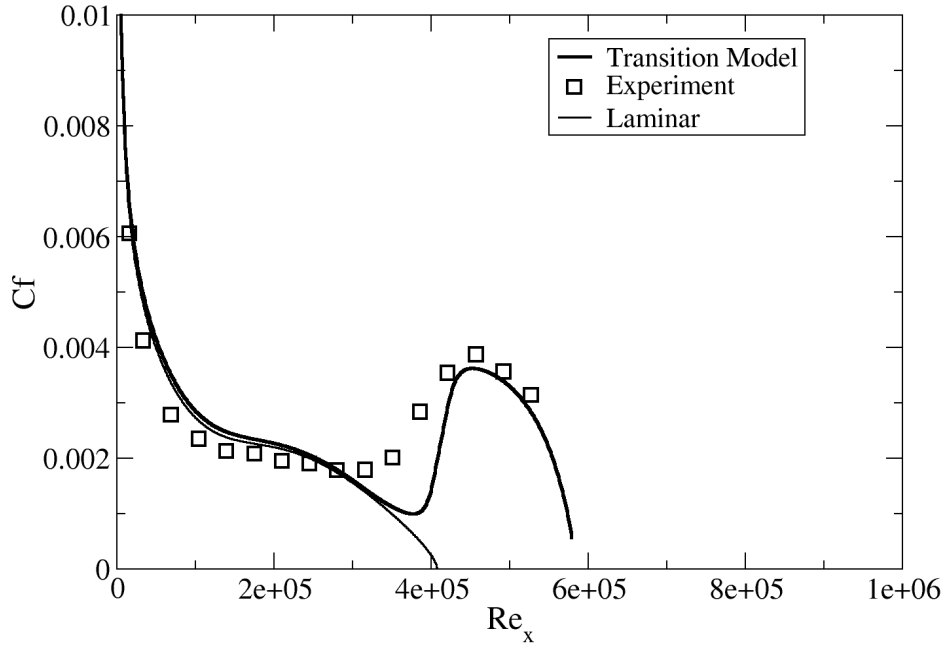

Figure 4.11 Predicted skin friction (Cf) for the T3C2 test case (transition near the suction peak).

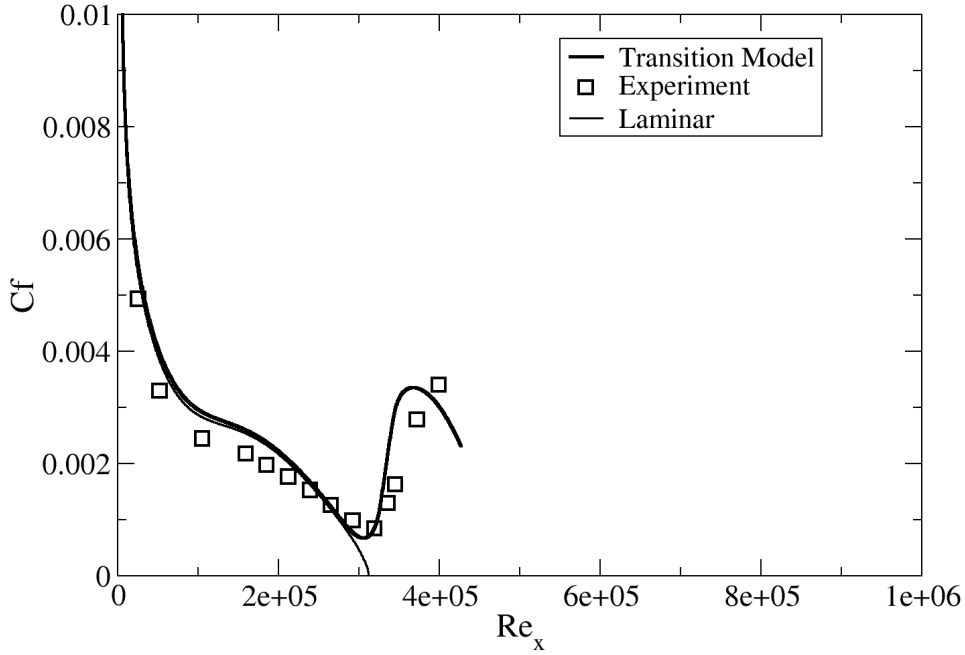

Figure 4.12 Predicted skin friction (Cf) for the T3C3 test case (transition in an adverse pressure gradient).

For the last T3C test case, T3C4, the Reynolds number is so low that the laminar boundary layer separates at a Re_x of 129 000, undergoes separation-induced transition and then reattaches as a turbulent boundary layer. Because there is a laminar separation this case was computed with the Navier-Stokes code CFX-5 using the grid shown in Figure 4.4. The predicted skin friction for the T3C4 test case is shown in Figure 4.13 and is in good agreement with the experimental data. This test case was actually used to calibrate the modification for separation induced transition which is described in Chapter 3. The velocity vectors from the laminar separation to the turbulent reattachment are shown in Figure 3.9.

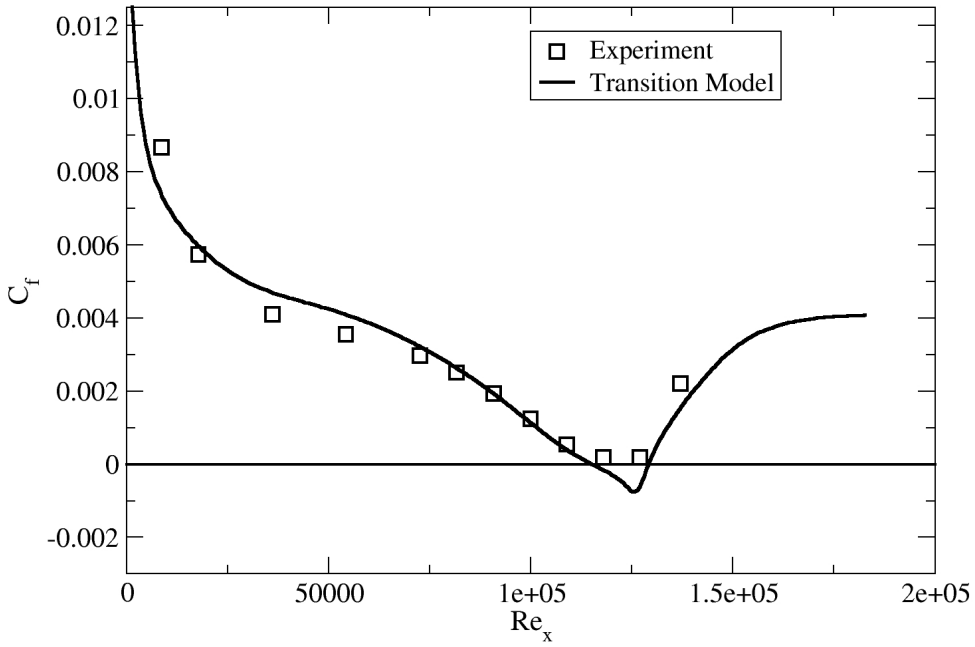

Figure 4.13 Predicted skin friction (Cf) for the T3C4 test case (separation induced transition)

The last test case in this chapter is used to investigate the transition model's ability to predict relaminarization. According to Mayle (1991), relaminarization should occur in a strong favourable pressure gradient when the acceleration parameter ($K = (\nu/U^2)dU/dx$) exceeds 3×10^{-6}. Conversely, transition should never occur until the acceleration parameter drops below 3×10^{-6}. A hypothetical test case has been proposed in order to test the ability of the new transition model to predict relaminarization. The test case is identical to T3A until a Reynolds number of $Re=3\times10^5$, at which point a strong favourable pressure gradient is imposed (see Figure 4.14) in the boundary layer code. The skin friction calculated by the boundary layer code for the laminar, transitional and turbulent cases are shown in Figure 4.15. From Figure 4.15 the model does in fact predict relaminarization once the acceleration parameter exceeds 3×10^{-6}. It also predicts retransition downstream once the strong favourable pressure gradient has subsided. However, since this was a hypothetical testcase, in the future the model will need to be validated against an actual experiment where relaminarization was present.

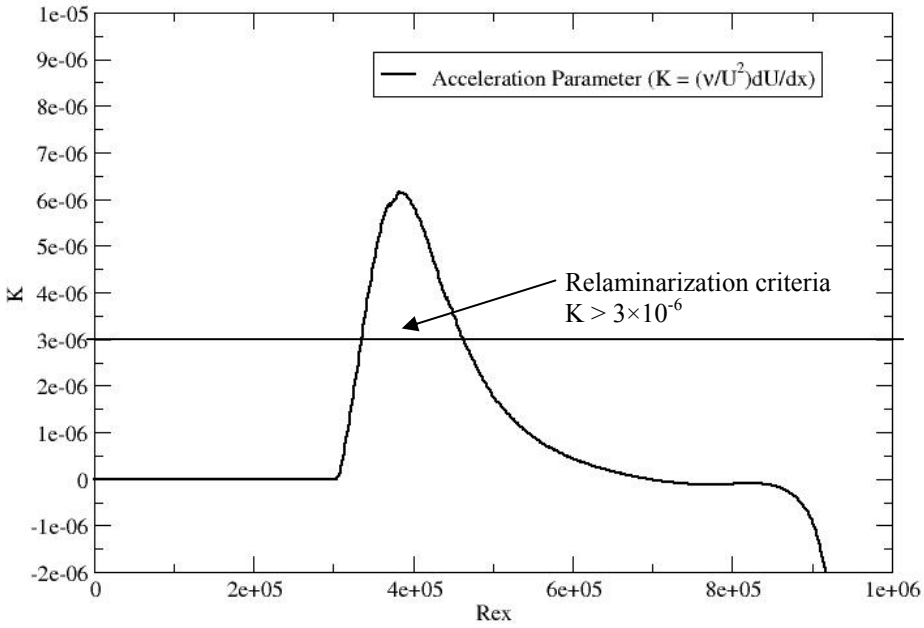

Figure 4.14 Acceleration parameter (K) for the relaminarization test case.

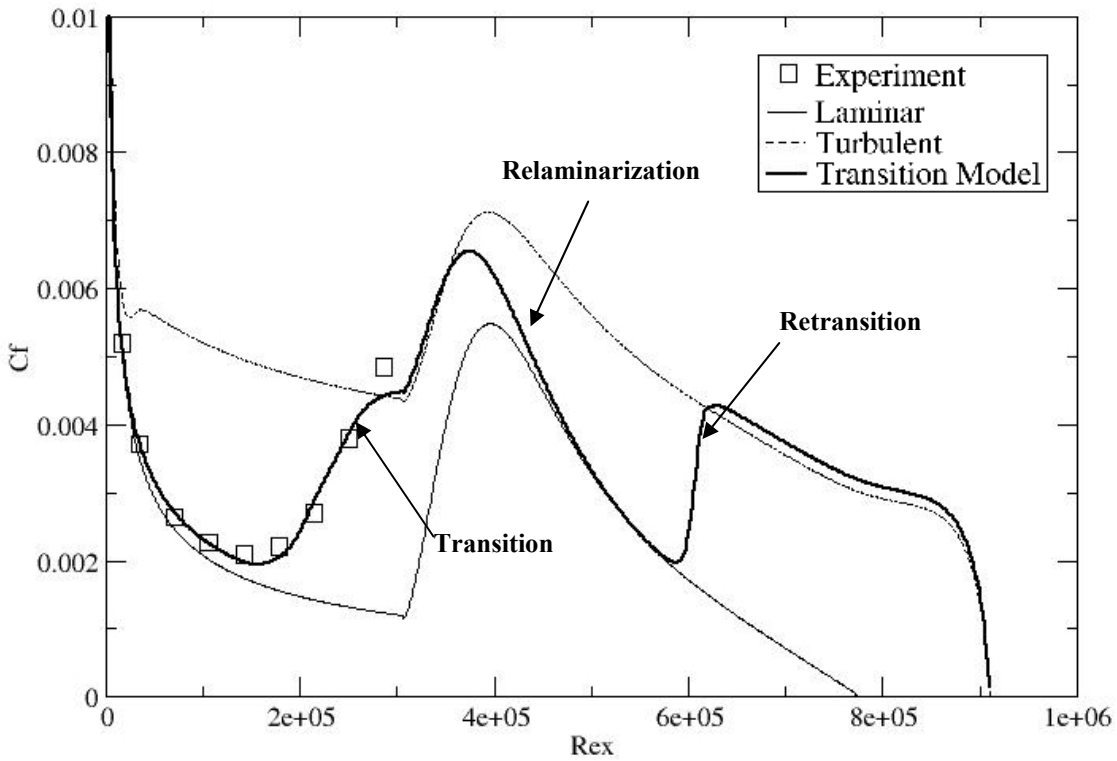

Figure 4.15 Predicted skin friction for the hypothetical relaminarization test case.

This concludes the flat plate validation chapter of the new transition model. The model has been shown to predict with reasonable accuracy the combined effects of freestream turbulence, strong pressure gradients and separation on transition. It has also been shown that the model does not suffer from any hysteresis in the predicted transition location which is an important criteria for predicting unsteady-state transition effects. Finally the model has been shown to predict relaminarization at the experimentally observed acceleration parameter (K) of 3×10^{-6} (Mayle, 1991). The remainder of this thesis will focus on validating the transition model for both 2D and 3D test cases of increasing complexity.

Chapter 5
2D Test Cases

5.1 Introduction

This chapter describes the results obtained with the transition model for a variety of 2D aeronautical and turbomachinery flows. The 2D aeronautical test cases include the Aerospatiale A airfoil (Chaput, 1997), GE wind turbine airfoil (Langtry et al., 2004), the McDonnell Douglas 30P-30N 3-element flap configuration (Klausmeyer and Lin, 1997) and the drag crisis of a cylinder (Achenbach, 1968). For the wind turbine airfoil the transition model predictions have been extensively validated against the X-Foil (Drela and Giles, 1987) code and the available experimental data at various angles of attack. X-Foil uses an e^n method for transition prediction and is regarded as one of the best tools available for predicting natural transition on airfoils. The 2D turbomachinery test cases include a high-pressure turbine stator vane (Genoa, Ubaldi et al 1996), highly loaded compressor cascade (Zierke and Deutsch, 1989), a low-pressure turbine blade (Pak-B, Suzen et al., 2003), a transonic turbine guide vane cascade (VKI MUR, Arts et al. 1990) and unsteady transition due to wake impingement (T106, Steiger et al, 2003). All simulations have been computed with CFX-5.

The best practice grid guidelines for the transition model (see Appendix) were used to generate all of the grids. As a result, the grids in the computations had a maximum y^+ of approximately one, wall normal expansion ratios between 1.1 and 1.2 and at least 100 nodes were present in the streamwise direction in order to properly resolve the laminar, transitional and turbulent boundary layers. A summary of the inlet conditions for all the test cases described in this chapter is given in Table 5.1. Where possible, the inlet turbulence levels were specified in order to match the experimentally measured freestream turbulence intensity. If the freestream turbulence was not known in the experiment than an educated guess was made for the inlet values such that at the leading edge of the body the values were representative of a typical wind tunnel. For the aeronautical cases, the decay of freestream turbulence as it convects downstream from the inlet to the body typically caused the local value near the leading edge of the body to be less than half of the inlet FSTI value quoted in Table 5.1.

Case	$Re_x = \rho c U_o/\mu$ ($x10^6$)	Mach $= U_o/a$ where speed of sound (a) $= (\gamma RT)^{0.5}$	Chord (c) (m)	FSTI (%)	μ_t / μ
Aerospatiale A Airfoil	2.1	0.15	0.6	0.2	10
Wind Turbine Airfoil	4.0	0.22	0.8	0.1	10
30P-30N Flap, AoA = 8.1°	9.0	0.2	0.5588	0.6	2.5
Drag Crisis of a Cylinder	0.05 – 2.0	0.1	0.3	0.3	5
Genoa Turbine Blade	0.36	0.08	0.1973	1.5	1.5
Zierke and Deutsch Compressor Incidence = -1.5°	0.47	0.1	0.2152	0.18	2.0
Pak-B Low-Pressure Turbine Blade	0.05, 0.075, 0.1	0.03	0.075	0.08, 2.35, 6.0	6.5 - 30
VKI MUR Transonic Guide Vane	0.26	Inlet: 0.15 Outlet: 1.06	0.037	1.0, 6.5	11, 1000
T106 Cascade Unsteady Wake/Blade Interaction	0.078	0.02	0.17	0.1	1.0

Table 5.1 Inlet conditions for the 2D test cases.

5.2 Aeronautical Test Cases

5.2.1 Aerospatiale A Airfoil

The Aerospatiale A airfoil was designed at Aerospatiale in 1986 and was tested in the ONERA F1 1.5 by 3.5 m wind tunnel (Chaput, 1997). It should also be noted that a second experiment has since been performed in the F2 wind tunnel and somewhat different results were obtained for this airfoil with respect to lift, drag as well as pressure and skin friction distributions. The F1 results at 13.3° angle of attack are widely accepted as the most accurate with the exception of the trailing edge velocity profiles, which are believed to be more accurate in the F2 results (Haase et al., 1997). Consequently, in this thesis the F1 results are used for all of the comparisons with the exception of the velocity profiles, which are based on the F2 data. The grid used for the present computation is shown in Figure 5.1 and consists of approximately 130 000 nodes.

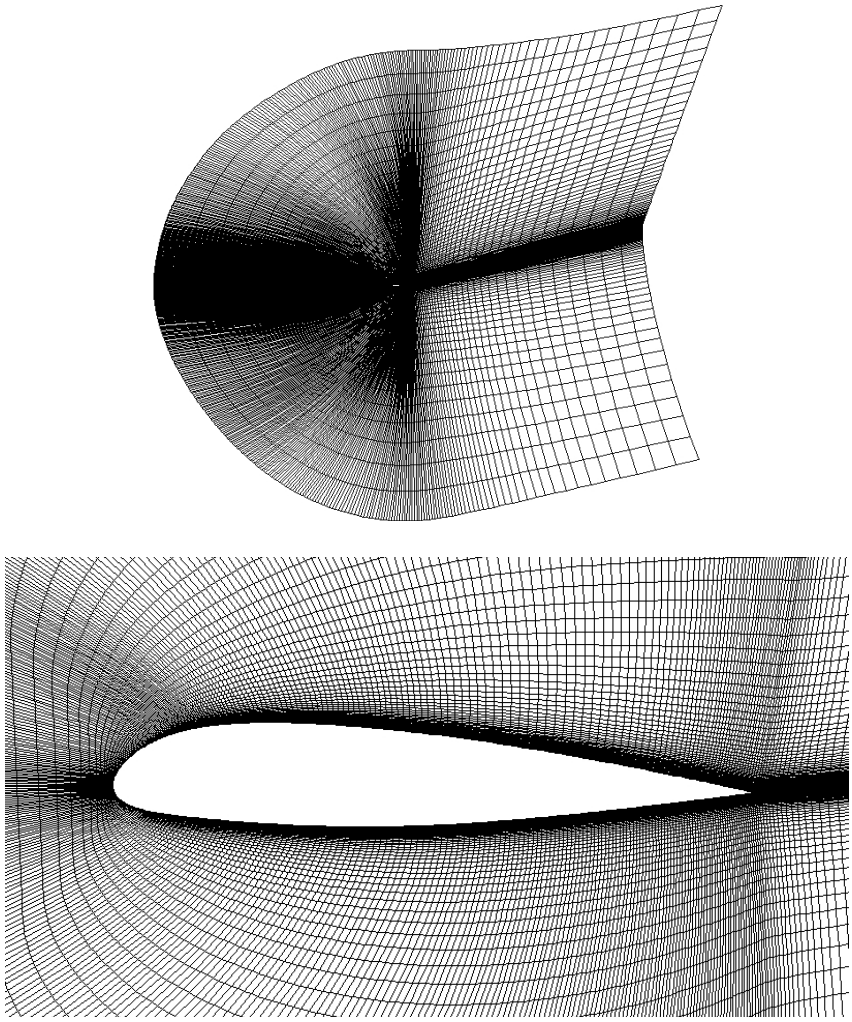

Figure 5.1 Grid used for the Aerospatial A computations (top) and close up of the same grid near the airfoil (bottom).

The Aerospatiale A airfoil has been the subject of a vast number of validation exercises (see for example Haase et al., 1997). This experiment is a particularly interesting test case for a transition model because there were no boundary layer trips placed on the suction side of the airfoil. Consequently, a laminar boundary layer develops and terminates in a laminar separation bubble at 12% of chord (see Figure 5.2) near the suction peak. This separation bubble causes separation-induced transition which then results in a turbulent boundary layer developing downstream. At the trailing edge, the turbulent boundary layer eventually separates due to the large adverse pressure gradient there. In RANS computations the laminar region is usually modeled by disabling the turbulence model up to the 0.12 chord position. A notable achievement was that LES computations performed by Mary and Sagaut (2002) who were able to actually predict the transition at the 0.12 chord position and the subsequent boundary layer development downstream.

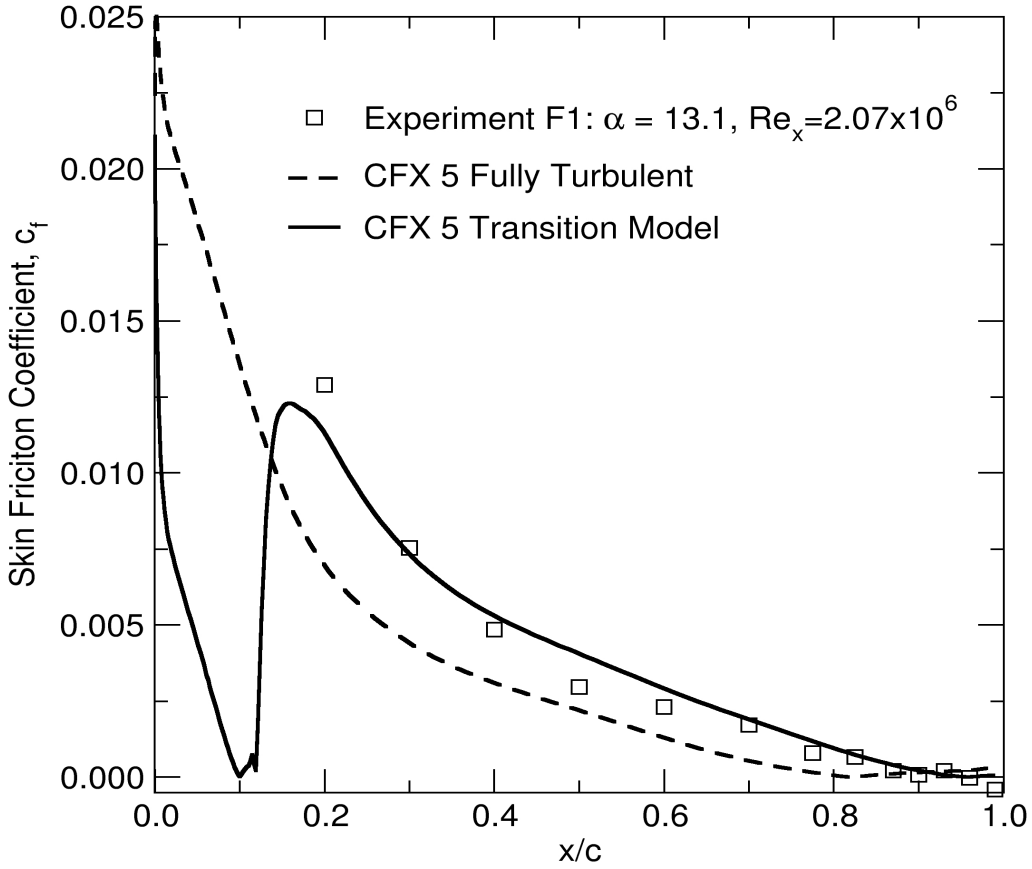

Figure 5.2 Skin friction on the suction side of the Aerospatial A Airfoil.

The pressure distribution obtained with the transition model is shown in Figure 5.3. The agreement with the experimentally measured pressure distribution is very good except in the trailing edge region where the flow separates in the experiment and remains attached (although just barely) in the transitional prediction. This can be seen clearly in boundary layer velocity profiles near the trailing edge shown in Figure 5.4. Also shown in Figure 5.3 is the fully turbulent pressure distribution which appears to be under-predicted compared to the experiment except in the trailing edge region where interestingly enough, the agreement appears to be quit good. The velocity profile near the trailing edge obtained with the fully turbulent computation also appears to be in better agreement with the experiment.

The lift and drag coefficients obtained with the transition model are 1.5706 and 0.1856 respectively. This compares quit well with the experimentally measured values of 1.562 and 0.0208. The fully turbulent solution under-predicted the lift and drag coefficients and gave values for the lift coefficient of 1.4531 and the drag coefficient of 0.1654.

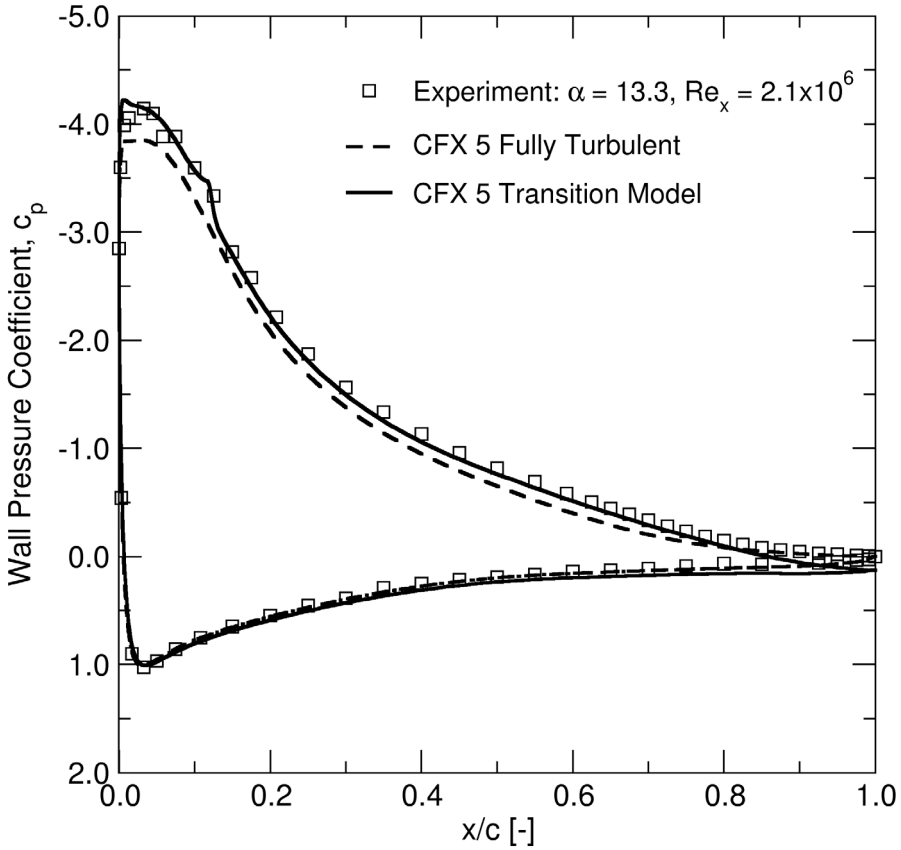

Figure 5.3 Pressure distribution around the Aerospatial A Airfoil.

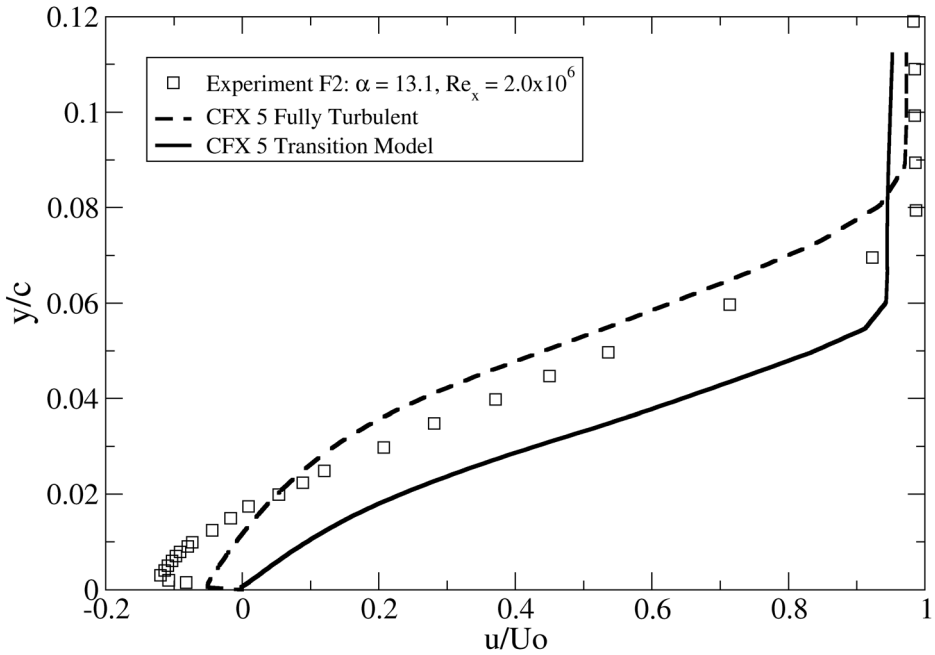

Figure 5.4 Velocity profiles near the trailing edge (x/c = 0.96) for the Aerospatial A Airfoil.

The differences between the transitional and fully turbulent solutions can be largely explained by the laminar flow on the leading edge, which alters the development of the boundary layer momentum deficit over the entire length of the airfoil. As a result, the fully turbulent solution actually under-predicts the skin friction compared to the experiment (see Figure 5.2). This also results in an early separation on the trailing edge (at least based on the skin friction measurements). It can be seen in Figure 5.2 that the transition model does a good job predicting the separation-induced transition at 12% chord. In addition, the subsequent increase in skin friction appears to be in good agreement with the experimentally measured skin friction. The one exception appears to be in the trailing edge region where the separation is not captured properly be the transitional solution.

5.2.2 Wind Turbine Airfoil

The testcase geometry is a 2D airfoil section, as typically used for GE wind-turbine blades. It operates in a low FSTI environment with a turbulence intensity of only around 0.1 percent at the leading edge. As a result, natural transition occurs on both the suction and pressure surfaces. This test case has already been computed in Langtry et al. (2004) with some deviations from the experiments. The main issues in the previous study were that the transition location was too far upstream by about 5% chord and the drag was poorly predicted, particularly at the higher angles of attack. The deficiency in the onset predictions was largely related to the empirical correlations for transition onset in the low turbulence intensity regime. This was not surprising, as the transition model was original developed primarily for predicting bypass transition in turbomachinery flows. In order to improve the predictions of natural transition, the empirical correlation for transition onset in this thesis has been re-calibrated for both low and high turbulence intensities. The poor predictions of the drag coefficient were caused by inadequate grid resolution in the wake region of the airfoil. In the present thesis a refined grid has been used, resulting in much better drag predictions for all angles of attack. Further grid refinement did not have any significant effect on the predicted drag coefficient. The refined grid consisted of 160 000 nodes and is shown in Figure 5.5.

The inlet values for the turbulence intensity and viscosity ratio have been selected in order to match the transition location at zero angle of attack. They have then been kept at these values for all other angle of attack simulations. A similar calibration for wind-tunnel conditions is typically done with the e^n method as well. The transition locations vs. angle of attack predicted by the transition model are shown in Figure 5.6 (top). Wind tunnel results and XFOIL (v6.8) predictions (where transition is predicted by the e^N method) are plotted for comparison. The experimental data were obtained using a

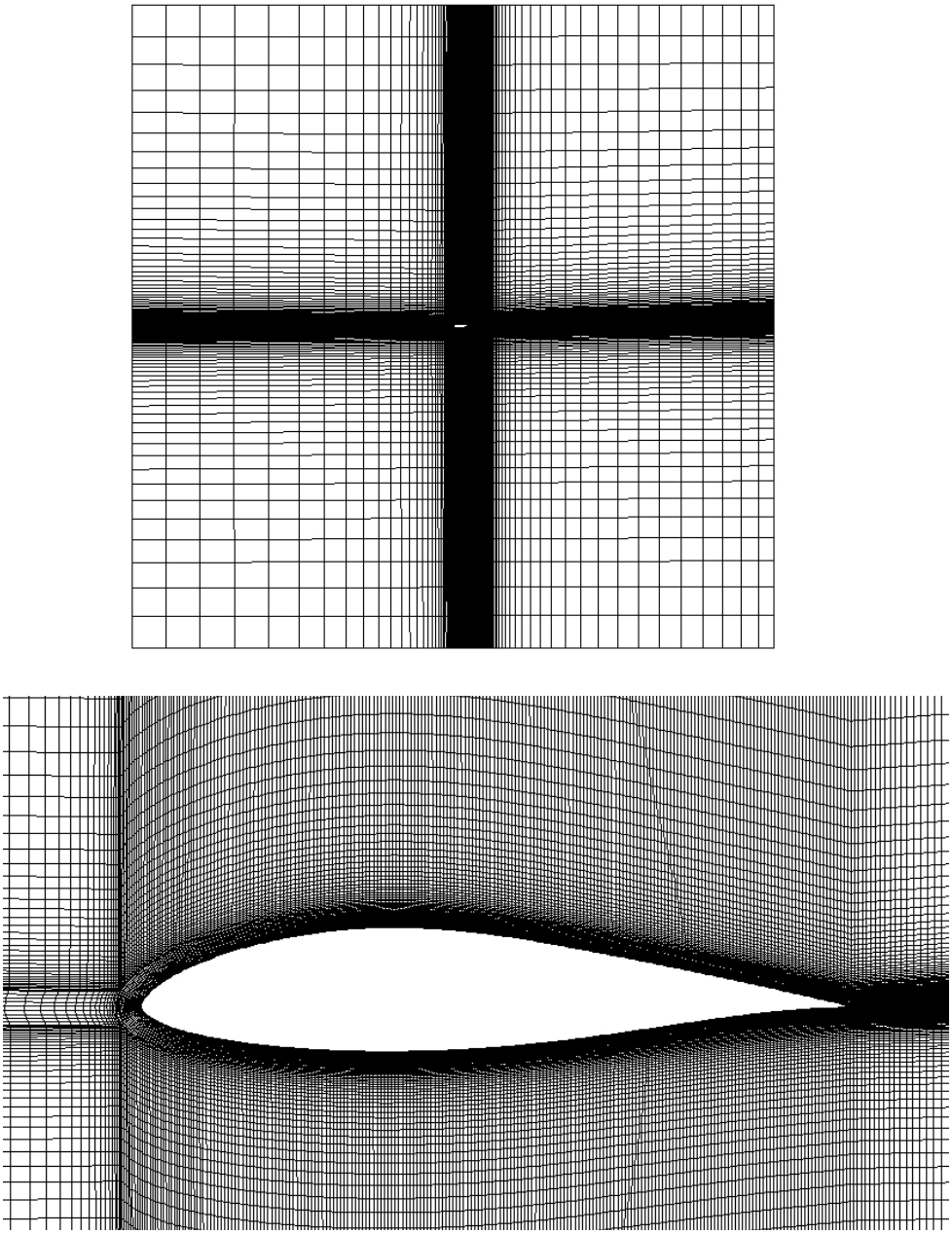

Figure 5.5 Grid used for the wind turbine airfoil computations (top) and close up of the same grid near the airfoil (bottom).

stethoscope method. At the moderate angles of attack transition occurs on both the suction and pressure side due to a small laminar separation bubble that acts like a transition trip. At the higher angles of attack Natural transition occurs before the laminar boundary separates and the flow remains attached. With the new empirical correlations, the transition model captures the dependence of the transition location on the angle of attack in very good agreement with the data. Figure 5.6 (bottom) shows the predicted drag coefficient as a function of angle of attack. Included are wind tunnel measurements

as well as results from a transitional computation using the XFOIL code and from fully turbulent simulations. The drag coefficient predictions from the transitional computation are also in very good agreement with the experimentally measured drag. The scale on the y-axis has been purposely omitted because the experimental drag values are proprietary to GE.

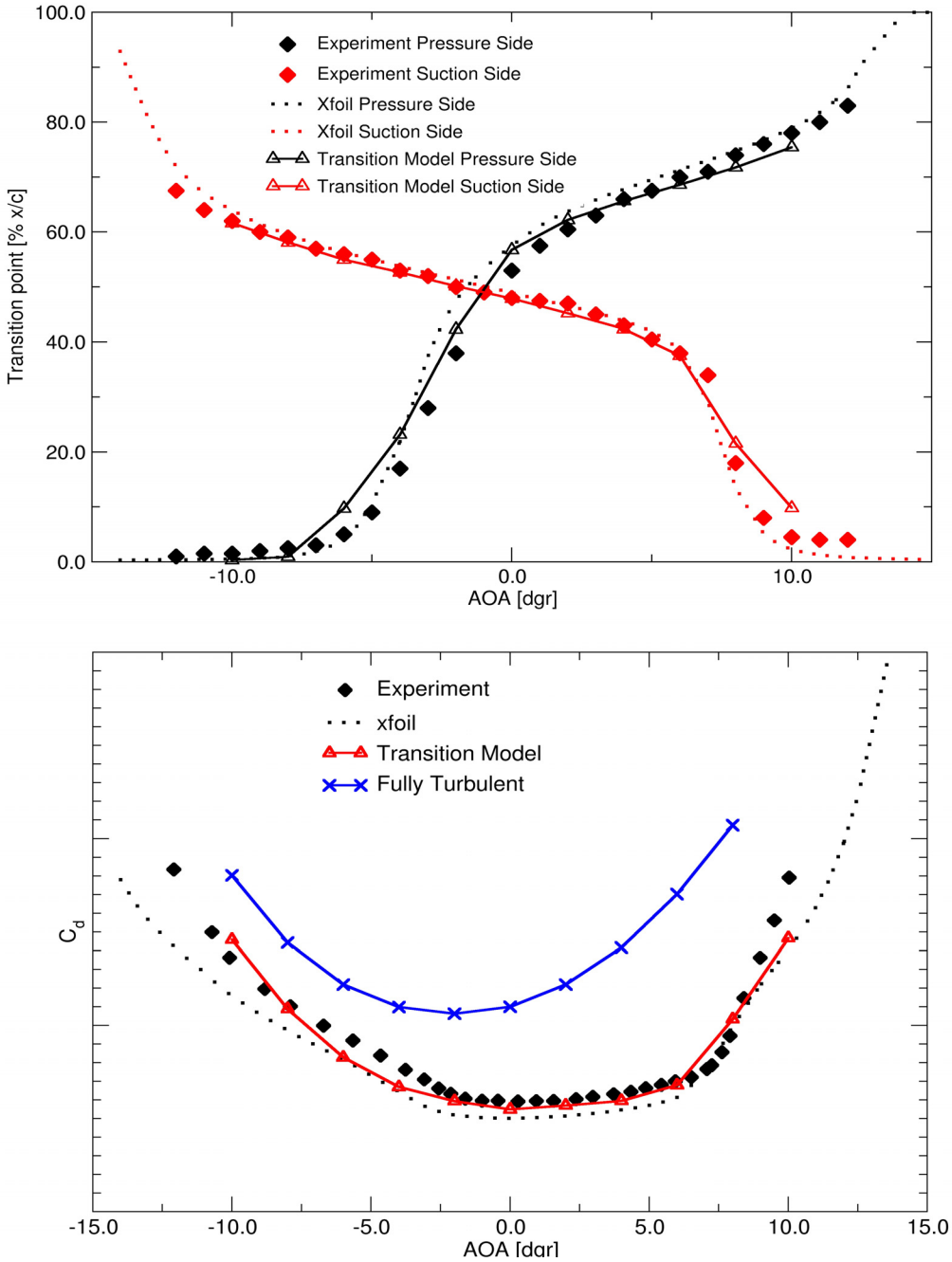

Figure 5.6 Predicted transition location (top) and drag coefficient (bottom) as a function of angle of attack for the wind turbine airfoil.

5.2.3 McDonald Douglas 30P-30N Flap

The McDonald Douglas 30P-30N flap configuration was originally a test case for the High-Lift Workshop/CFD Challenge that was held at the NASA Langley Research Center in 1993 (Klausmeyer and Lin, 1997). It is a very challenging test case for a transition model because of the large changes in pressure gradient and the local freestream turbulence intensity around the various lifting surfaces. The experiment was performed in the Langley Low Turbulence Pressure Tunnel and the transition locations were measured using hot films on the upper surface of the slat and flap and on both the upper and lower surfaces of the main element (Rumsey et al., 1998). The skin friction was also measured at various locations using a Preston tube (Klausmeyer and Lin, 1997). For the present comparison the Reynolds number of $Re = 9\times10^6$ and an angle of attack of $\alpha=8°$ was selected. Based on the best practice grid guidelines the resultant grid used for the computation consisted of 500 000 nodes and is shown in Figure 5.7.

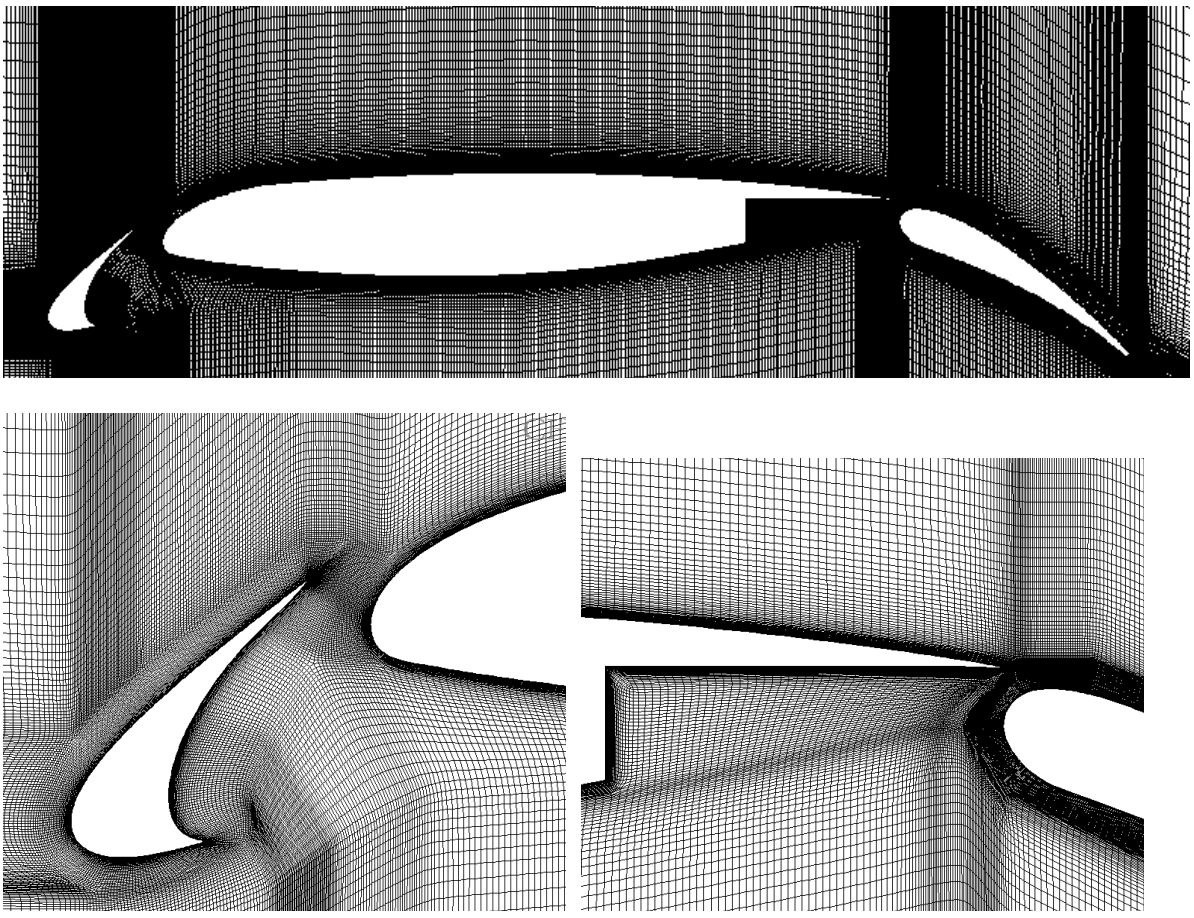

Figure 5.7 Close up of the grid used to compute the McDonald Douglas 30P-30N flap test case.

The predicted streamlines around the flap are shown in Figure 5.8. Clearly visible are three regions of re-circulating flow on the pressure side of the slat, the flap housing in the main element and the trailing edge of the flap.

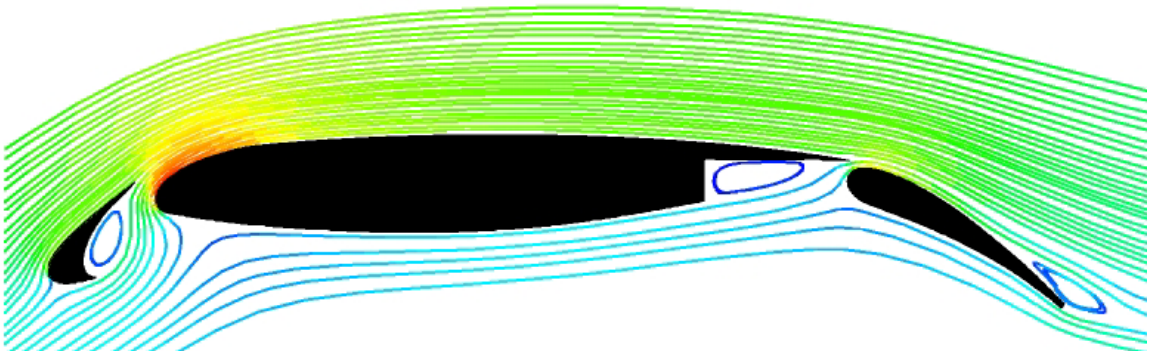

Figure 5.8 Predicted streamlines coloured by the local velocity around the McDonald Douglas 30P-30N flap.

A contour plot of the predicted turbulence intensity around the flap is shown in Figure 5.9. Also indicated are the various transition locations that were measured in the experiment (Exp.) as well as the locations that were predicted by the transition model (CFD). As no information was available on the freestream turbulence level in the experiment, the inlet turbulence values for this case were estimated so that the slat transition location matched the experiment. The transition locations on the main element and the flap are the outcome of selecting that freestream turbulence level. In the computations, the onset of transition was judged as the location were the skin friction first started to increase due to the production of turbulent kinetic energy in the boundary layer. In general the agreement between the measured and predicted transition locations is good. The worst error is on the lower surface of the main element where the predicted transition location was too far downstream by approximately 6% of the cruise airfoil chord, c.

The predicted skin friction on the upper surface of the flap is compared to the experimentally measured value in Figure 5.10. The predicted transition location is in reasonably good agreement with the experiment, however, the turbulent skin friction appears to have been slightly over predicted. This could be the result of transition being predicted slightly too far downstream on the flap surface, thereby shifting the virtual origin of the turbulent boundary layer. This would also effect the size of the trailing edge separation on the flap, which is most likely being under-predicted in the present results.

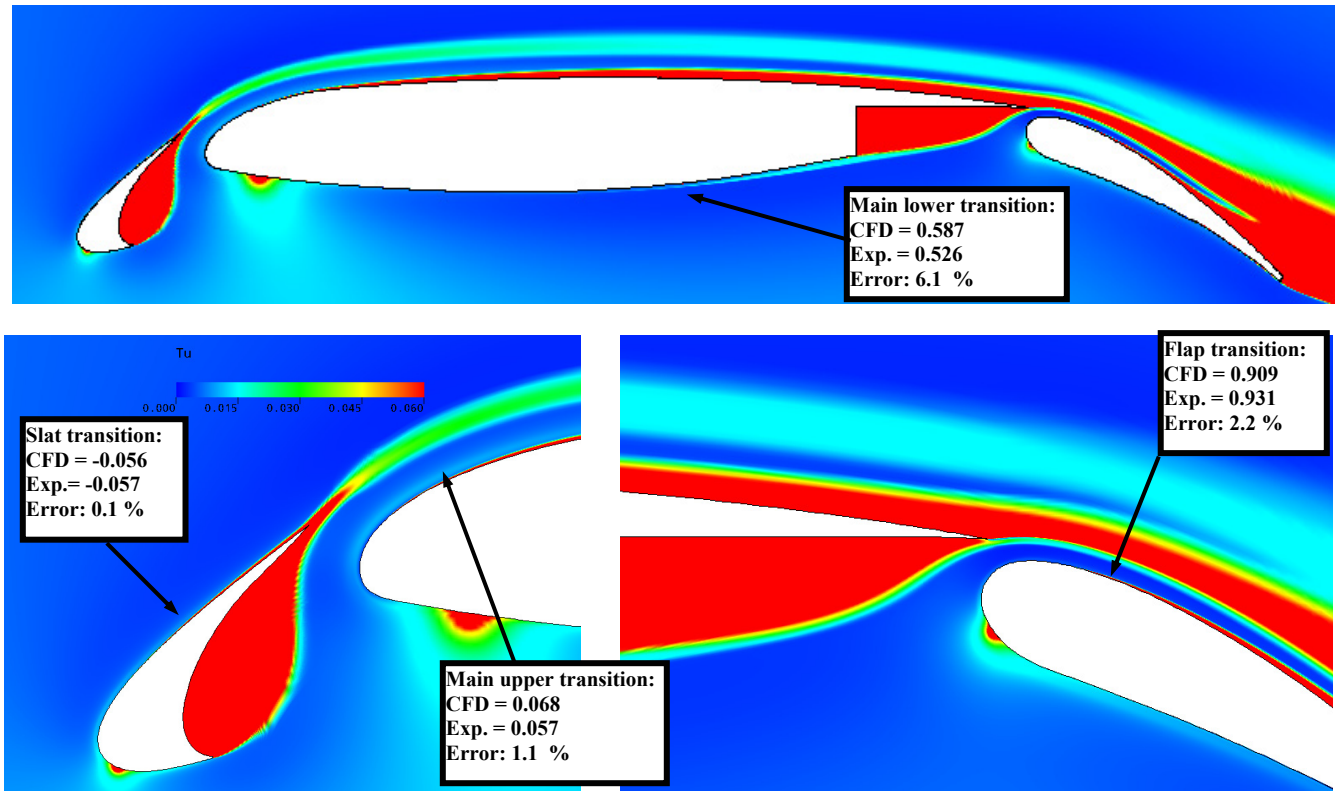

Figure 5.9 Contour of turbulence intensity (Tu) around the McDonald Douglas 30P-30N flap as well as the measured (Exp.) and predicted (CFD) transition locations (x/c) as a function of the cruise airfoil chord (c = 0.5588 m).

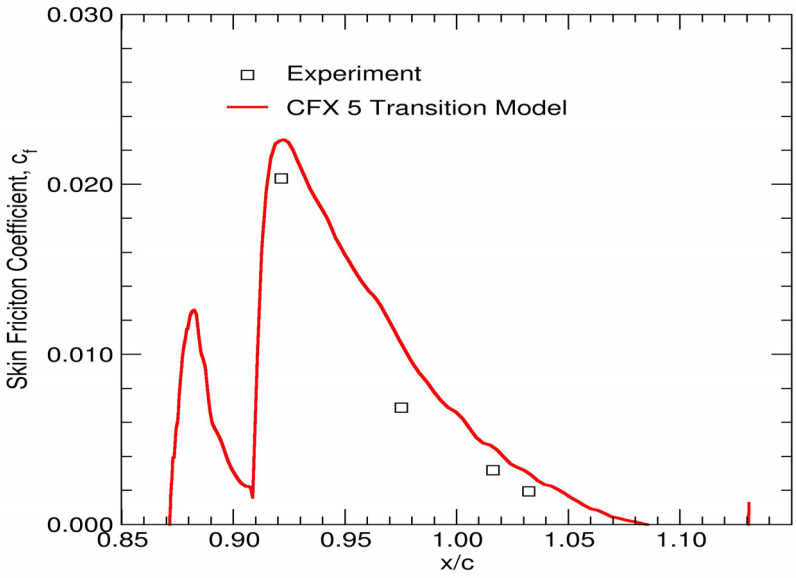

Figure 5.10 Skin friction on the upper surface of flap for the McDonald Douglas 30P-30N flap test case.

5.2.4 Drag Crisis of a Cylinder in Crossflow

One of the most challenging applications for any turbulence closure level is the prediction of the drag crisis of a cylinder in crossflow (see for example the LES results of Wang et al. 2001). Even on a RANS level, this simulation would require a fully unsteady-state simulation and most likely even a partial resolution of the 3D turbulent structures in the wake. In order to reduce the numerical effort, the current simulations with the transition model have been computed in unsteady-state mode on a 2D grid. The grid consisted of 183 000 nodes and is shown in Figure 5.11. Due to time constraints the fully turbulent simulations have been obtained with symmetric steady-state simulations.

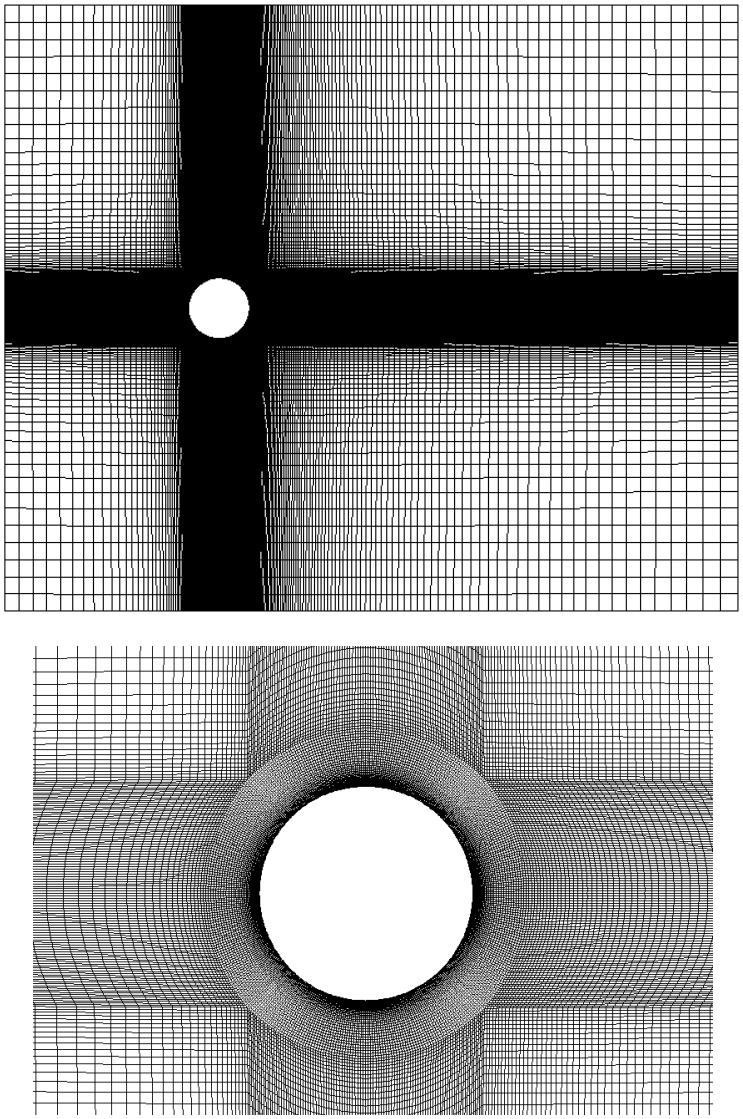

Figure 5.11 Grid used for the drag crisis of a cylinder computations (top) and close up of the same grid near the cylinder (bottom).

The predicted drag coefficient for a varying Reynolds number is shown in Figure 5.12. While the agreement with experiments is not perfect, it appears that the transition model can in principle predict the appropriate Reynolds number range at which the separation on the cylinder switches from a laminar separation to a turbulent one. For the present simulations, only about 30 time steps per vortex shedding period have been used in the unsteady simulations. It is possible that smaller time steps are required to properly capture the drag coefficient. However, what is more likely is that a hybrid RANS-LES approach such as Detached Eddy Simulation (DES) will be required to predict this case correctly. Instantaneous skin friction distributions predicted by the transition model for various Reynolds numbers are shown in Figure 5.13. The x-axis in Figure 5.13 is the cylinder arc length in degrees where –90° is the leading edge, 0° is the mid-chord location and +90° is the trailing edge. The results are for three different flow regimes, demonstrating laminar separation, laminar separation with turbulent reattachment and finally transition before the laminar separation point. It should be noted that these effects are beyond the ability of most engineering transition models in use today.

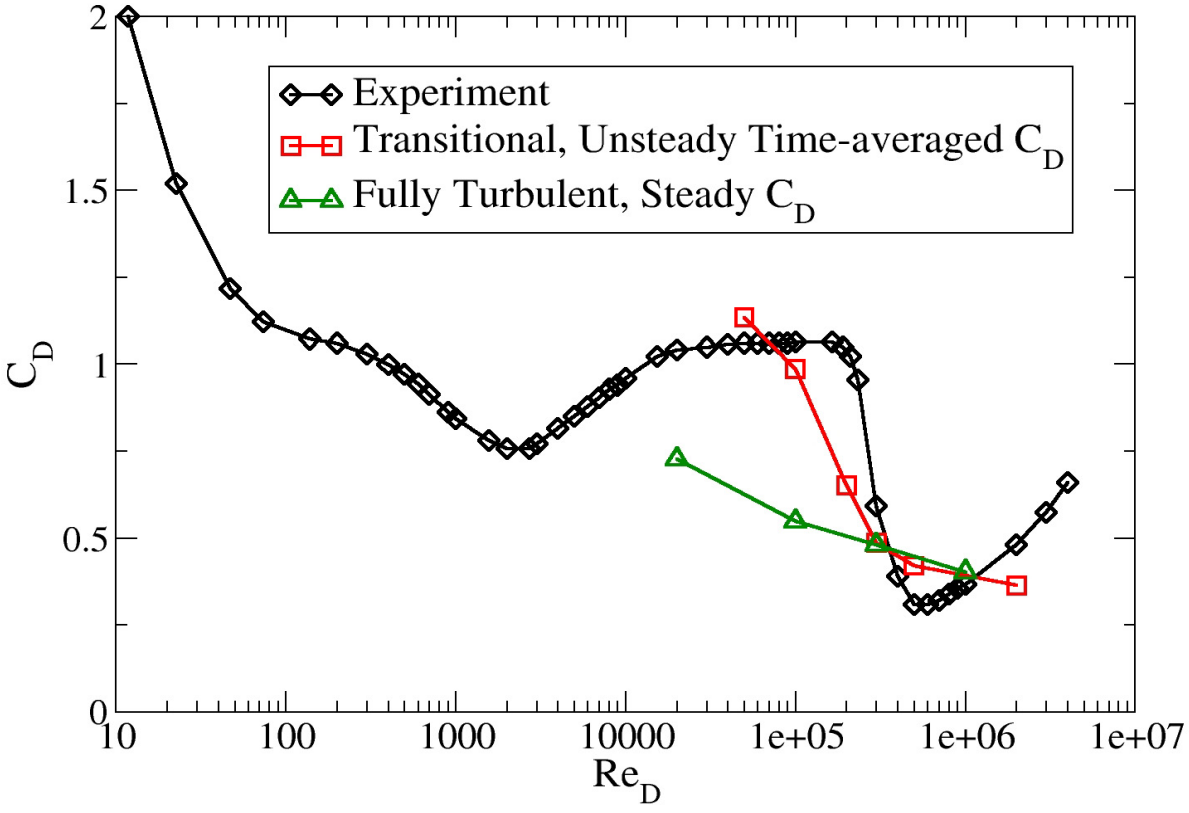

Figure 5.12 Drag crisis of a cylinder in cross-flow.

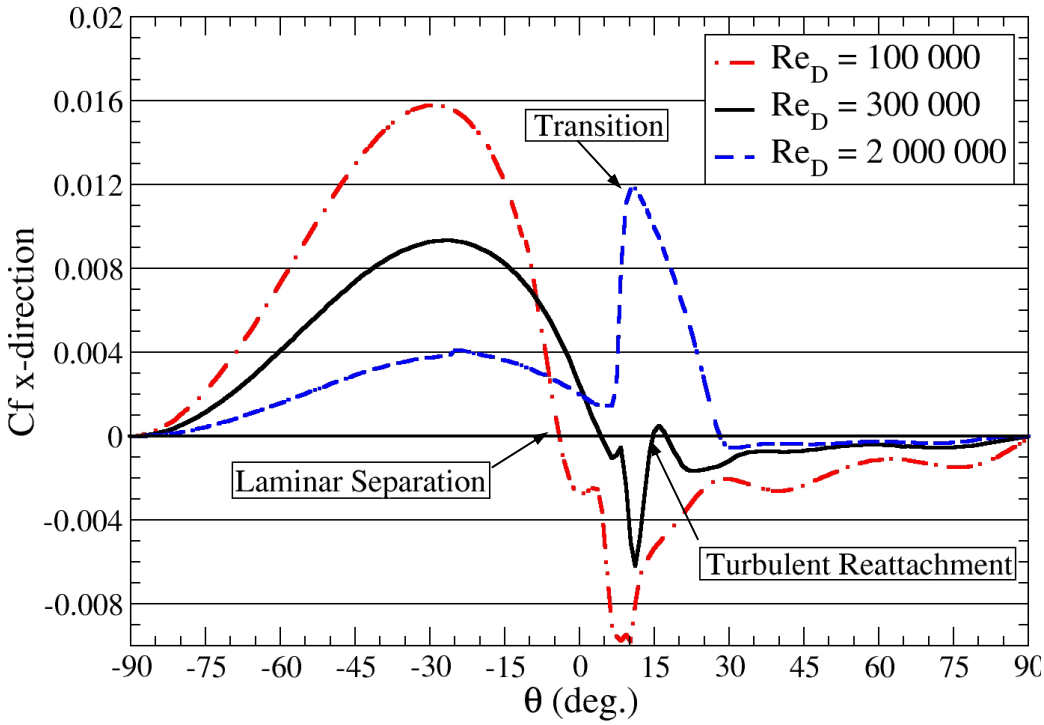

Figure 5.13 Predicted instantaneous skin friction, Cf, for a cylinder in cross-flow at Reynolds numbers (Re_D) of 100 000, 300 000 and 2 million.

5.3 Turbomachinery Test Cases

5.3.1 Genoa Turbine Cascade

The transition on the suction side of the Genoa turbine cascade was experimentally investigated by Ubaldi et al (1996). In the experiment, the freestream turbulence intensity was approximately 1%. The pressure side of the blade was completely laminar while on the suction side transition occurred at mid-chord. The grid used in the computation consisted of 86 000 nodes and is shown in Figure 5.14. The flow entered axially (in this case in the x-direction) and the incidence angle with the blade leading edge was zero degrees.

The velocity distribution computed with the transition model and compared to the experimental measurements (which are based on pressure tap measurements) is shown in Figure 5.15. On the pressure side the boundary layers are accelerated from the leading edge to the trailing edge. On the suction side the boundary layer is strongly accelerated until approximately the 0.3 chord location at which point a weak adverse pressure gradient is encountered.

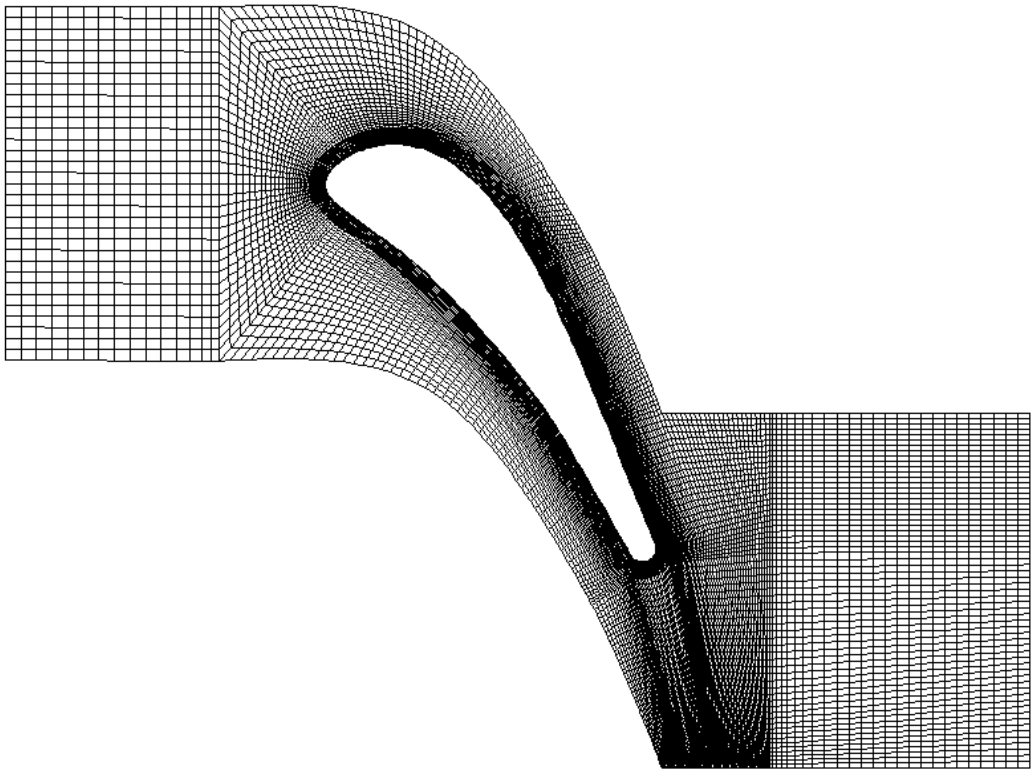

Figure 5.14 Mesh used to compute the Genoa turbine blade.

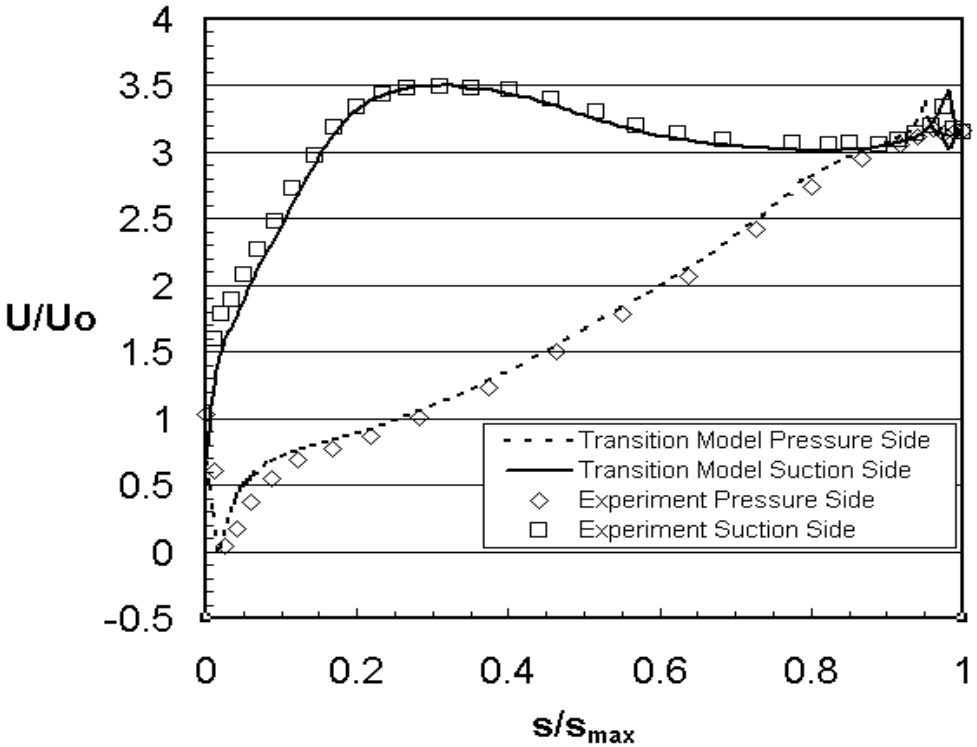

Figure 5.15 Velocity distribution (U/Uo) around the Genoa turbine blade.

The normalized suction side friction velocity for the Genoa test case is shown in Figure 5.16. The onset of transition is predicted slightly early. However, based on the two different measurements there does appear to be some experimental uncertainty in the exact location of transition onset. For this test case, the pressure side of the blade was completely laminar both in the experiment and in the prediction.

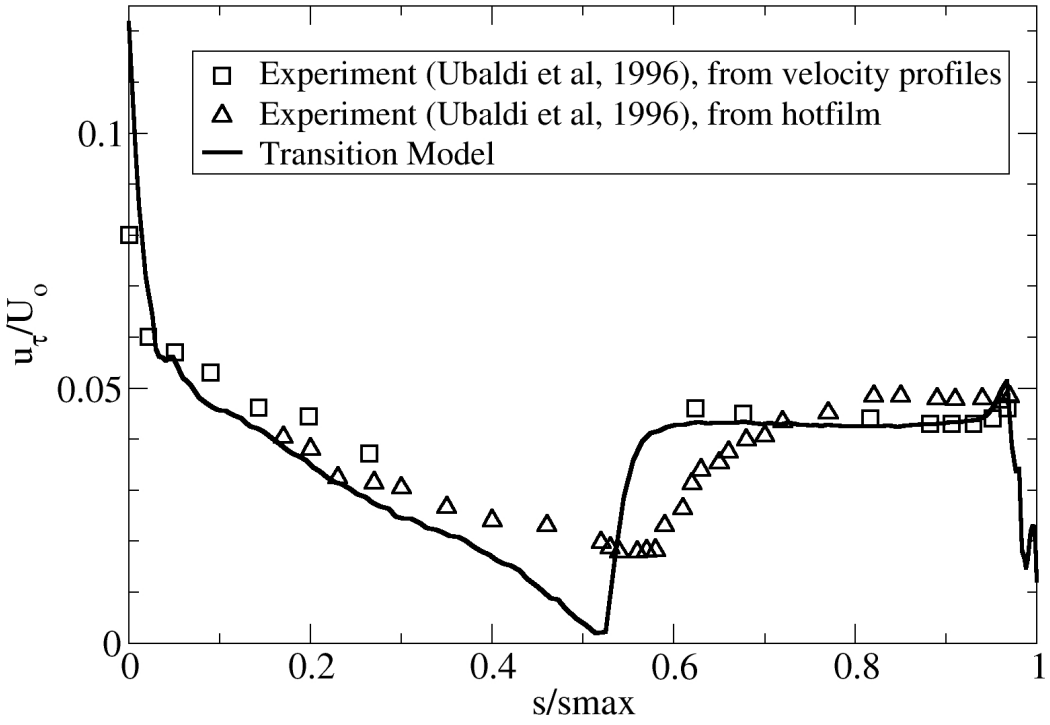

Figure 5.16 Normalized wall friction velocity distributions (u_τ/U_o) on the suction side of the Genoa cascade.

5.3.2 Zierke and Deutsch Compressor Cascade

The flow field around this compressor blade was experimentally investigated by Zierke and Deutsch (1989). The case computed in this thesis is for a leading edge incidence angle of –1.5°. The experimental wind tunnel had a relatively low freestream turbulence level of 0.18 percent. The grid used for the CFD computations consisted of 86,000 nodes and is shown in Figure 5.17. The pressure distribution for the Zierke compressor is shown in Figure 5.18 and appears to be in relatively good agreement with the experiment. On the suction side the boundary layer is decelerated from the leading edge to the trailing edge while on the pressure side the flow is decelerated from the leading edge until the 0.75 chord location at which point it undergoes an acceleration.

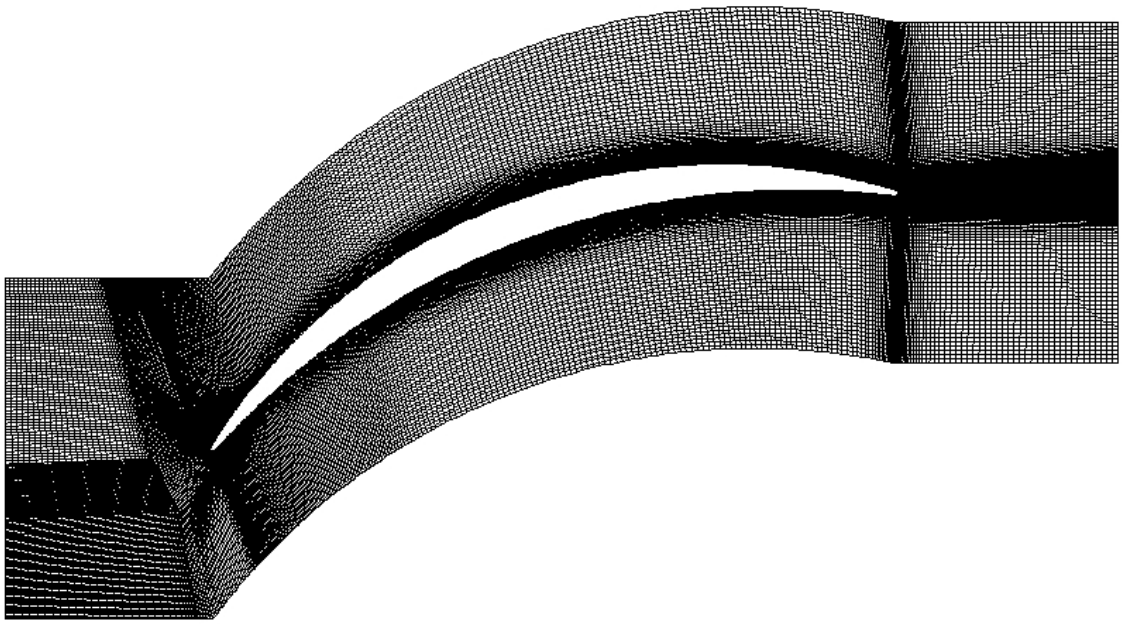

Figure 5.17 Mesh used to compute the Zierke and Deutsch compressor blade.

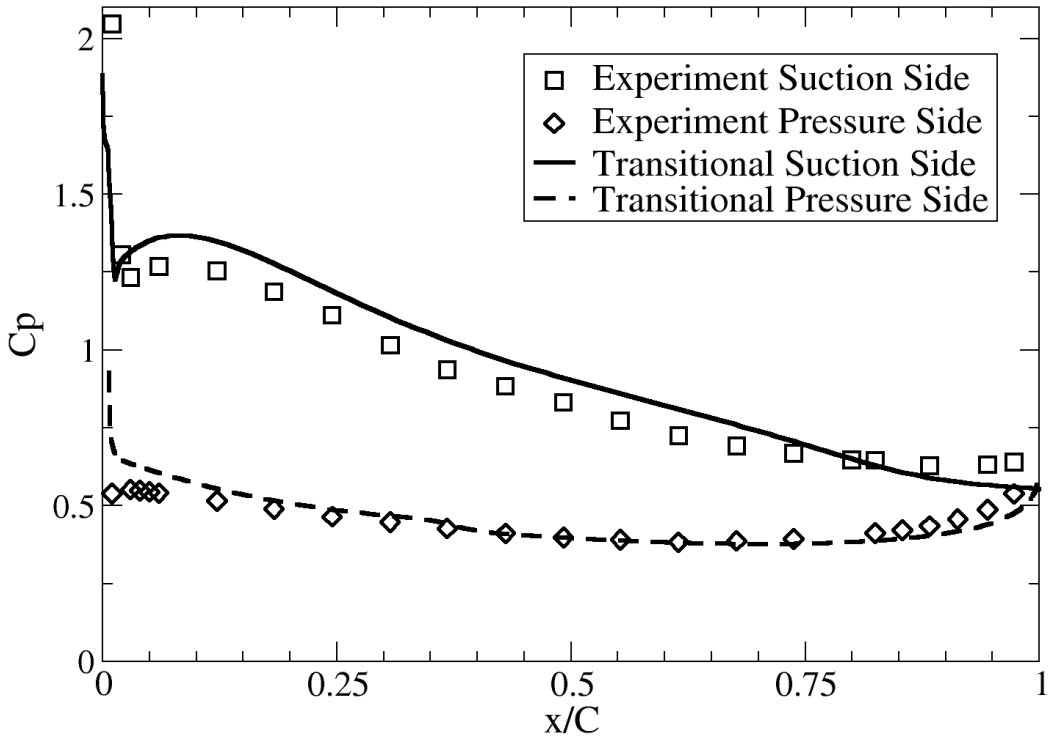

Figure 5.18 Pressure distribution (Cp) around the Zierke and Deutsch compressor blade.

The contours of turbulence intensity (Tu) predicted by the transition model for the Zierke and Deutsch compressor blade are shown in Figure 5.19. On the suction side, transition occurs at the leading edge due to a small leading edge separation bubble. This can be seen clearly in Figure 5.20 which is a close up of the leading edge region. The velocity streamlines clearly indicate the presence of a small leading edge separation bubble and the turbulence intensity (Tu) contour indicate that this separation causes the boundary layer to transition to turbulent flow. If the leading edge separation bubble had not tripped the boundary layer to fully turbulent, the trailing edge separation would probably occur at a different position, which would in turn affect the profile loss of the blade. This would seem to bolster the arguments made by Tain and Cumpsty (2000) that a leading edge separation can have a profound effect on the subsequent boundary layer development. On the pressure side, transition occurs at about mid-chord also due to the presence of a laminar separation. This can be seen clearly in the skin friction distribution shown in Figure 5.21. On the pressure side the skin friction is negative from the 0.25 until the 0.5 chord position, at which point the flow transitions and reattaches. The reattachment location appears to be in good agreement with the experimental measurement. On the suction side, the flow is fully turbulent due to the leading edge separation bubble. Overall, there is a significant amount of scatter in the experimentally measured skin friction, however, in principal the transition model appears to be predicting the major flow features correctly (i.e. fully turbulent suction side, transition at mid-chord on the pressure side).

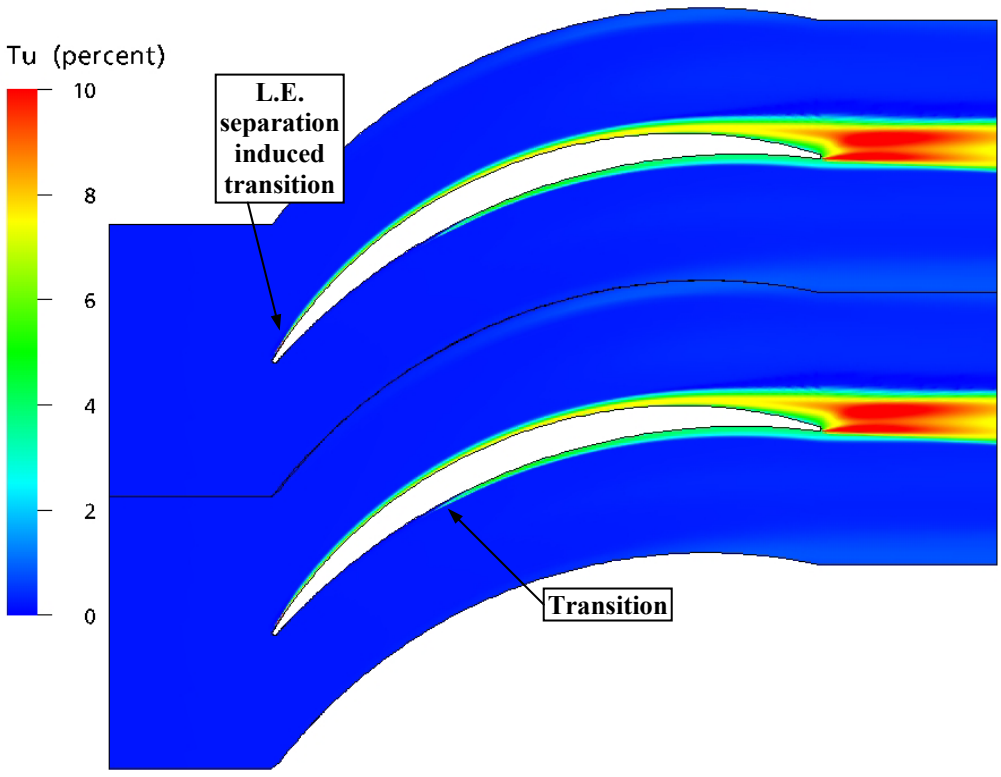

Figure 5.19 Contour of turbulence intensity, Tu, around the Zierke and Deutsch compressor.

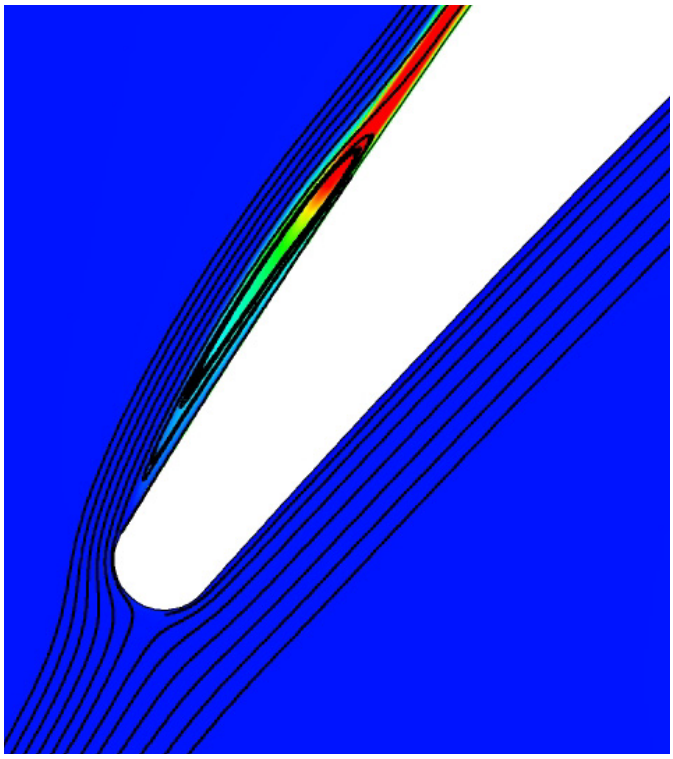

Figure 5.20 Close up of the Zierke compressor leading edge showing the velocity streamlines and a contour of the turbulence intensity, Tu.

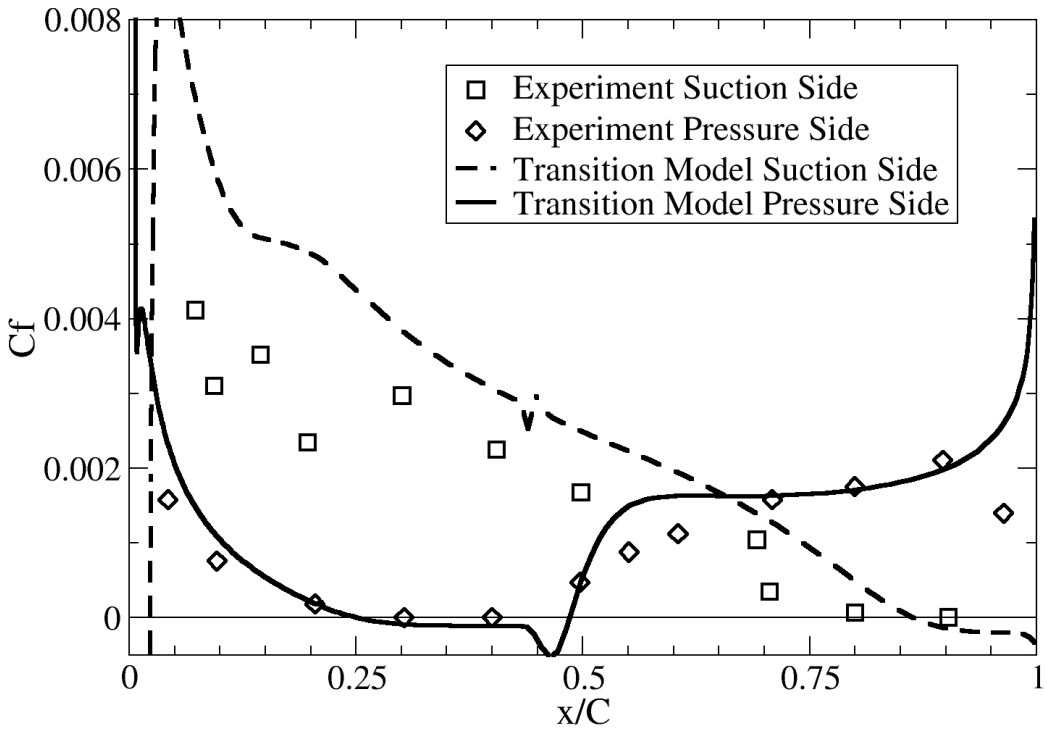

Figure 5.21 Skin friction (Cf) distribution for the Zierke and Deutsch compressor.

5.3.3 Pratt and Whitney Pak-B Low Pressure Turbine Cascade

The Pratt and Whitney PAK-B low pressure turbine blade is a particularly interesting airfoil because it has a loading profile similar to the rotors found in many modern aircraft engines (Dorney et al., 2000). The low-pressure rotors on modern aircraft engines are extremely challenging flow fields. This is because in many cases the transition occurs in the free shear layer of a separation bubble on the suction side (Mayle, 1991). The onset of transition in the free shear layer determines whether or not the separation bubble will reattach as a turbulent boundary layer and, ultimately, whether or not the blade will stall. The present transition model would therefore be of great interest to turbine designers if it can accurately predict the transition onset location for these types of flows.

Huang et al. (2003) conducted experiments on the PAK-B blade cascade for a range of Reynolds numbers and turbulence intensities. The experiments were performed at the design incidence angle for Reynolds numbers of 50,000, 75,000, and 100,000 based on inlet velocity and axial chord length, with turbulence intensities of 0.08%, 2.35% and 6.0% (which corresponded to values of 0.08%, 1.6%, and 2.85% at the leading edge of the blade). The computed pressure coefficient distributions obtained with the transition model and fully turbulent are compared to the experimental data for the 75 000 Reynolds number, 2.35% turbulent intensity case in Figure 5.22. The agreement with experiment is quite good except on the suction side where a pressure plateau due to a laminar separation turbulent reattachment exists. The fully turbulent computation completely misses this phenomena because the boundary layer remains attached over the entire length of the suction surface. The transition model appears to do a reasonably good job predicting the pressure plateau due to the laminar separation and the subsequent turbulent reattachment location. The pressure side was predicted to be fully attached and laminar.

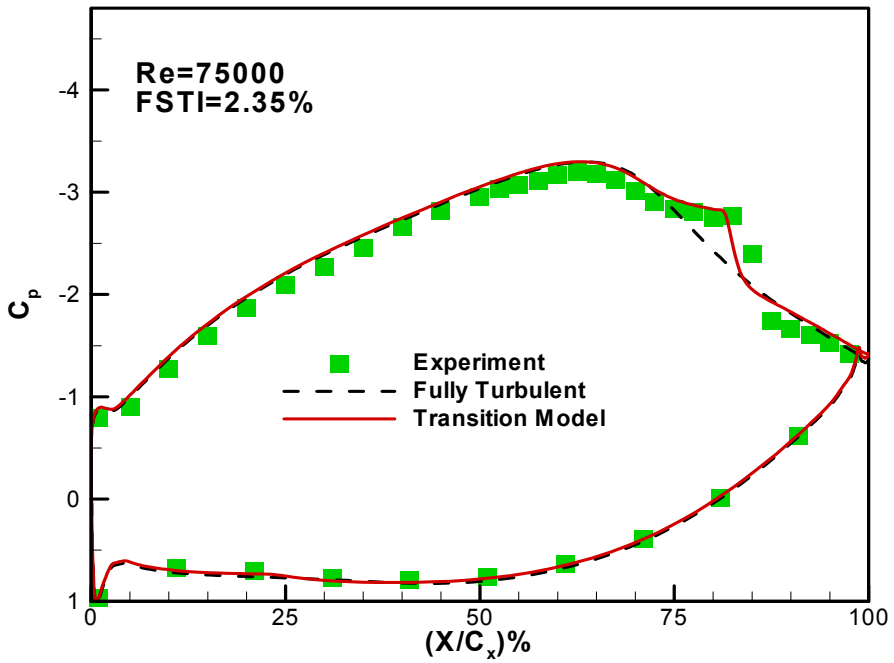

Figure 5.22 Predicted blade loading for the Pak-B Low-Pressure turbine at a Reynolds number of 75 000 and a freestream turbulent intensity (FSTI) of 2.35%.

The computed pressure coefficient distributions for various Reynolds numbers and freestream turbulence intensities compared to experimental data are shown in Figure 5.23. In this figure, the comparisons are organized such that the horizontal axis denotes the Reynolds number whereas the vertical axis corresponds to the freestream turbulence intensity of the specific case. As previously mentioned, the most important feature of this testcase is the extent of the separation bubble on the suction side, characterized by the plateau in the pressure distribution. The size of the separation bubble is actually a complex function of the Reynolds number and the freestream turbulence value. As the Reynolds number or freestream turbulence decrease, the size of the separation and hence the pressure plateau increases. The computations with the transition model compare well with the experimental data for all of the cases considered, illustrating the ability of the model to capture the effects of Reynolds number and turbulence intensity variations on the size of a laminar separation bubble and the subsequent turbulent reattachment.

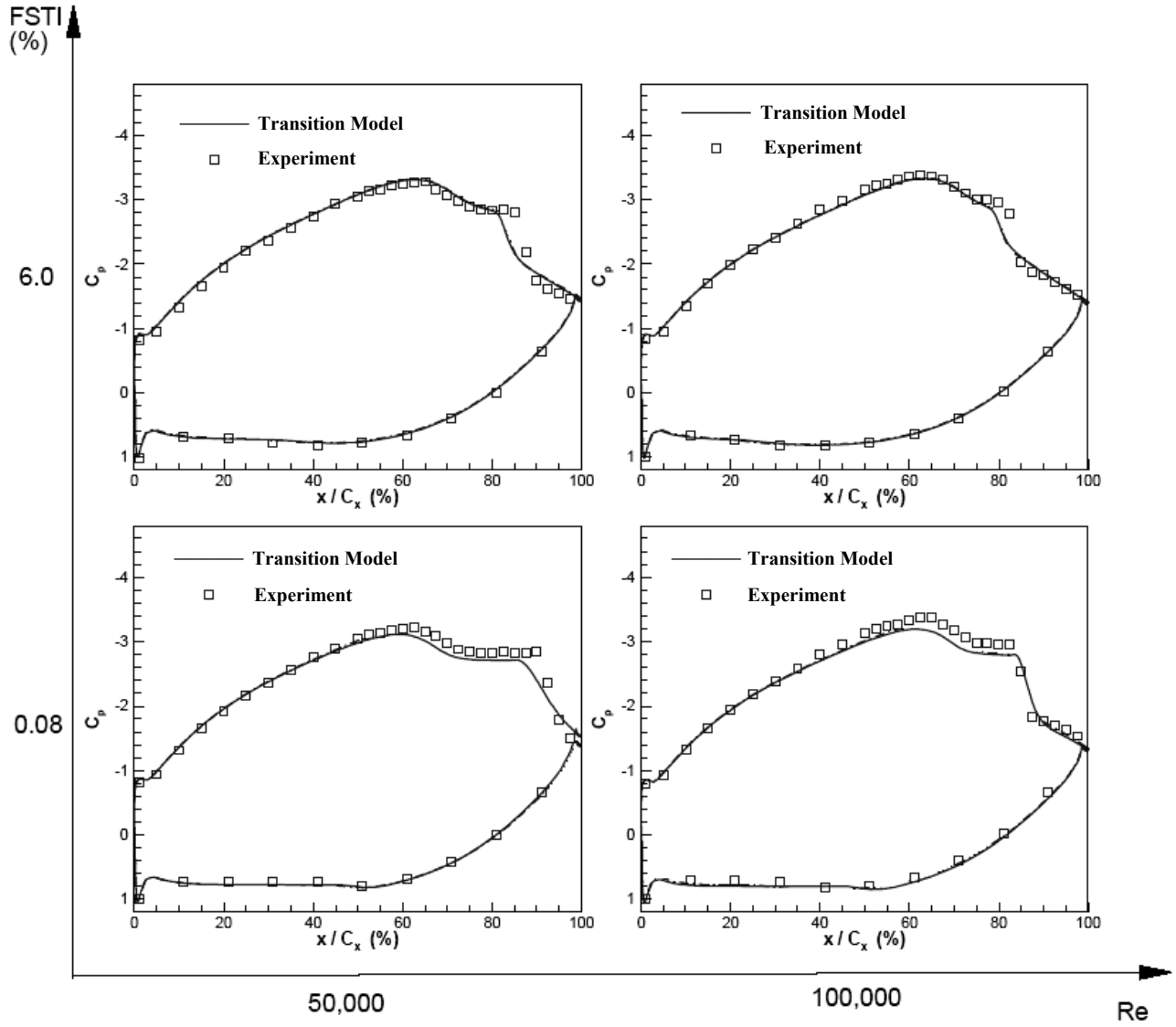

Figure 5.23 Blade loading for the Pak-B Low-Pressure turbine at various freestream turbulence intensities (FSTI) and Reynolds numbers (Re).

5.3.4 Von-Karman Institute (VKI) Transonic Turbine Cascade

This turbine blade was experimentally investigated by Arts et al. (1990) and is a very good test case for the ability of the transition model to predict the effect of transition on the heat transfer of a transonic turbine blade. The case computed in this thesis is for two different freestream turbulence intensities of 6.0% and 1.0% with an exit Mach number of 1.06. The grid consisted of 70 000 nodes and is shown in Figure 5.24. The total temperature at the inlet was 416.4° K and the wall temperature in the CFD computations was specified as a constant value of 299.75° K. The heat transfer coefficient (H) was then calculated based on the predicted heat flux divided by the difference between the inlet total temperature and the wall temperature. The isentropic Mach number around the turbine blade is shown in Figure 5.25. On the pressure side the flow undergoes a strong acceleration along the entire length of the blade. On the suction side the flow is also strongly accelerated until the 0.045 position, at which point it would appear that a shock impinges on the surface. This causes a strong local deceleration and afterwards the flow continues to accelerate towards the trailing edge.

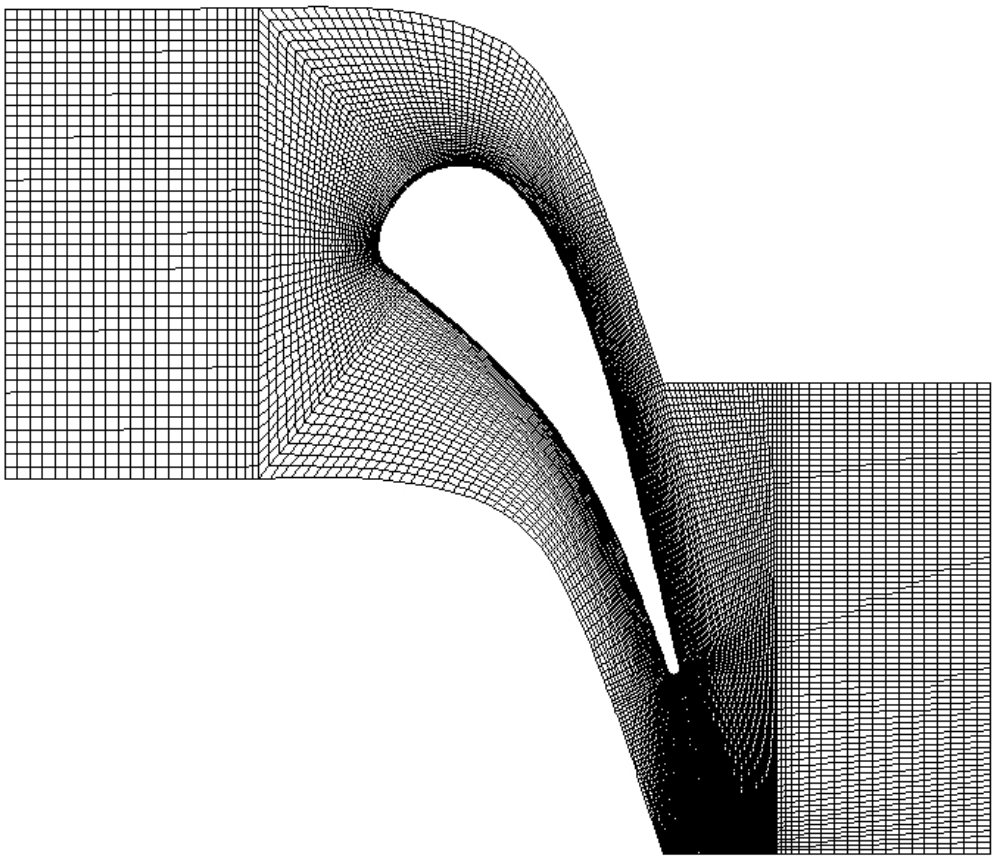

Figure 5.24 Mesh used to compute the VKI transonic turbine blade.

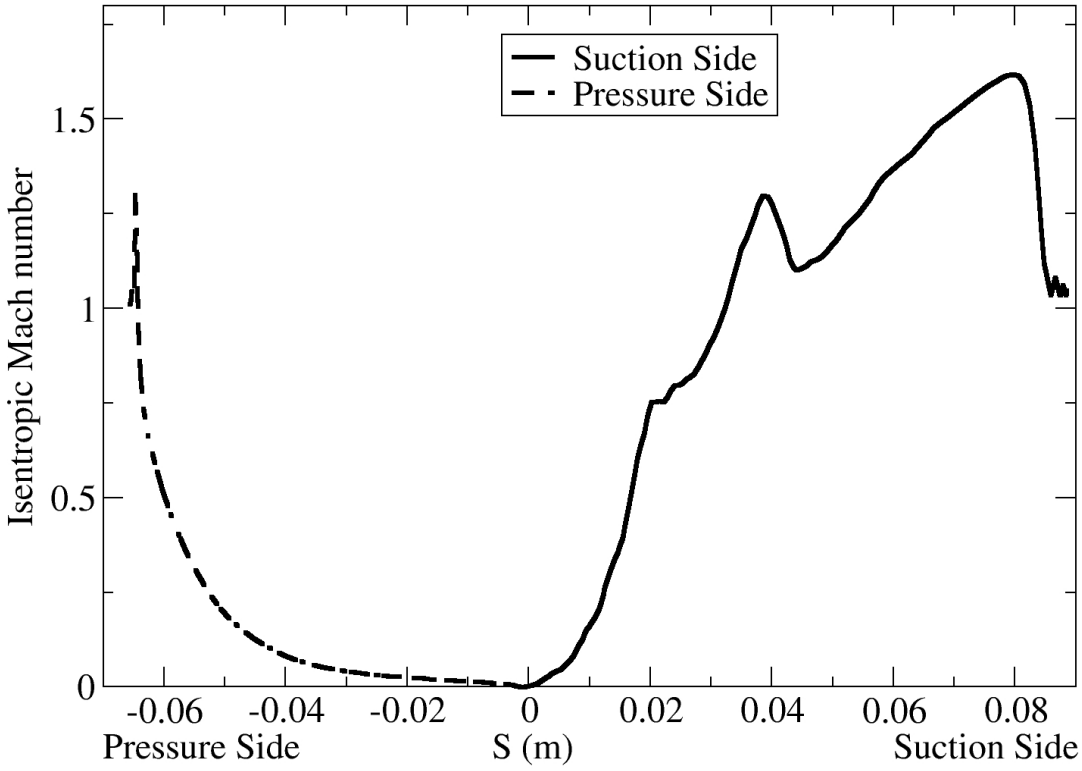

Figure 5.25 Isentropic Mach number around the VKI transonic turbine.

The surface heat transfer coefficient (H) for the VKI MUR 241 (FSTI = 6.0%) and MUR 116 (FSTI = 1.0%) test cases is shown in Figure 5.26. The strong acceleration on the suction side for the MUR 241 case keeps the flow laminar until a shock near the mid chord, whereas for the MUR 116 case the flow is laminar until right before the trailing edge. It would appear that the shock acts almost like a boundary layer trip and if the freestream turbulence is large enough, as is the case for MUR 241, transition will occur due to the strong local deceleration. If the freestream turbulence is too small (i.e. MUR 116) then the laminar boundary layer passes through the locally decelerated region and continues downstream in a laminar state. For the MUR 241 case, downstream of transition there appears to be a significant amount of error between the predicted turbulent heat transfer and the measured value. It is possible that this is the result of a Mach number effect on the transition length (Steelant and Dick, 2001). At present, no attempt has been made to account for this effect in the present transition model. Mach number effects could be incorporated into future correlations, if found consistently important.

The pressure side heat transfer is of particular interest for this case. For both cases transition did not occur on the pressure side, however, the heat transfer was significantly increased for the high turbulence intensity case. It is believed that large freestream levels of turbulence can buffet the laminar boundary layer and increase the heat transfer and skin friction. From a modeling standpoint the effect was caused by the large freestream

viscosity ratio necessary for MUR 241 to keep the turbulence intensity from decaying below 6%, which is the freestream value quoted in the experiment (Arts et al., 1990). This led to an increase in the eddy viscosity inside the laminar boundary layer for the MUR 241 case. This can be seen clearly in the pressure side velocity and eddy viscosity profiles shown in Figure 5.27. From the velocity profiles both the pressure side MUR 116 and MUR241 boundary layers appear to resemble strongly accelerated laminar profiles. However, the MUR 241 velocity profile is fuller than the MUR 116 velocity profile. This is caused by the increased eddy viscosity which is essentially zero inside the boundary layer for the MUR 116 case but is approximately five times the dynamic viscosity for the MUR 241 case. The enhanced heat transfer for the MUR 241 case on the pressure side was also present in the experiment and the effect appears to be physical.

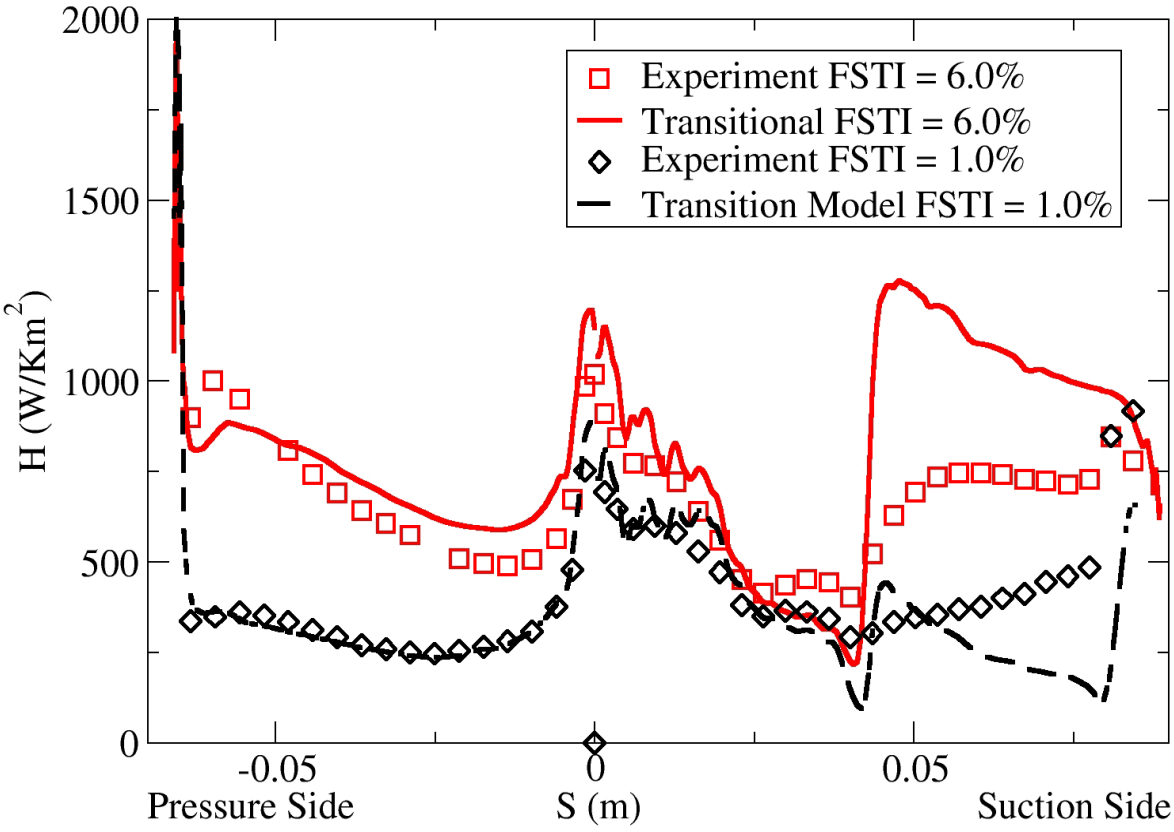

Figure 5.26 Predicted heat transfer coefficient (H) for the VKI MUR241 (FSTI = 6.0%) and MUR116 (FSTI = 1.0%) test cases.

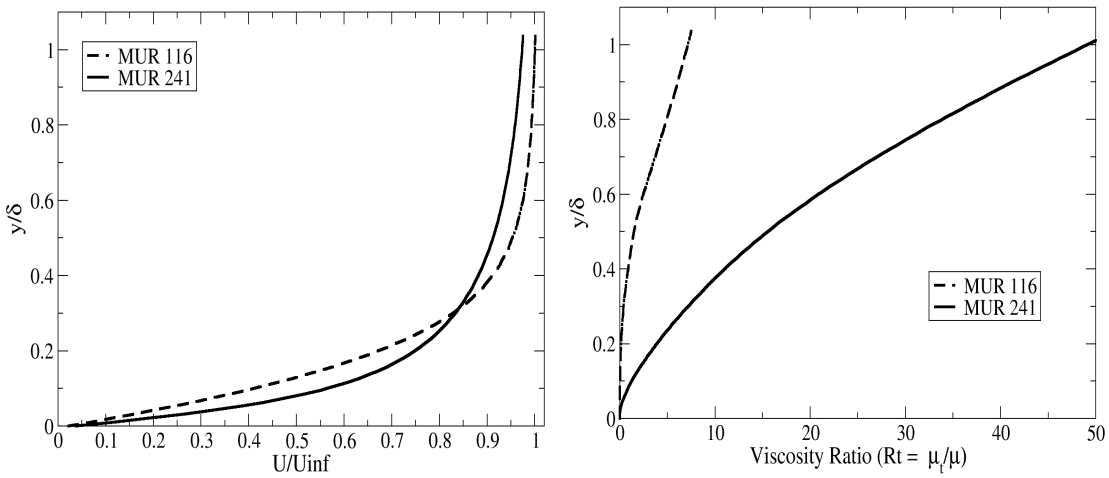

Figure 5.27 Velocity profile (left) and eddy viscosity ratio (right) in the accelerated laminar boundary layer on the pressure side (at S = -0.017) for the VKI MUR241 (FSTI = 6.0%) and MUR116 (FSTI = 1.0%) test cases.

5.3.5 Unsteady Wake/Blade Interaction on the T106 Cascade

In the previous test cases the new transition model has been shown to predict transition reasonably well in steady attached and separated flows. However, in gas turbine engines the mean flow is not steady. It is now believed that transition on actual engine blades is strongly influenced by the unsteady wakes from the upstream blade rows. There is a growing body of experimental evidence that suggests that the unsteady wakes can have a profound impact on the suction side separation bubbles and hence the losses of low pressure turbine blades (e.g., Howell et al., 2001). For this reason, turbomachinery designers will eventually need to be able to investigate both the steady-state and unsteady –state behaviour of their blade designs in order to improve efficiency . This next test case will therefore attempt to validate the new transition model for the prediction of unsteady wake-induced transition on a low pressure turbine blade.

A computational investigation of the effects of unsteady wake/blade interaction on transition and separation in low-pressure turbines has been performed by the University of Kentucky authors in Langtry et al. (2004) in order to simulate the experiments performed by Stieger et al. (2003). These experiments were conducted in order to investigate the effects of periodically passing wakes on laminar-to-turbulent transition and separation in low-pressure turbines. The test section involved a T106 turbine blade cascade subject to a wake passing from a moving bar wake generator. The flow conditions correspond to a Reynolds number of 91,077 based on chord and inlet velocity and a freestream turbulence level of 0.1%. The details of the T106 cascade are summarized in Table 5.2. The bar was included in the computational domain the extent of which is illustrated in Figure 5.28.

Chord	198mm
Blade stagger	59.3°
Cascade and bar pitch	158mm
Inlet flow angle	37.7°
Design exit flow angle	63.2°
Bar diameter	2.05mm
Axial Distance: bars to LE	70mm
Flow Coefficient (U_{axial}/U_{bar})	0.83

Table 5.2 T106 cascade details.

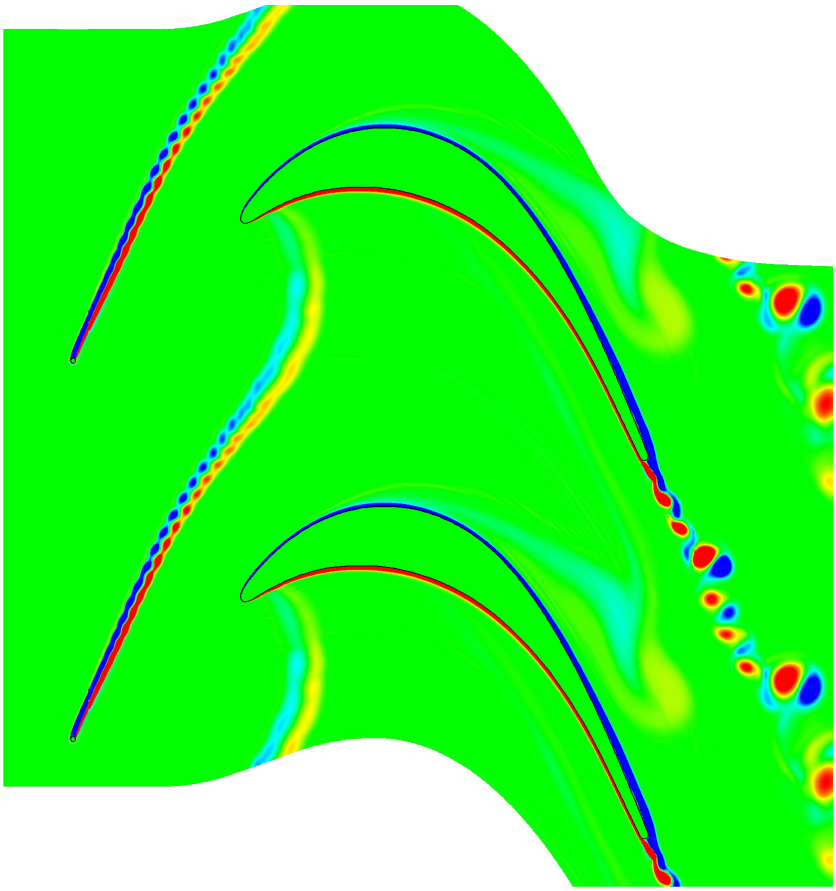

Figure 5.28 Computational domain used to compute the T106 test case. Note: contours of vorticity are shown.

The computed velocity profile of the bar wake at x/C = -0.04 before it enters the blade passage is compared to the experiment in Figure 5.29. The computation is in good agreement with the experiment, illustrating that the wake from the moving bars is captured accurately. The computed and experimental turbulent kinetic energy contours at various time levels are shown in Figure 5.30. In this figure the computed results are shown in the right hand side and the experimental data on the left. The computed results agree well with the experiments. The evolution of the wake and its interaction with the boundary layer on the blade appears to be captured well.

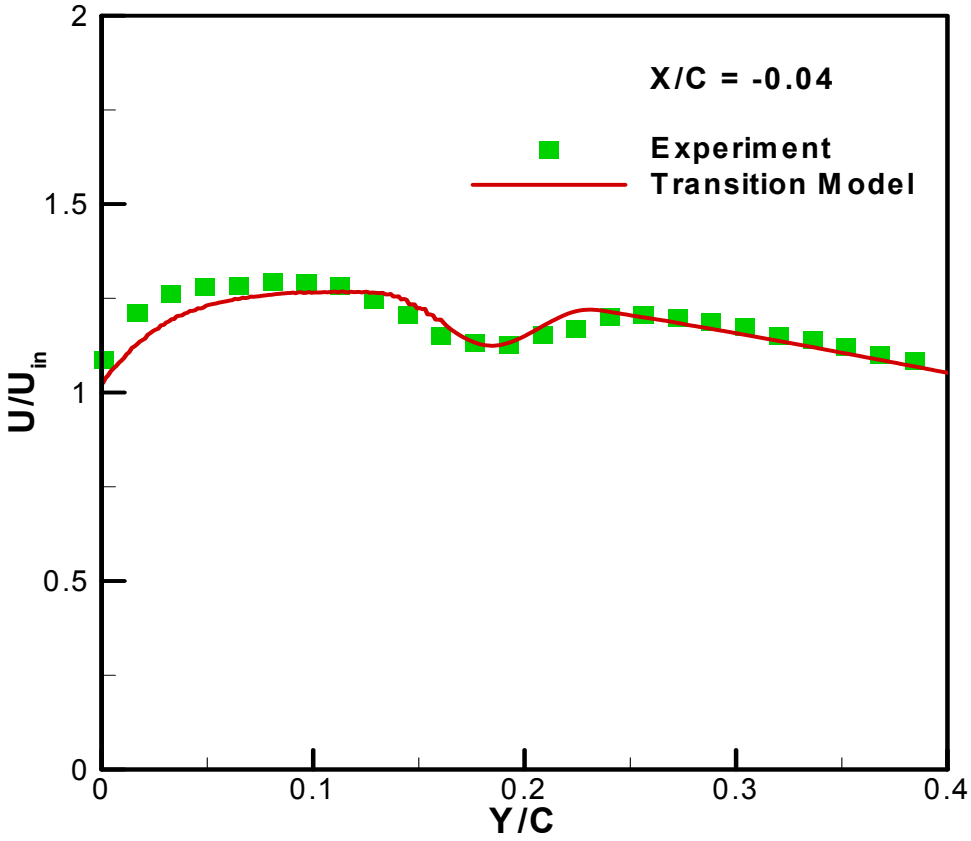

Figure 5.29 Velocity profile at x/C=-0.04 for T106 case.

The computed transition model pressure coefficient distribution as compared to experiment are shown in Figure 5.31. Both the wake-free (steady) computation and experiment are given along with the time-averaged pressure distributions from the unsteady-state experiments and computations. In the wake-free computation the size of the predicted separation region is slightly larger than in the experiment. The time-averaged pressure distribution from the unsteady-state experiments indicates that the laminar separation bubble on the suction side is completely suppressed due to the unsteady impinging wake. The computations predicted a partial suppression of the separation bubble as indicated by the pressure distribution shown in Figure 5.31.

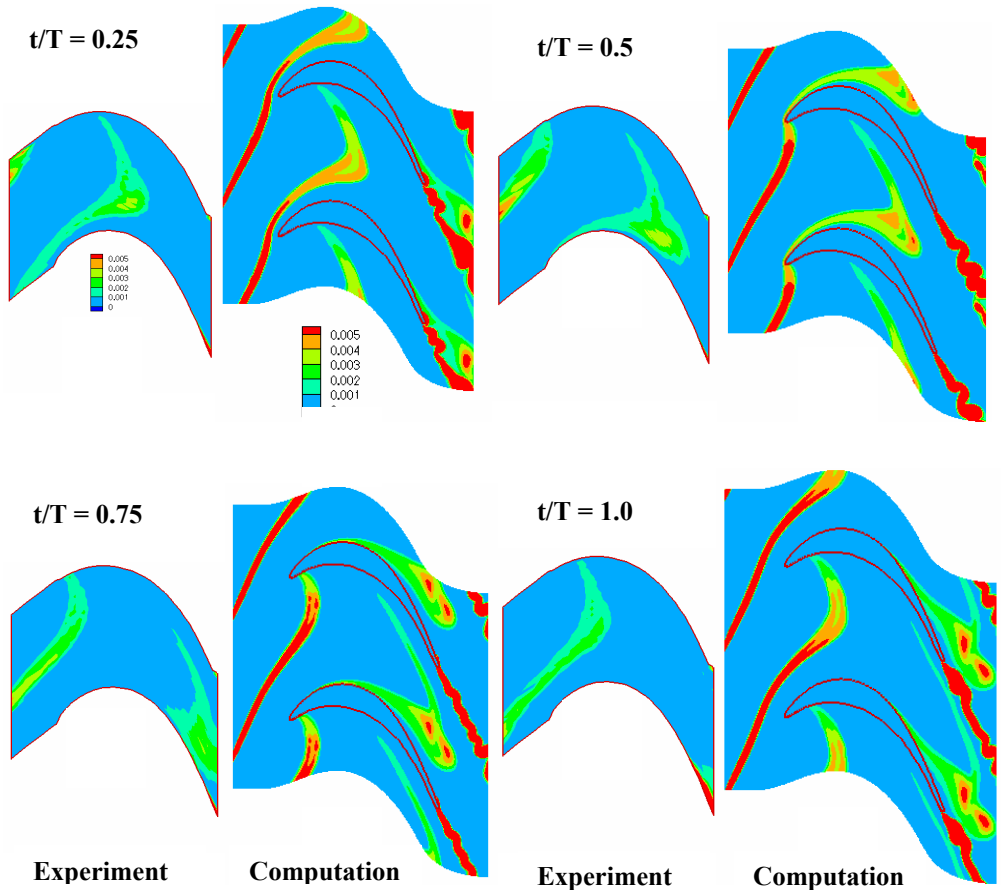

Figure 5.30 Contours of turbulent kinetic energy at various wake passing periods (t/T). Note: the left figure at each time is the experimental data, the right figure is the CFD computation

The predicted time variation of the skin friction coefficient on the suction surface of the blade is shown in Figure 5.32. The flow is separated for a large portion of time over the aft part of the suction surface. However, at a wake passing time (t/T) of 0.5 early transition appears at the 70% chord location, which is approximately where the wake is located at that point in time. There also appear to be regions of reverse flow in the turbulent patch downstream of the transition location. Similar regions of reverse flow in the turbulent patch were observed by Stieger et al. (2003) in the experiment using a particle image velocimetry method.

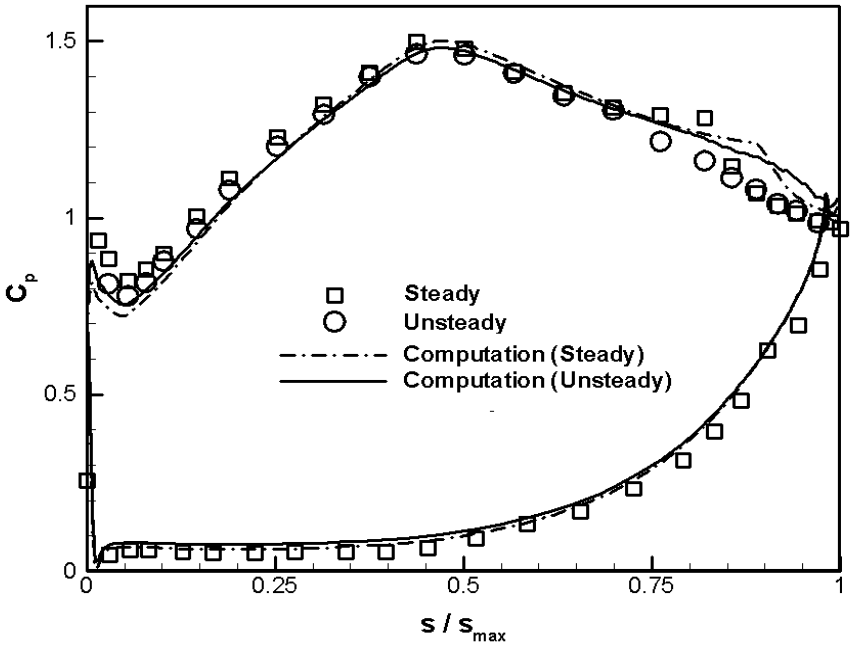

Figure 5.31 Comparison of computed transition model and experimental pressure coefficient distributions for the T106 test case.

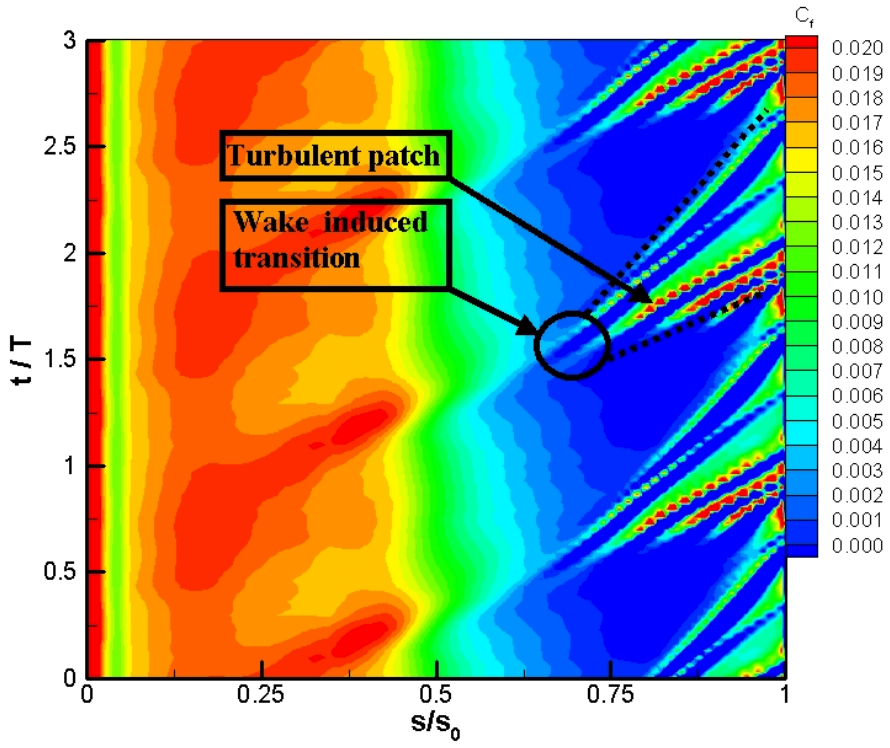

Figure 5.32 Computed phase averaged skin friction coefficient distribution on the suction surface of T106 blade. Note: Negative values of skin friction are cut off and shown as dark blue.

The time-averaged velocity profiles at nine stations along the suction surface are compared to the experimental data in Figure 5.33. The simulations agree well with the data except in the near wall region of the last three stations where the computations indicate separated flow but the experiment indicates attached flow. Note that the current model already over-predicts the steady-state separation bubble. This could be the main

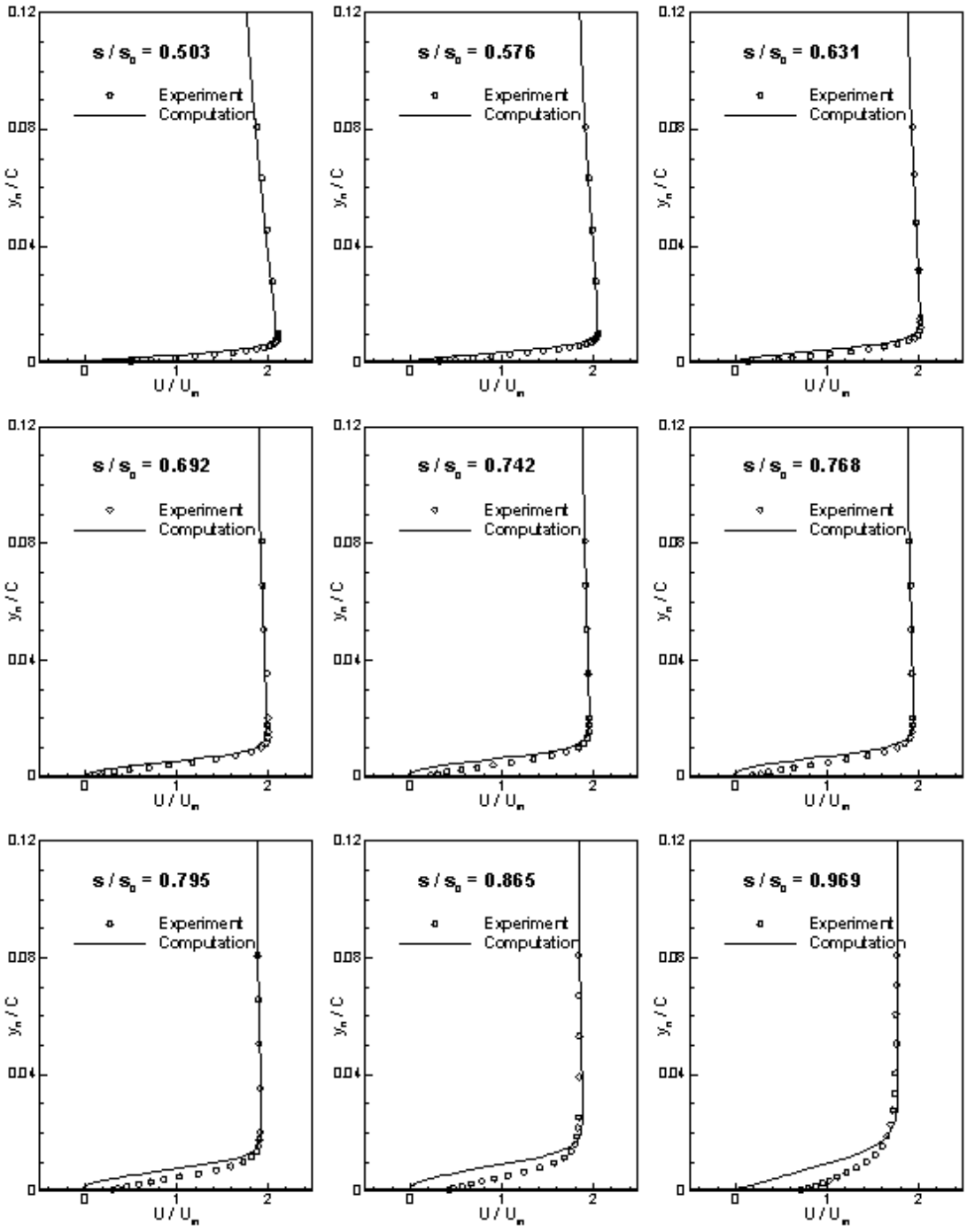

Figure 5.33 Comparison of computed and experimental mean velocity profiles at various streamwise locations on the suction surface of T106 blade.

reason why the unsteady-state simulations did not lead to a fully time-averaged attached flow. The fact that the laminar separation was not predicted correctly by the CFD is somewhat puzzling. It is possible that there could be some 3D flow features in the experiment that cannot be captured by the 2D CFD simulation. This is an area that should be further investigated in the future, either by attempting to model the 3D features of the wind tunnel or by using experimental data from another facility that does not have any significant 3D effects.

This concludes the chapter on the 2-D test cases for the transition model. In general, very good agreement with the available experimental data was obtained. The model appears to do a good job predicting the combined effects of turbulence intensity, pressure gradients and separation on transition. Encouraging first results were also obtained for unsteady wake-induced transition effects but this aspect of the model will need to be validated more extensively against additional experimental test cases. The next chapter will detail the 3-D test cases that have been used to validate the transition model.